CALIFORNIA CURRENT INTEGRATED ECOSYSTEM ASSESSMENT (CCIEA) CALIFORNIA CURRENT ECOSYSTEM STATUS REPORT, 2020

A report of the NOAA CCIEA Team to the Pacific Fishery Management Council, March 5, 2020.

Editors: Dr. Chris Harvey (NWFSC), Dr. Toby Garfield (SWFSC), Mr. Greg Williams (PSMFC), and Dr. Nick Tolimieri (NWFSC)

1 INTRODUCTION

Section 1.4 of the 2013 Fishery Ecosystem Plan (FEP) established a reporting process wherein NOAA provides the Pacific Fishery Management Council (Council) with a yearly update on the status of the California Current Ecosystem (CCE), as derived from environmental, biological, economic and social indicators. NOAA's California Current Integrated Ecosystem Assessment (CCIEA) team is responsible for this report. This is our 8th report, with prior reports in 2012 and 2014-2019.

This report summarizes CCE status based on data and analyses that generally run through 2019. Highlights are summarized in Box 1.1. Appendices provide additional information or clarification, as requested by the Council, the Scientific and Statistical Committee (SSC), or other advisory bodies.

Box 1.1: Highlights of this report

- **In 2019, the system experienced weak to neutral El Niño conditions, average to slightly positive Pacific Decadal Oscillation (PDO), and very weak North Pacific circulation**
- **A large marine heatwave emerged in mid 2019, similar in size and intensity to the 2013-2016 "Blob," but it weakened by December, and we do not yet know what effects it had**
- **Several ecological indicators implied average or above-average productivity in 2019:**
  - The copepod community off Oregon was high in cool-water, lipid-rich species in summer
  - Anchovy densities continued to increase along most of the coast
  - Juvenile Chinook and coho salmon catches off Oregon and Washington were average
  - Sea lion pup growth on San Miguel Island was above average
- **However, there was evidence of unfavorable conditions in 2019, particularly off central and northern California:**
  - Krill densities off central and northern California and Oregon were very low
  - Pyrosomes (warm-water tunicates) were abundant in the central CCE
  - Juvenile rockfish, a key forage group in this region, had low abundance
  - Seabird colonies at the Farallon Islands and Año Nuevo had poor production
- **Indicators are consistent with average to below-average salmon returns in 2020**
- **Above-average reports of whale entanglements occurred for the 6th straight year**
- **West Coast fishery landings in 2018 declined 8% relative to 2017; revenue declined 7%**
- **Fishery diversification remains relatively low on average across all vessel classes**
- **We introduce two new indicators in this year's report:**
  - Proportional distribution of commercial fishing revenue among coastal communities
  - Habitat compression, which measures how climate and ocean forcing compresses cooler upwelling habitat along the coast

Throughout this report, most indicator plots follow the formats illustrated in Figure 1.1.

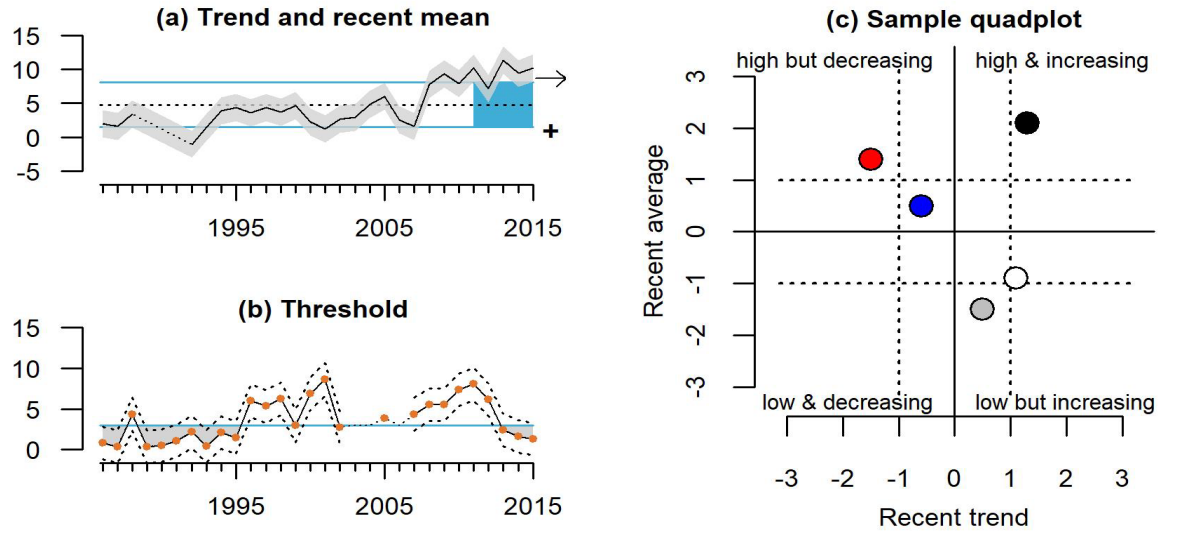

Figure 1.1 (a) Sample time-series plot, with indicator data relative to the mean (black dotted horizontal line) and 1.0 s.d. (solid blue lines) of the full time series. Dotted black line indicates missing data, and points (when included) indicate data. Arrow at the right indicates if the trend over the evaluation period (shaded blue) was positive, negative or neutral. Symbol at the lower right indicates if the recent mean was greater than, less than, or within 1.0 s.d. of the long-term mean. When possible, times series indicate observation error (gray envelope), defined for each plot (e.g., s.d., s.e., 95% confidence intervals); (b) Sample time-series plot with the indicator plotted relative to a threshold value (blue line). Dashed lines indicate upper and lower observation error, again defined for each plot. Dotted black line indicates missing data; (c) Sample quadplot. Each point represents one normalized time series. The position of a point indicates if the times series was increasing or decreasing over the evaluation period and whether the mean recent years of the time series (recent trend) was above or below the long-term average (recent mean). Dashed lines represent ±1.0 s.d. of the full time series.

2 SAMPLING LOCATIONS

Figure 2.1a shows the CCE and headlands that define key biogeographic boundaries. We generally consider areas north of Cape Mendocino to be the "Northern CCE," areas between Cape Mendocino and Point Conception the "Central CCE," and areas south of Point Conception the "Southern CCE." Figure 2.1a also shows sampling locations for most regional oceanographic data (Sections 3.2 and 3.3). Key transects are the Newport Line off Oregon, the Trinidad Line off northern California, and the CalCOFI grid further south. This sampling is complemented by basin-scale observations and models.

Freshwater ecoregions in the CCE are shown in Figure 2.1b, and are the basis by which we summarize indicators for snowpack, streamflow and stream temperature (Section 3.5).

Figure 2.1c indicates sampling locations for most biological indicators, including zooplankton (Section 4.1), forage species (Section 4.2), juvenile salmon (Section 4.3), California sea lions (Section 4.6) and seabirds (Section 4.7).

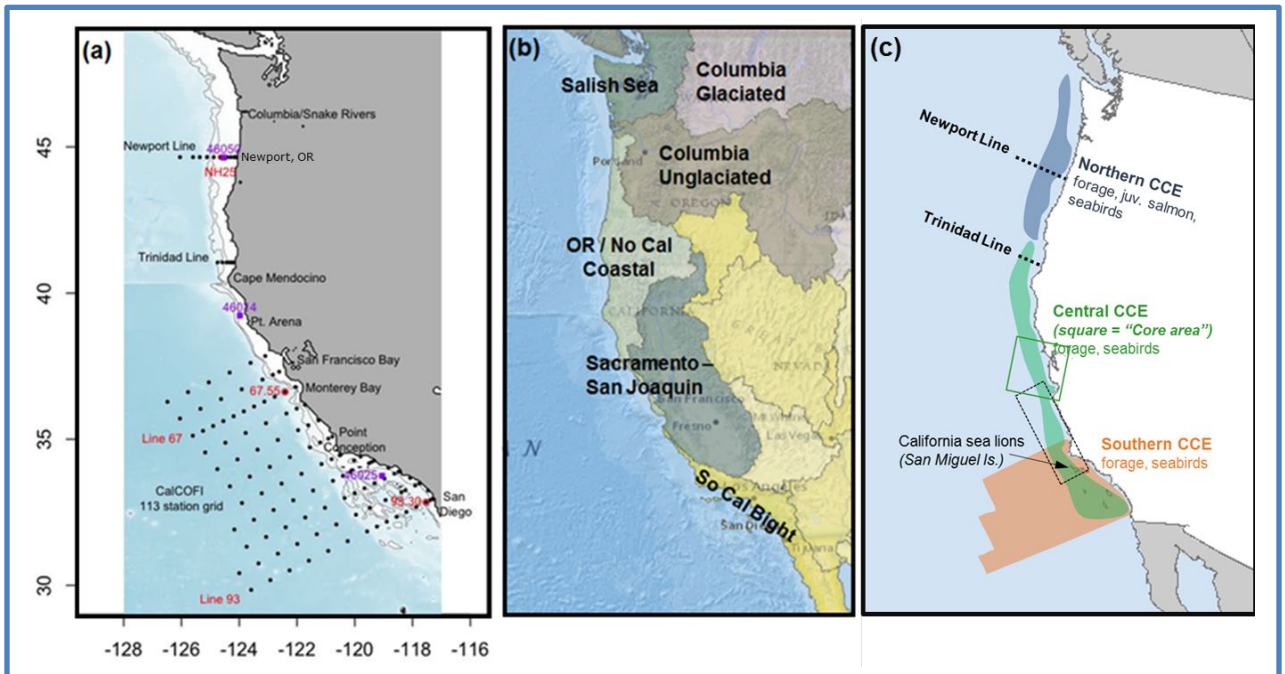

Figure 2.1. Map of the California Current Ecosystem (CCE) and sampling areas: (a) key geographic features and oceanographic sampling locations; (b) freshwater ecoregions, where snowpack and hydrographic indicators are measured; and (c) biological sampling areas for zooplankton (Newport Line, Trinidad Line), pelagic forage, juvenile salmon, seabirds, and California sea lions. Solid box = core sampling area for forage in the Central CCE. Dotted box approximates foraging area for adult female California sea lions from the San Miguel colony.

3 Climate and Ocean Drivers

The CCE has experienced exceptional ocean warming over the past seven years, due to a mixture of El Niño events and large marine heat waves, including the record heatwave of 2014-2016. This general trend continued in 2019: a weak El Niño event occurred in winter and spring, and a marine heatwave originated in the North Pacific in the summer. El Niño impacts included below-average upwelling during winter and spring 2019 in the central and southern CCE, and above-average spring water temperatures in the south. The heatwave that emerged in the summer was mostly constrained offshore outside of the upwelling zone. It is too early to connect any specific responses in the CCE to this new marine heatwave, but ecosystem impacts can be expected if it reemerges in spring 2020.

The following subsections provide in-depth descriptions of basin-scale, regional-scale, and hydrologic indicators of climate and ocean variability in the CCE.

3.1 Basin-Scale Indicators

To describe large-scale physical ecosystem states, we report three indices. The Oceanic Niño Index (ONI) describes the equatorial El Niño Southern Oscillation (ENSO). An ONI above 0.5°C indicates El Niño conditions, which usually correspond to lower primary production, weaker upwelling, poleward transport of equatorial waters and species, and more storms to the south in the CCE. An ONI below -0.5°C means La Niña conditions, which usually lead to higher productivity. The Pacific Decadal Oscillation (PDO) describes Northeast Pacific sea surface temperature anomalies (SSTa) that may persist in regimes for many years. Positive PDOs are associated with warmer waters and lower productivity in the CCE, while negative PDOs indicate cooler waters and higher productivity. The North Pacific Gyre Oscillation (NPGO) is a signal of sea surface height, indicating changes in ocean circulation that affect source waters for the CCE. Positive NPGOs are associated with increased equatorward flow and higher surface salinities, nutrients, and chlorophyll-*a*. Negative NPGOs are associated with decreases in such values, less subarctic source water, and lower CCE productivity.

The ONI indicated that a weak El Niño, which began in September 2018, continued through June 2019 (Figure 3.1.1, top). The ONI only recorded a high of 0.9°C (compared to 2.6°C during the strong 2015-2016 El Niño). The ONI was neutral by the end of 2019, and NOAA's Climate Prediction Center forecasts a ~65% chance for neutral ENSO conditions to persist through spring 2020. The PDO has experienced a downward trend from the high positive values of 2013-2016, and was generally neutral in 2019, with values >1.0 only occurring during April-June (Figure 3.1.1, middle). These PDO values were thus above normal, but not nearly as high as in past major El Niño events (1982, 1998, 2016) and the 2013-2016 marine heatwave (the "Blob"). The NPGO in 2019 continued an extended period of negative values, which began in late 2016 (Figure 3.1.1, bottom). Values from October 2017 to June 2019 were among the lowest NPGO values for the whole record since 1950. Thus, the three basin-scale indices provide a mixed signal of general conditions in the CCE: the ONI and NPGO were consistent with lower productivity, while the PDO was neutral, implying average productivity. Seasonal values for basin-scale indices are in Appendix D.1.

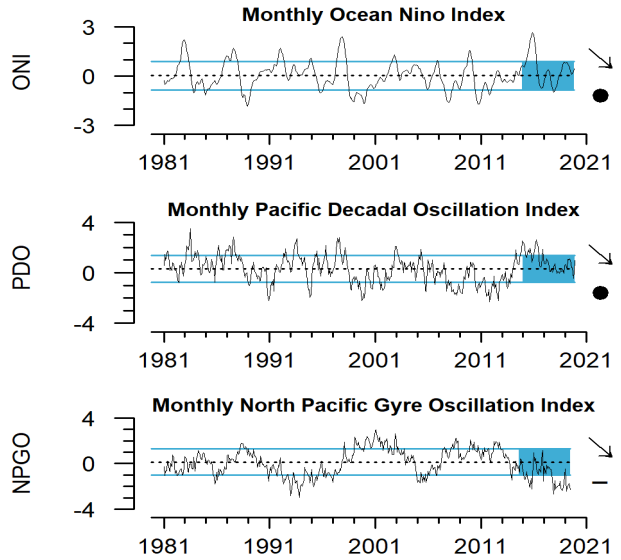

Figure 3.1.1 Monthly values of the Ocean Nino Index (ONI), Pacific Decadal Oscillation (PDO), and the North Pacific Gyre Oscillation (NPGO) from 1981-2019. Mean and s.d. for 1981-2010 not the full time series. Lines, colors, and symbols are as in Fig. 1.

Bering Sea and Gulf of Alaska warming extended into the northeast Pacific during 2019 (Figure 3.1.2, left). Positive SST anomalies increased and the spatial extent of warming expanded over the course of 2019, with the warmest anomalies and greatest spatial extent occurring in summer and fall. Winter SST measurements were ~0.5°C warmer than average along the coast, while warming anomalies were 0.5 to 1.0°C above long-term mean for most cells above 48°N (Figure 3.1.2, upper left). Summer 2019 anomalies were more extreme, representing the development of another marine heatwave (see Section 7.2 for additional detail). A quarter of the grid cells had the highest recorded temperature anomalies since 1982 (Figure 3.1.2, lower left). Along the West Coast, summer 2019 anomalies ≥1 SD occurred north of Monterey Bay, while coastal anomalies to the south were neutral.

Five-year average SST anomalies demonstrate the extended warming that the CCE has experienced for many years. The 5-year average winter SSTa in the CCE was generally ≥1 SD above average, with slightly cooler but still positive anomalies closer to shore (Figure 3.1.2, upper middle). The 5-year average summer SSTa was positive for most of the Northeast Pacific, again with some slightly cooler warm anomalies in the coastal CCE (Figure 3.1.2, lower middle). Trends in winter SSTa over the last 5 years have been negative (Figure 3.1.2, upper right), due to recent years being cooler than the winters associated with the 2013-2016 marine heatwave. Summer 5-year trends along the coast were positive north of Cape Mendocino and negative to the south (Figure 3.1.2, lower right). Summer trends were mixed in the rest of the Northeast Pacific.

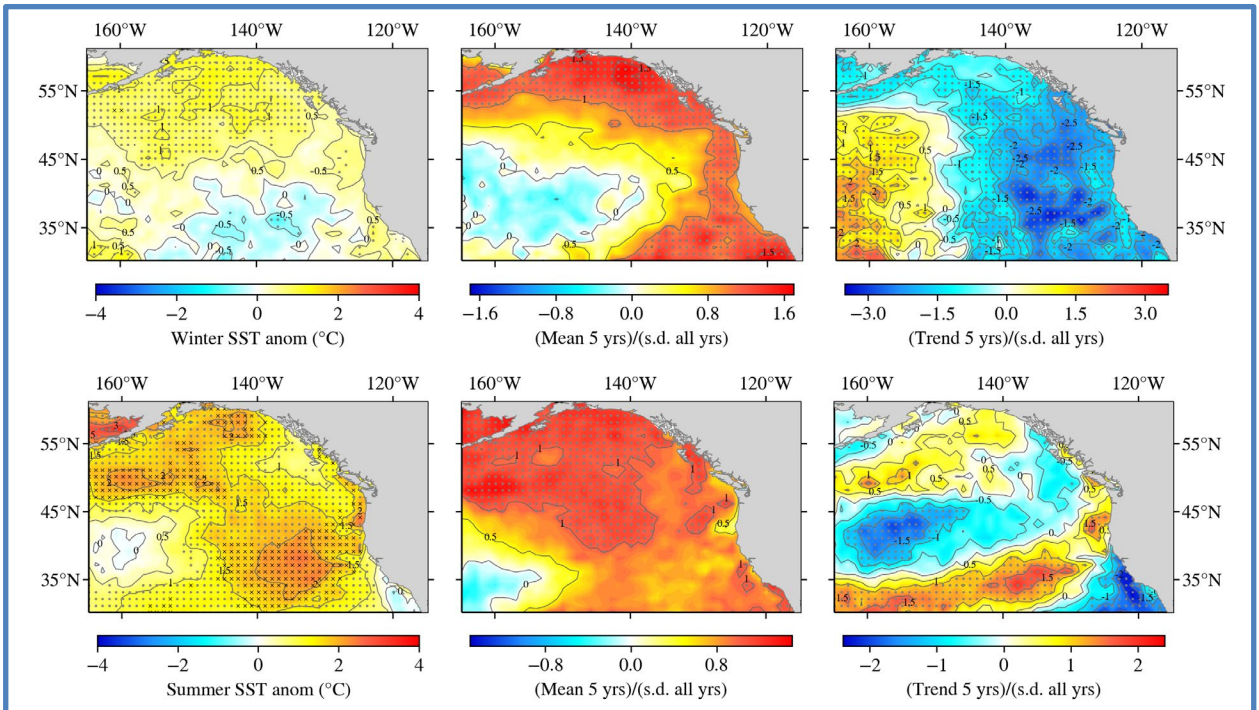

Figure 3.1.2 Left: Sea surface temperature (SST) anomalies in 2019, based on 1982-present satellite time series in winter (Jan-Mar; top) and summer (July-Sept; bottom). Center: Mean SST anomalies for 2015-2019. Right: trends in SST anomalies from 2015-2019. Black circles mark cells where the anomaly was >1 s.d. above the long-term mean (left, middle) or where the trend was significant (right). Black x's mark cells where the anomaly was the highest in the time series.

Depth profiles of temperatures off Newport, Oregon and San Diego show that the warming in 2019 was mostly confined to surface waters, and that seasonal patterns differed in the north and south. At NH25 off Newport, temperature anomalies through spring 2019 were small and variable in sign, but then rose to strongly positive (>1°C) anomalies during the late summer and early fall 2019, constrained to the upper 25 m of the water column (Figure 3.1.3, top). The subsurface water off Newport remained warmer than normal into the fall. CalCOFI station 93.30 off San Diego had large positive anomalies (>1°C) in winter and spring 2019 in the upper 50 m depth layer (Figure 3.1.3, bottom). By summer 2019, most of the water column had cooled to negative anomalies, though the upper 10 m still had large positive anomalies. Figure 3.1.3 also shows how persistent the warm anomalies at depth have been since 2014 at both stations, and the relative dominance of warm water at depth off San Diego since at least 1997.

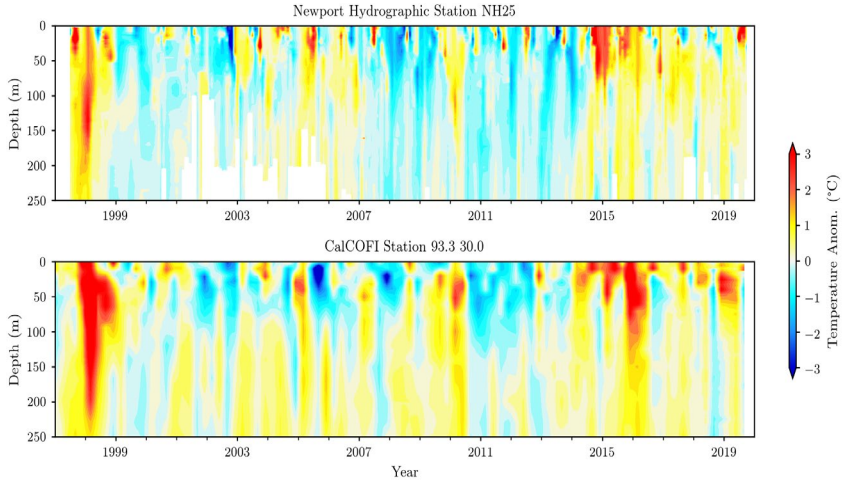

Figure 3.1.3 Time-depth temperature anomalies for stations NH25 (July 1997 to October 2019) and CalCOFI 93.30 (January 1997 to October 2019). For location of stations see Fig. 2.1a.

3.2 Regional Climate and Ocean Indicators

Upwelling in the CCE occurs when equatorward winds move deep, cold, nutrient-rich water to the surface layer, fueling the high seasonal production in the CCE food web. On average, upwelling peaks in late April near San Diego, mid June off Point Arena in Central California, and late July off Newport, Oregon. Nutrient delivery by upwelling also varies in space: vertical flux of nitrate at Point Arena is an order of magnitude greater than at Newport or San Diego. Jacox et al. (2018) developed models to estimate the vertical transport of water (Cumulative Upwelling Transport Index; CUTI) and nitrate flux (Biologically Effective Upwelling Transport Index; BEUTI) for the CCE.

In 2019, upwelling volume (CUTI) at 45°N during winter and spring was slightly above the long-term mean, while at 33°N and 39°N CUTI values varied around or below the mean (Figure 3.2.1, left). Nitrate fluxes (BEUTI) in winter and spring 2019 were mostly average coastwide, except for some below-average periods in winter and spring at 39°N (Figure 3.2.1, right). In summer, CUTI was generally average or below-average in the north, but average to above-average in the central and southern regions. However, nitrate fluxes in the summer were average to above-average in all regions (Figure 3.2.1, right).

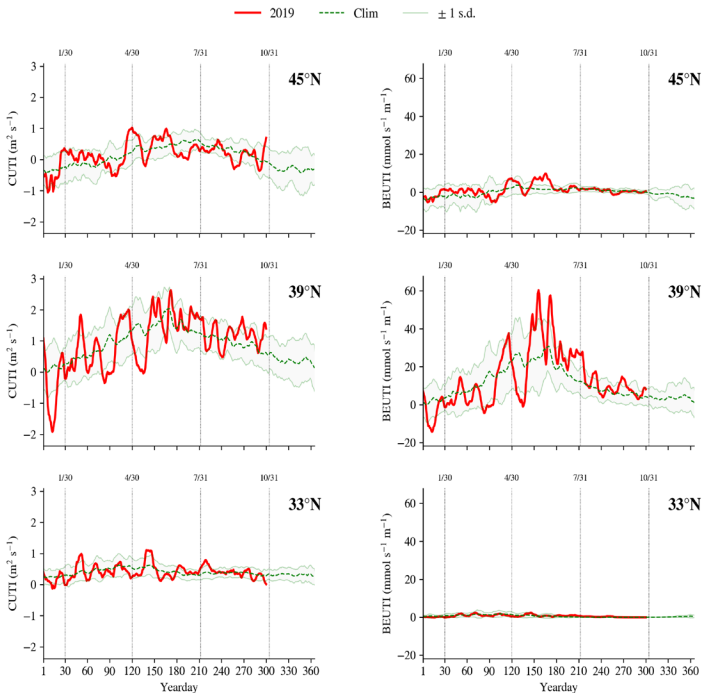

Figure 3.2.1 Daily 2019 values of Coastal Upwelling Transport Index (CUTI; left) and Biologically Effective Upwelling Transport Index (BEUTI; right) from Jan. 1–Sept. 1, relative to the 1988-2019 climatology average (green dashed line) ±1 s.d. (shaded area), at latitudes 33°, 39°, and 45°N. Vertical lines mark the end of January, April, July and October.

3.3 Hypoxia and Ocean Acidification

Dissolved oxygen (DO) is dependent on processes such as currents, upwelling, air-sea exchange, primary production, and respiration. Low DO can compress habitat and cause stress or die-offs for sensitive species. Waters with DO levels <1.4 ml/L (2 mg/L) are considered hypoxic.

Near-bottom DO measurements at station NH05 (5 nautical miles off of Newport, Oregon) fell below the hypoxia threshold in August 2019 but rebounded by September (Figure 3.3.1, top). This was a similar intensity of hypoxia to 2018, although the 2018

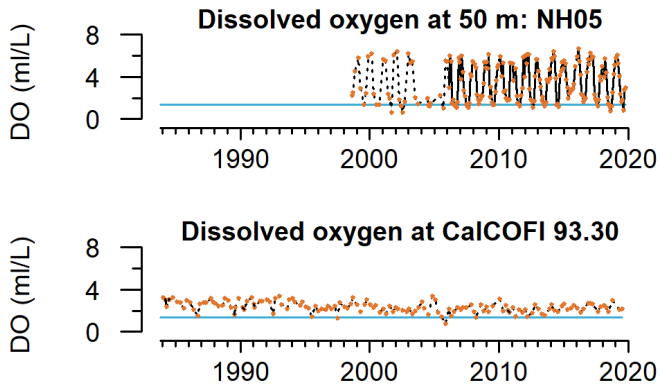

Figure 3.3.1 Near-bottom dissolved oxygen off Newport, OR (Station NH05) and San Diego, CA (CalCOFI 93.30) through 2019. The blue line is the hypoxic threshold of 1.4 ml dissolved oxygen per liter. Dotted black line indicates missing data. Lines, colors, and symbols are as in Fig. 1.

hypoxic period off Newport lasted from June to September. Off San Diego at CalCOFI station 93.30, near-bottom DO was above the hypoxia threshold in spring and summer cruises (Figure 3.3.1, bottom), and DO values throughout the CalCOFI region were close to average (Appendix D.3). DO maps and time series for additional stations off Oregon and Southern California are in Appendix D.3.

Ocean acidification, caused by increased levels of atmospheric CO_2, lowers pH and carbonate in seawater and can be stressful to shell-forming organisms and other species (Chan et al. 2008, Feely et al. 2008, Bednaršek et al. 2020). Off Newport Oregon, levels of aragonite (a form of calcium carbonate) near the seafloor in 2019 were similar to 2018, and lower than in the anomalous years of 2014–2015. More of the water column was above the saturation threshold in 2019 than in 2017 or 2018. For space considerations, we present ocean acidification data in Appendix D.3.

3.4 Harmful Algal Blooms

Blooms of the diatom *Pseudo-nitzschia* can increase concentrations of the toxin domoic acid in coastal waters, creating harmful algal blooms (HABs). Domoic acid can enter the food web via filter feeders like razor clams. Because domoic acid can cause amnesic shellfish poisoning in humans, fisheries for razor clams, Dungeness crab and other species are closed when concentrations exceed regulatory thresholds for human consumption. Extremely toxic HABs of *Pseudo-nitzschia* may coincide with warm events in the CCE, such as the 2014-2016 marine heatwave (Appendix E).

In 2019, elevated levels of domoic acid occurred in razor clams and Dungeness crabs in parts of Oregon and California, while low levels of domoic acid were detected in Washington razor clams and Dungeness crabs (Figure 3.4.1). Domoic acid levels extended years-long closures of razor clam fisheries in southern Oregon and northern California, and closed all of Oregon razor clam fisheries in December 2019 (Appendix E). Domoic acid contributed to delayed openings of Dungeness crab fisheries in 2019 in southern Oregon and in parts of central California, and northern California rock crab fisheries have been closed in some areas since 2015 (Appendix E). In contrast, there were no domoic acid-related razor clam or Dungeness crab closures in Washington in 2019 (Figure 3.4.1), or in Southern California fisheries for rock crab and spiny lobster (Appendix E).

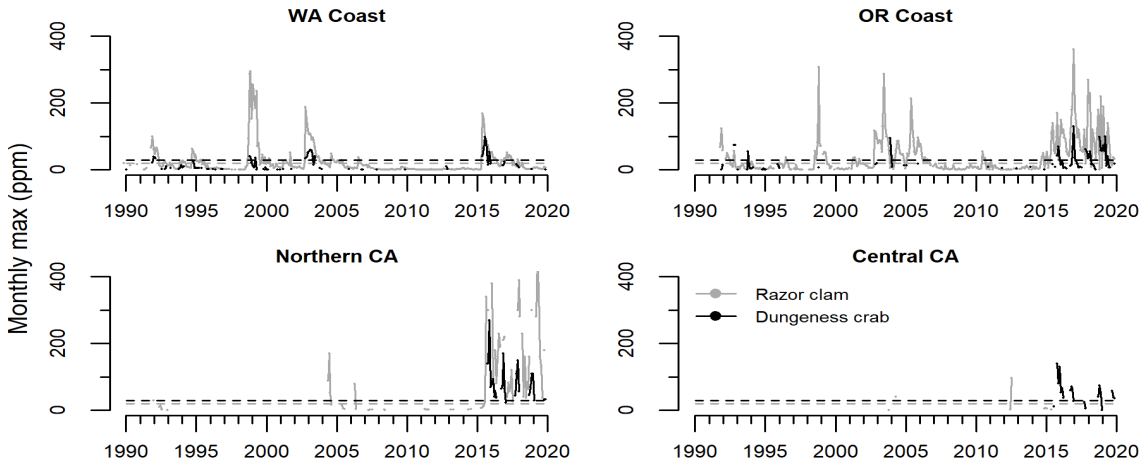

Figure 3.4.1 Monthly maximum domoic acid concentration (ppm) in razor clams (gray) and Dungeness crab viscera (black) through 2019 for WA, OR, northern CA (Del Norte to Humboldt counties), and central CA (Sonoma to San Luis Obispo counties). Horizontal dashed lines are the management thresholds of 20 ppm (clams in gray) and 30 ppm (crabs in black).

3.5 Hydrologic Indicators

Freshwater conditions are critical for salmon populations and West Coast estuaries. Hydrologic

indicators presented here are snowpack, streamflow and stream temperature, summarized by ecoregion (Figure 2.1b) or by salmon evolutionarily significant units (ESUs, Waples 1995). Snow-water equivalent (SWE) is the water content in snowpack, which provides cool freshwater in the spring, summer and fall months. Maximum streamflow in winter and spring is important for habitat formation and removal of parasites, but extreme discharge relative to historic averages can scour salmon nests (redds). Below-average minimum streamflow in summer and fall can restrict habitat for juvenile salmon and migrating adults. High summer temperatures can impair physiology and cause mortality.

In 2019, SWE in the two northern regions (Salish Sea/WA Coast and Columbia River Glaciated) declined relative to 2018 (Figure 3.5.1), and drought conditions were declared in parts of Washington. In contrast, SWE was above average in 2019 for Sacramento/San Joaquin and coastal California and Oregon. All regions have increasing trends, due to rebounds since the extreme lows of 2015 (Figure 3.5.1).

As of February 1st, SWE in 2020 is mixed. Most stations are average to below average, although portions of Washington, eastern Oregon, Idaho, and parts of interior northern California are above average (Appendix F). Because SWE values typically do not peak until early spring, the official measure of SWE will be on April 1, 2020.

Minimum streamflows were consistent with SWE, with generally increasing trends since lows in 2015, particularly in central and southern ecoregions (Appendix F). Maximum flows have experienced increasing 5-year trends in the Southern California Bight, Sacramento/San Joaquin, and Unglaciated Columbia Basin, but decreasing trends in the Salish Sea/WA Coast ecoregion (Appendix F). Maximum August stream temperatures have not exhibited strong trends except for the Salish Sea/WA Coast ecoregion, where they have increased over the past 5 years (Appendix F).

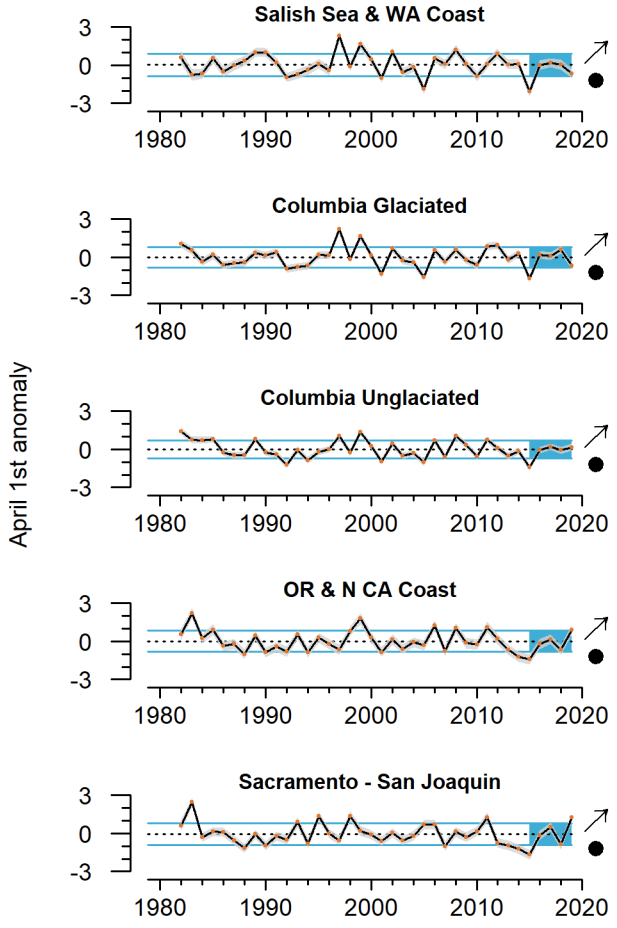

Figure 3.5.1 Anomalies of April 1st snow-water equivalent (SWE) in five freshwater ecoregions of the CCE through 2019. Ecoregions are mapped in Fig. 2.1. Error envelopes represent the 2.5% and 97.5% upper and lower credible intervals. Symbols to the right follow those in Fig. 1, but were evaluated based on whether the credible interval overlapped zero (slope of the 5-year trend) or the long-term mean (5-year mean).

We also summarized streamflows at the finer scale of individual Chinook salmon ESUs. These results are presented in quad plots, showing flow anomalies and 95% credible intervals to indicate ESUs with significant short-term trends or recent averages that differ from long-term means. With the exception of Salish Sea, northern coastal sites and the Lower Columbia, maximum flows have generally increased since 2015 (Figure 3.5.2, left; Appendix F). Because high rates of winter flow are generally beneficial for juvenile salmon in inland regions but detrimental to northern coastal populations, these trends suggest improving flow conditions during egg incubation across much of

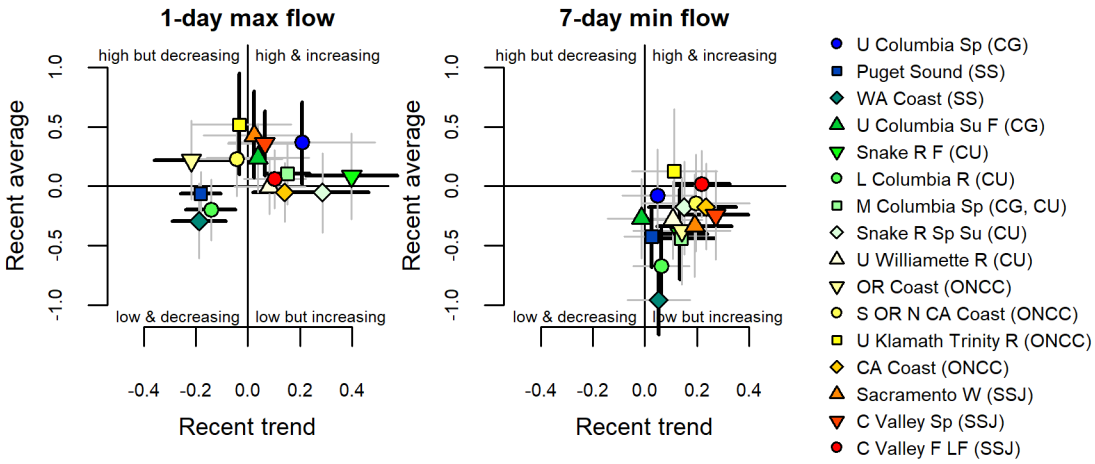

Figure 3.5.2 Recent (5-year) trend and average of anomalies in maximum and minimum flow in 16 freshwater Chinook salmon ESUs in the CCE through 2019. Symbols of ESUs are color-coded from north (blue) to south (orange). Error bars represent the 2.5% and 97.5% upper and lower credible intervals. Grey error bars overlap zero. Heavy black error bars differed from zero.

the CCE. Minimum flows were generally below average but increasing since the very low flows of 2015, with the strongest short-term increases in southern and inland ESUs (Figure 3.5.2, right; Appendix F). ESUs in the northwest tended to be the furthest below average, including three Columbia Basin ESUs, Puget Sound, and the Washington Coast.

4 Focal Components of Ecological Integrity

The CCIEA team examines many indicators related to the abundance and condition of key species and the dynamics of ecological interactions and community structure. Many CCE species and processes respond very quickly to changes in ocean and climate drivers, while other responses may not manifest for many years. These dynamics are challenging to predict. In 2019, ecological indicators implied average to above-average productivity in the northern and southern portions of the CCE, but average to below-average conditions in the central CCE. The marine heatwave that developed in mid 2019 may have affected portions of the system later in the year, but we have relatively little data to demonstrate impacts at this time.

4.1 Copepod Biomass Anomalies and Krill Size

Copepod biomass anomalies represent variation for northern copepods, which are cold-water species rich in wax esters and fatty acids, and southern copepods, which are smaller and have lower fat content and nutritional quality. In summer, northern copepods usually dominate the zooplankton community along the Newport Line (Figure 2.1a,c), while southern copepods dominate in winter. Positive values of northern copepods correlate with stronger returns of Chinook salmon to Bonneville Dam and coho salmon to coastal Oregon (Peterson et al. 2014). El Niño events and positive PDO regimes can increase southern copepods (Keister et al. 2011, Fisher et al. 2015).

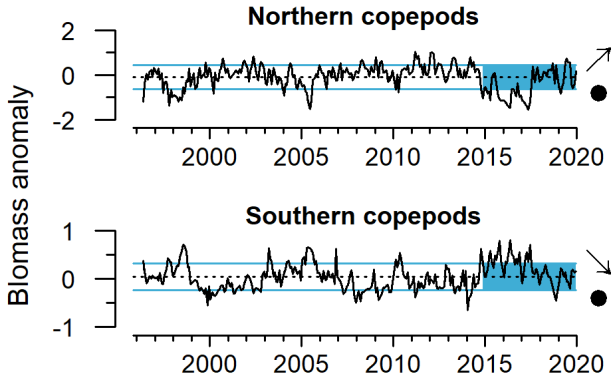

Figure 4.1.1 Monthly northern and southern copepod biomass anomalies from station NH05, 1996-2019. Lines, colors and symbols are as in Fig. 1.

In 2019, northern copepods continued an overall increasing trend since the extreme lows during the 2014-2016 heatwave. They were ~1 s.d. above the mean in spring-summer 2019, but declined by September (Figure 4.1.1, top). The spring-summer anomaly was among the highest of the time series, despite weak El Niño conditions. However, the northern copepods appeared relatively late and declined relatively early, resulting in a short duration of the northern copepod community. Southern copepods were near-average for most of 2019, continuing a decline since the heatwave (Figure 4.1.1, bottom). These values suggest average to above-average feeding conditions for pelagic fishes off central Oregon in 2019, with the best copepod ratios in the summer.

Krill are among the most important prey for fishes, mammals and seabirds in the CCE. The key species *Euphausia pacifica* has been sampled multiple times per season off of Trinidad Head (Figure 2.1a,c) since late 2007. Mean length of adult *E. pacifica* is an indicator of krill as a resource for predators. *E. pacifica* length cycles from short individuals in winter that grow into longer individuals by summer. *E. pacifica* lengths were very low during the first half of 2019 (Figure 4.1.2), coincident with El Niño conditions during the 2018-2019 winter. This marked a decrease relative to 2018, when lengths were generally above average and consistent with conditions associated with typical seasonal upwelling. Krill lengths had been gradually increasing after poor growth at the onset of the 2014-2016 heatwave. The 2019 results suggest that krill production in the northern CCE continues to be impacted by ocean forcing such as recent warming and the weak NPGO.

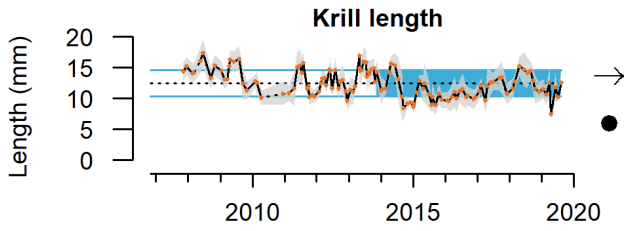

Figure 4.1.2 Mean krill carapace length (mm) off of Trinidad Head, CA from 2007-2019. Grey envelope indicates +/- 1.0 s.d. Lines, colors, and symbols are as in Fig. 1.

4.2 Regional Forage Availability

The CCE forage community is a diverse portfolio of species and life history stages, varying in behavior, energy content, and availability to predators. The species summarized below represent a substantial portion of the available forage in the CCE. *We consider these regional indices of relative forage availability and variability, not indices of stock biomass of coastal pelagic species (CPS).*

The regional surveys that produce CCE forage data use different methods (e.g., gear, timing, survey design), which makes regional comparisons difficult. We use cluster analysis (Thompson et al. 2019a) to identify and compare regional shifts in forage composition. Co-occuring species cluster on the y-axis, and yearly abundance estimates are indicated by color (red = abundant, blue = rare); temporal shifts in forage composition are marked by vertical lines. Related time series are in Appendix G.

Northern CCE: The northern CCE survey off Washington and Oregon (Figure 2.1c) targets juvenile salmon in surface waters, but also samples surface-oriented fishes, squid and jellies. This forage assembly has had several recent shifts since the onset of the 2014-2016 marine heatwave (Figure 4.2.1). Since the most recent shift prior to 2018, market squid,

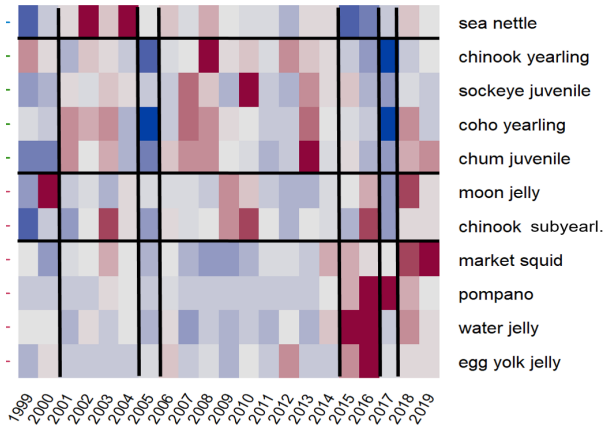

Figure 4.2.1 Cluster analysis of key forage species in the northern CCE through 2019. Horizontal lines indicate clusters of typically co-occurring species. Vertical lines indicate temporal shifts in community structure. Colors indicate relative abundance (red = abundant, blue = rare).

juvenile coho and chum salmon, and several jellies have been abundant. Some species that were abundant during the previous marine heatwave (e.g., pompano, water jelly, egg yolk jelly) were less abundant in 2018-2019. Related surveys off Oregon and southern Washington indicated that krill abundance was very low in 2019, and has been for several years (Appendix G.1).

Central CCE: Data presented here are from the "Core area" of a survey (Figure 2.1c) that targets pelagic juvenile rockfishes, but also samples other pelagic species. Since 2018, this forage base has been dominated by anchovy, with adult anchovy more abundant in 2019 than any previous year surveyed (Figure 4.2.2; Appendix G.2). Adult sardine in 2019 were the most abundant in a decade, though not as abundant as in the 2000s. Market squid remained abundant, as did several myctophids. However, juvenile rockfish, hake, and flatfish, which had been abundant from 2013-2017, have declined to low abundances in the past two years. A concerning sign was that krill catches were the lowest of the time series (Appendix G.2).

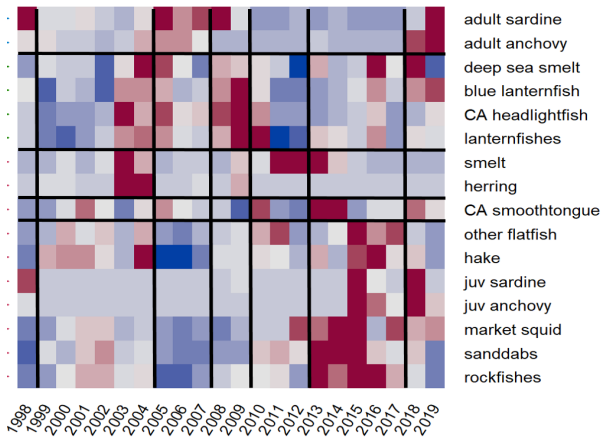

Figure 4.2.2 Cluster analysis of key forage species in the central CCE through 2019. Lines and colors are as in Figure 4.2.1.

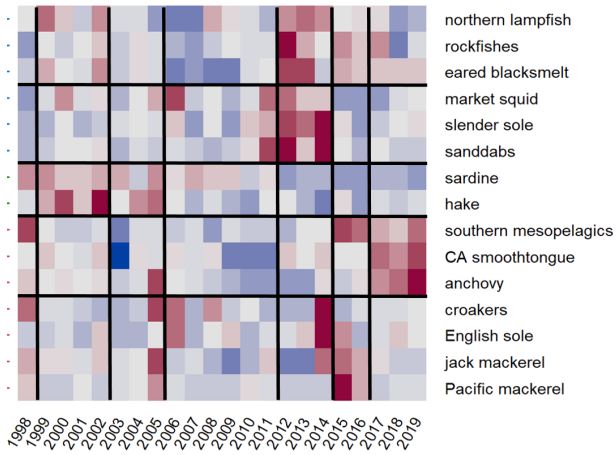

Figure 4.2.3 Cluster analysis of key forage species in the southern CCE through 2019. Lines and colors are as in Figure 4.2.1.

Southern CCE: Forage data for the Southern CCE (Figure 2.1c) come from CalCOFI larval fish surveys. The larval biomass of forage species is assumed to correlate with regional abundance of adult forage species. The southern forage assemblage has experienced 6 substantial shifts from 1998-2019. Since 2017, the community has been characterized by abundant larval anchovy and warm-water mesopelagic fishes (Figure 4.2.3; Appendix G.3). Larval anchovy abundance was the greatest it has been in the history of the CalCOFI time series. Larvae of other forage species were near long-term averages (e.g., rockfish, English sole, market squid) or below average (cool water mesopelagics, sardine, mackerels, sanddabs).

Pyrosomes, a warm-water pelagic tunicate, have been abundant in different regions of the CCE since the onset of warming in 2014. They cause fouling of fishing gear and have likely affected food web dynamics. Pyrosome distribution shifted considerably in 2019: after reaching extreme densities off of Washington and Oregon in 2017 and 2018, they were nearly absent in 2019. In contrast, pyrosome densities off of California were similar to densities from 2015-2016 (Miller et al. 2019; Appendix G.4).

4.3 SALMON

Chinook salmon escapement: For indicators of the abundance of naturally spawning Chinook salmon, we examine trends in natural spawning escapement from different populations to compare status

and coherency in production dynamics across their range. We summarize escapement trends in quad plots; time series are shown in Appendix H. Most escapement data are updated through 2018.

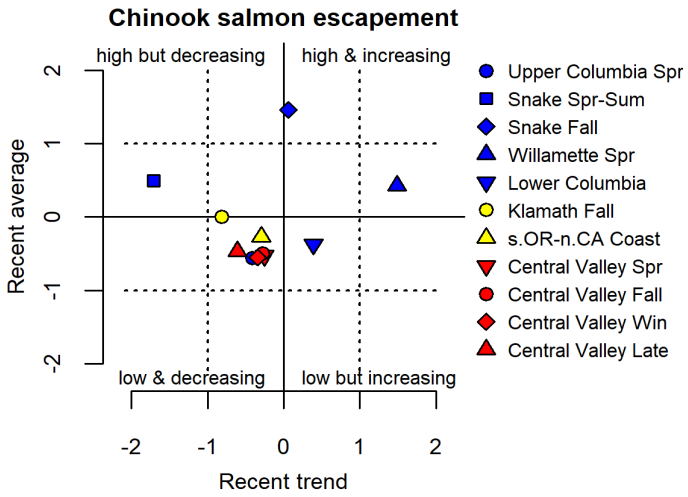

Figure 4.3.1 Recent (10-year) trend and average of Chinook salmon escapement through 2018. Recent trend indicates the escapement trend from 2008-2018. Recent average is mean natural escapement (includes hatchery strays) from 2008-2018. Lines, colors, and symbols are as in Fig. 1.

Escapements of California Chinook salmon ESUs over the last decade were within 1 s.d. of long-term means (Figure 4.3.1), though 2018 escapements were among the lowest on record in several ESUs, particularly in the Central Valley (Appendix H.1). California ESUs had neutral trends over the last decade, though some sharp declines occurred ~5 years ago (Appendix H.1). In the Northwest, most mean escapements in the past decade were within 1 s.d. of average; the exception was above-average Snake River Fall Chinook escapements, due to relatively large escapements from 2009 to 2016 (Appendix H.2). Escapement trends for Northwest stocks over the past decade were mostly neutral, but Willamette Spring Chinook had a positive trend while Snake River Spring-Summer Chinook had a negative trend.

Juvenile salmon abundance: Annual catches of juvenile coho and Chinook salmon from surveys during June in the Northern CCE (Figure 2.1c) can serve as indicators of salmon survival during their first few weeks at sea. In 2019, catches of subyearling Chinook, yearling Chinook, and yearling coho salmon were all very close to long-term averages (Figure 4.3.2). The 5-year catch trends were neutral but variable for all groups. Juvenile salmon captured off Oregon and Washington in 2019 generally appeared to be in good condition.

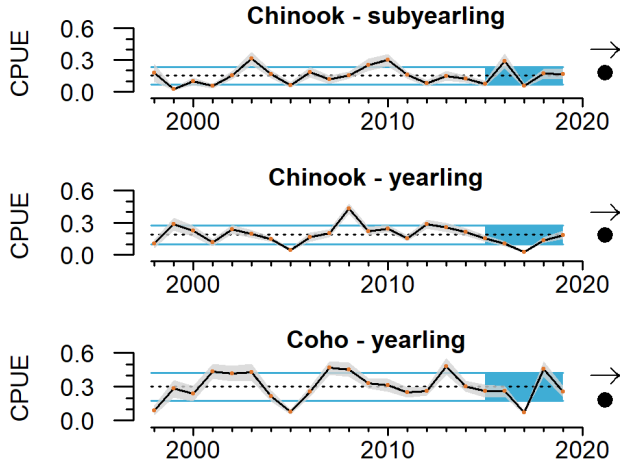

Figure 4.3.2 At sea juvenile salmon catch ($Log_{10}(no/(km + 1))$) from 1998 to 2019 for Chinook and coho salmon. Lines, colors, and symbols are as in Fig. 1.

Long-term associations between oceanographic conditions, food web structure, and salmon productivity (Burke et al. 2013, Peterson et al. 2014) support projections of returns of Chinook salmon to Bonneville Dam and smolt-to-adult survival of Oregon Coast coho salmon. The suite of indicators is depicted in the "stoplight chart" in Table 4.3.1, and includes many indicators shown elsewhere in this report (PDO, ONI, SSTa, deep temperature, copepods, juvenile salmon catch). Indicators for 2020 salmon returns reflect a range of conditions, from poor in smolt years 2016 and 2017 to more mixed conditions in smolt year 2018. Taken as a whole, these indicators are consistent with average returns of Chinook salmon to the Columbia River in 2020, relative to the past two decades. Conditions in smolt year 2019 were a mix of good, intermediate and poor conditions, consistent with average to

Table 4.3.2 "Stoplight" table of basin-scale and local-regional conditions for smolt years 2016-2019 and projected adult returns in 2020 for coho and Chinook salmon that inhabit coastal Oregon and Washington waters in their marine phase. Green/circle = "good," yellow/square = "intermediate," and red/diamond = "poor," relative to long-term time series.

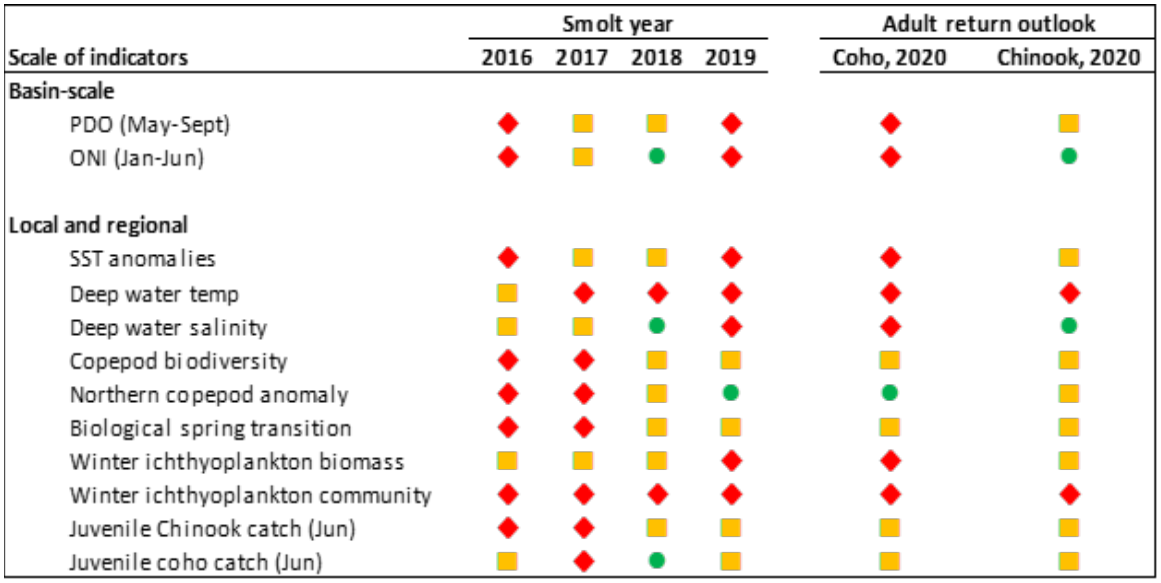

below-average returns of coho to the Oregon coast in 2020. A related quantitative model indicates a probability of modest increases in returns of Fall Chinook in the Columbia River relative to 2018 and 2019, but returns of Spring Chinook that are similar to 2017-2019 (Appendix H.3).

At the request of several Council groups, we are working to develop similar indicator-based outlooks for returns of Chinook salmon in California. As a first iteration, a recent paper by Friedman et al. (2019) found that returns of naturally produced Central Valley fall run Chinook salmon were correlated with spawning escapement of parent generations, egg incubation temperature between October and December at Red Bluff Diversion Dam (Sacramento River), median flow in the Sacramento River in the February after fry emergence, and a marine predation index based on the abundance of common murres at Southeast Farallon Island. For fall Chinook salmon cohorts returning to the Central Valley in 2020, these four indicators imply relatively low returns for age-3 Chinook salmon, the dominant age group for this system (Table 4.3.2). Age-3 fish returning in 2020

Table 4.3.1 Table of conditions for naturally produced Central Valley fall run Chinook salmon returning in 2020, from spawning years 2016-2018. Indicators reflect each cohort's parent generation escapement, egg incubation temperature, flow during juvenile stream residence, and seabird predation in the early marine phase. Heavy outline and boldfaced type indicates age-3 Chinook salmon, the dominant age class returning to the Central Valley.

Spawning Escapement (t=0)	Incubation Temperature (Oct-Dec t=0)	February Median Flow (t+1)	Seabird Marine Predation Index (t+1)	Chinook Age in Fall 2020
2016: 56,000 (low)	11.8°C (poor)	48,200 cfs (very high)	Near average	4
2017: 18,000 (very low)	**11.8°C (poor)**	**5,525 cfs (very low)**	**Near average**	**3**
2018: 72,000 (low)	11.7°C (poor)	21,700 cfs (high)	Near Average	2

were the progeny of a very low escapement year (2017), experienced poor incubation temperature in the 2017-2018 winter, and very low streamflow in early 2018, likely coupled with typical predation pressure as they went to sea later in 2018. Age-4 fish (produced in 2016) and age-2 jacks (2018) have somewhat more mixed signals thanks to better juvenile flow regimes.

4.4 Groundfish Stock Abundance

The CCIEA team regularly presents the status of groundfish biomass and fishing pressure based on the most recent stock assessments. This year's report includes updated information for 10 stocks (big and longnose skates, 3 cabezon substocks, Pacific hake, sablefish, cowcod and combined gopher/black-and-yellow rockfish), plus many catch-only projections. This leaves splitnose rockfish as the only full assessment done prior to 2010.

All assessed stock biomasses are above limit reference points (LRPs); thus, no assessed stocks were considered overfished (Figure 4.4.1, x-axis). Yelloweye rockfish is still rebuilding toward its target reference point (TRP), but cowcod is now above its TRP. Only two stocks (rougheye and greenstriped rockfish) are above the proxy for overfishing (Figure 4.4.1, y-axis). Stocks of black rockfish (CA, WA) and China rockfish (CA) were updated with recent catches, indicating that fishing rates have moved below the overfishing proxy.

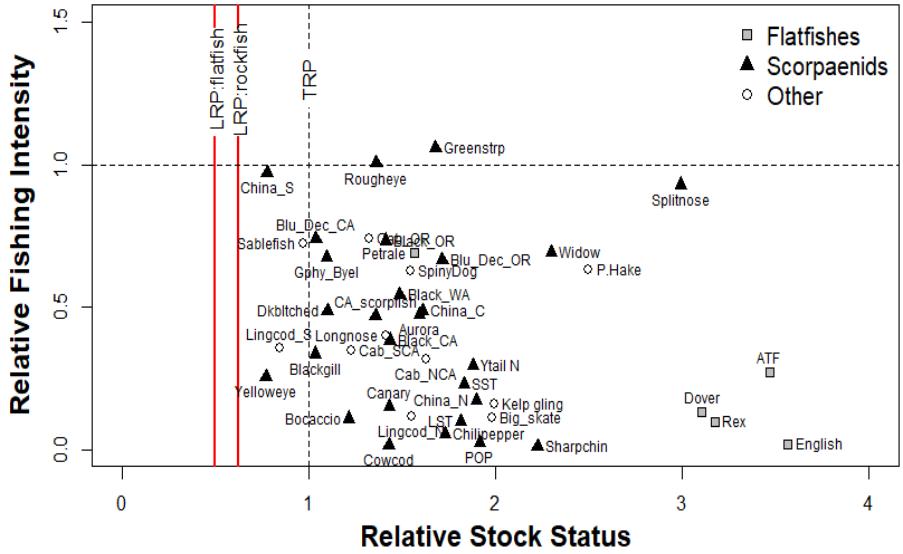

Figure 4.4.1 Stock status of groundfish. X-axis: Relative stock status is the ratio of spawning output (in millions of eggs) of the last to the first years in the assessment. Y-axis: Relative fishing intensity is based on stock-specific Spawning Potential Ratios (SPR); plotted values are (1-SPR)/(1-SPR$_{MSY}$ proxy). Horizontal line = fishing intensity rate reference. Vertical lines = biomass target reference point (dashed line) and limit reference point (solid line; left of this line indicates overfished status). Symbols indicate taxonomic group. All points are from the most recent Council-adopted stock assessments.

4.5 Highly Migratory Species

For highly migratory species (HMS), we have been presenting quad plots of recent averages and trends of biomass and recruitment from the most up-to-date stock assessments. These assessments (which range from 2015-2018) have not been updated since last year's ecosystem status report, and thus we have no new information on HMS indicators at this time. Available HMS time series (identical to those in last year's report) are in Appendix I.

4.6 Marine Mammals

Sea lion production: California sea lions are sensitive indicators of prey availability in the central and southern CCE (Melin et al. 2012): sea lion pup count at San Miguel Island relates to prey availability and nutritional status for gestating females from October to June, while pup growth at San Miguel from birth to age 7 months is related to prey availability to lactating females from June to February.

Indicators in Figure 4.6.1 are current through the 2018 pup cohort. These indicators represent the

third consecutive year of average or above average values following 2015, the worst year in the time series. In 2018, pup births were 24% above the long term average and contributed to an increasing trend in pup count over the past 5 years (Figure 4.6.1, top). Pup growth rates were slightly lower than for the 2017 cohort, but were still above the long-term average and supported a short-term increasing trend (Figure 4.6.1, bottom). These improvements coincide with a shift in the nursing female diet. Favorable ocean conditions for anchovy and sardine have resulted in the return of anchovy as the most frequently occurring prey (present in >85% of diets) in the past four years and the resurgence of sardine in the diet in 2018 (48%). Hake, market squid, and Pacific and jack mackerel also had high occurrence in 2018, resulting in a diverse diet of high quality prey for nursing females that likely contributed to the positive trends in the population indices. Preliminary data from the 2019 cohort indicate a 12% decrease in pup count from 2018, which is still above the long-term average. However, pups were in excellent condition through 3 months of age (fall 2019), likely due to the abundance of anchovies supporting nursing adult females; we will provide further updates on the 2019 cohort in our presentation at the March 2020 PFMC meeting.

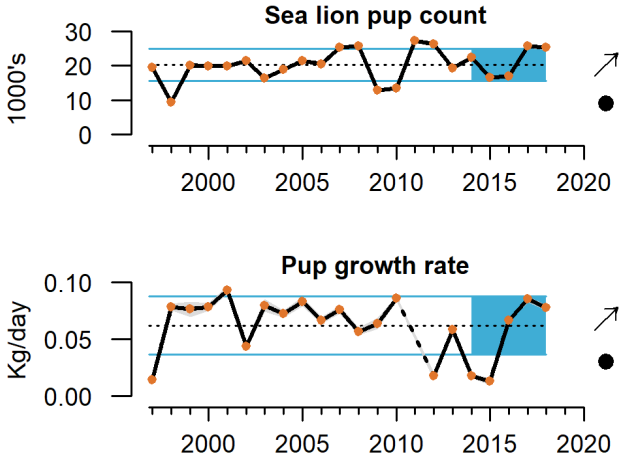

Figure 4.6.1 California sea lion pup counts, and estimated mean daily growth rate of female pups between 4-7 months on San Miguel Island for the 1997-2018 cohorts. Lines, colors, and symbols are as in Fig. 1.

Whale entanglement: The number of whale entanglements reported along the West Coast has increased considerably since 2014, particularly for humpback whales. While ~50% of entanglement reports cannot be attributed to a specific source, Dungeness crab fishing gear is the most common source that has been identified during this period. The dynamics of entanglement risk and reporting are complex, and they are affected by shifts in oceanographic conditions and prey fields, changes in whale populations, changes in distribution and timing of fishing effort, and increased public awareness leading to improved reporting.

In 2019, entanglement reports on the West Coast continued to be higher than prior to 2014, although fewer reports were received than in 2015-2018 (Figure 4.6.2). As in previous years, the majority of reports in 2019 were in California, though entanglements were known to include gear from all three West Coast states and included gear from commercial and recreational Dungeness crab, commercial rock crab, and gillnet fisheries. Significant actions were taken in 2019 to address the increased entanglement reports, including closures and delays of Dungeness crab seasons in California and late-season reductions of allowable

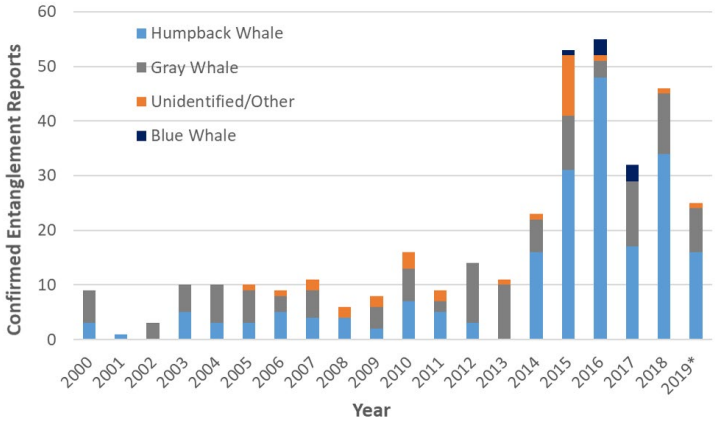

*Figure 4.6.2 Numbers of whales reported as entangled in fishing gear along the West Coast from 2000-2019. *2019 data are preliminary.*

Dungeness crab gear in Washington in response to entanglement risk, and commitments by all three West Coast states to develop conservation plans to reduce entanglements in Dungeness crab fisheries. While these actions likely contributed to reducing entanglement risks in 2019, other factors such as continued exposure of whales to gear that was lost during the season or foraging in nearshore waters on abundant anchovy likely contributed to entanglement risks in 2019.

4.7 SEABIRDS

Seabird indicators (at-sea densities, productivity, diet, and mortality) constitute a portfolio of metrics that reflect population health and condition of seabirds, as well as links to lower trophic levels and other conditions in the CCE. To highlight the status of different seabird guilds and their ecological relationships multiple focal species are monitored throughout the CCE. The species we report on here and in Appendix J represent a breadth of foraging strategies, life histories, and spatial ranges.

Indicators of seabird colony productivity suggested that feeding conditions were patchy in 2019. Fledgling production at colonies in spring 2019 was average to above-average for multiple seabird species at Yaquina Head, Oregon. In contrast, multiple seabird species experienced extremely poor fledgling production off northern and central California (Figure 4.7.1), which reflects the forage patterns in the central CCE reported in Section 4.2. Low availability of krill likely contributed to poor production of Cassin's auklets, which mainly prey on krill. Low availability of juvenile rockfish forced piscivorous birds to prey-switch (Appendix J), which may have led to mismatches; for example, while anchovy were abundant in this region (Figure 4.2.2), they may have been too large for some seabird chicks to ingest.

As further evidence of poor or mismatched prey availability in this region, large numbers of dead, emaciated adult common murres were observed on beaches in northern California during the 2019 breeding season (Appendix J.3). No other large mortality events ("wrecks") of seabirds were observed in late 2018-early 2019 (Appendix J.3). However, unusually high post-breeding mortality of rhinoceros auklets occurred in fall 2019 off Washington and Oregon, suggesting poor feeding conditions in the northern CCE later in the year. Data collection for wrecks in fall/winter 2019-2020 is not complete as of the briefing book deadline, so data from this rhinoceros auklet mortality event are not yet available.

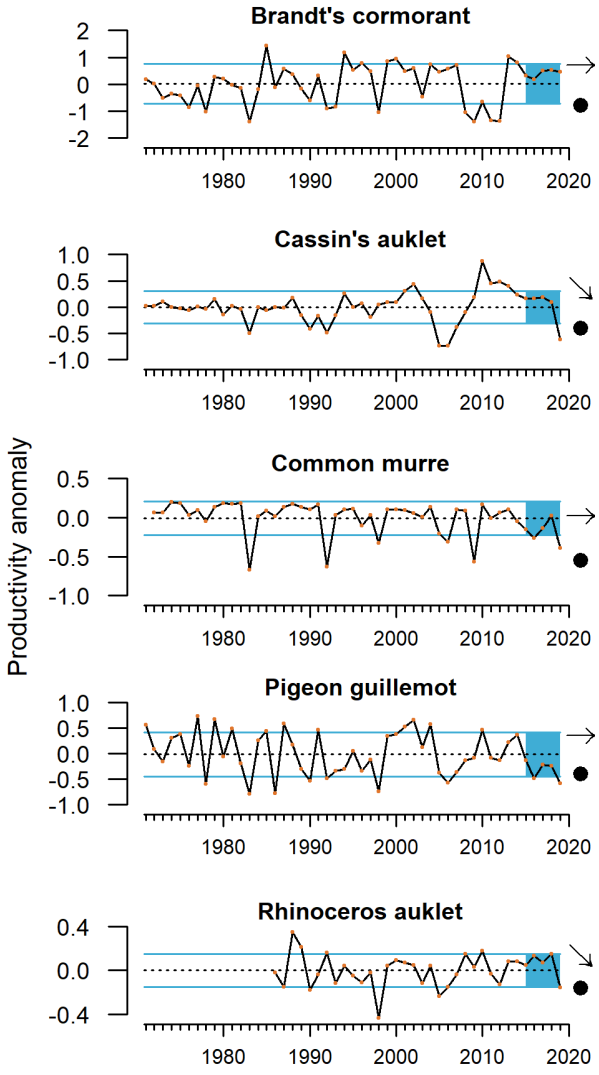

Figure 4.7.1 Standardized productivity anomalies (annual productivity, defined as the annual number of chicks fledged per pair of breeding adults, minus the long-term mean) for five seabird species breeding on Southeast Farallon Island through 2019. Lines, colors, and symbols are as in Fig. 1.

5 HUMAN ACTIVITIES

5.1 COASTWIDE LANDINGS BY MAJOR FISHERIES

Data for fishery landings are complete through 2018. Coastwide landings have been highly variable in recent years, driven by large Pacific hake landings and steep declines in CPS (Figure 5.1.1). Total landings decreased 8% from 2017 to 2018. Pacific hake landings increased to the highest levels of the time series from 2014–2018, and made up 63% of total coastwide landings in 2018. Commercial salmon landings were near the lowest of the time series over the last 5 years. Landings of groundfish (excluding hake) have been low since the mid-2000s, but showed slight increases in 2017 and 2018. Landings of CPS finfish were near the lowest of the time series, and market squid landings have decreased over the last 5 years. Shrimp landings have decreased, while landings of crab have increased over the last 5 years. Landings of HMS and Other species have been consistently within ±1 s.d. of long-term averages over the last 20+ years, although both are near lows for the time series. State-by-state landings are presented in Appendix K. We hope to have updates for 2019 landings by the time of the March 2020 presentation to the Council.

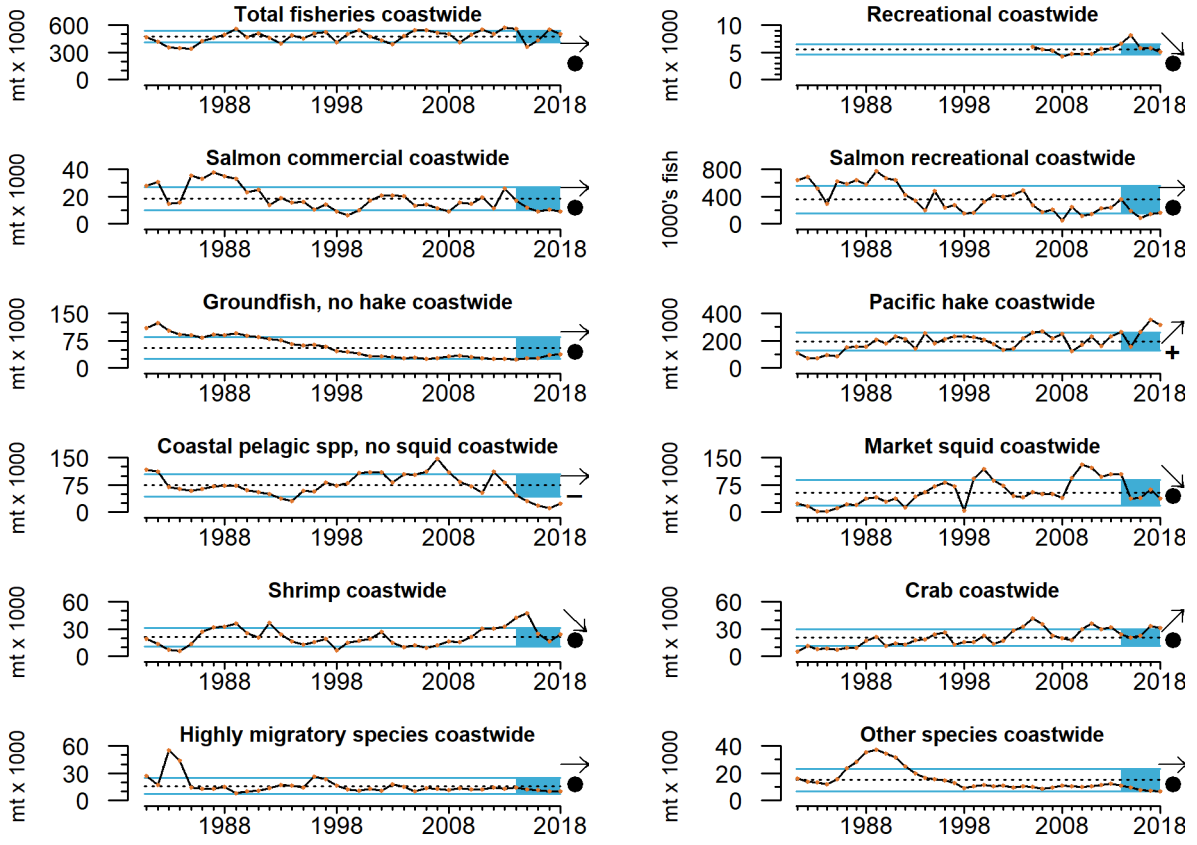

Figure 5.1.1 Annual landings of West Coast commercial (data from PacFIN) and recreational (data from RecFIN) fisheries, including total landings across all fisheries from 1981-2018. Lines, colors, and symbols are as in Fig. 1.

Recreational landings (excluding salmon and Pacific halibut) have decreased over the last 5 years (Figure 5.1.1), due to decreases in yellowfin tuna, yellowtail and lingcod landings in California and decreases in albacore and black rockfish landings in Oregon and Washington. Landings for recreationally caught Chinook and coho salmon showed no trends, but were at consistently low levels from 2014–2018. State-by-state recreational landings are in Appendix K.

Total revenue for West Coast commercial fisheries in 2018 was 7% lower than 2017, due to decreases in market squid, Pacific hake, groundfish and HMS. Revenue was within ± 1 s.d. of time series averages for most fisheries, except for crab (>1 s.d. above average) and CPS finfish (>1 s.d. below average). Shrimp revenue decreased sharply over the last 5 years, though it did increase in 2018 over 2017. Coastwide and state-by-state revenue data are presented in Appendix K.2.

5.2 Gear Contact with Seafloor

Benthic species, habitats and communities can be disturbed by natural processes and human activities (e.g., fishing, mining, dredging). The impacts of disturbance likely differ by seafloor type, with hard, mixed and biogenic habitats needing longer to recover than soft sediment. To illustrate spatial variation in bottom trawling activity, we estimated total distance trawled on a 2x2-km grid from 2002-2018. For each grid cell, we mapped the 2018 total distance trawled, the 2018 anomaly from the long-term mean and the most recent 5-year trend.

Off Washington, distance trawled in 2018 was above average and increasing in central waters (Figure 5.2.1 center and right, red cells), while northern and southern cells mostly experienced average or below-average bottom contact; trawl contact was decreasing in southern, nearshore waters (Figure 5.2.1 right, blue cells). Off Oregon, above average bottom contact in 2018 and increasing trends over the last 5 years were observed in several patches, the largest of which were off Central Oregon. Below-average anomalies in 2018 and decreasing trends were most concentrated off southern Oregon. In California, the most notable patches of above average bottom contact in 2018 and increased trawling over the last 5 years were just north of Cape Mendocino, while cells near the California-Oregon border and just north of San Francisco Bay experienced below-average bottom contact in 2018. Further information on methods and coastwide bottom trawl contact trends is available in Appendix L.

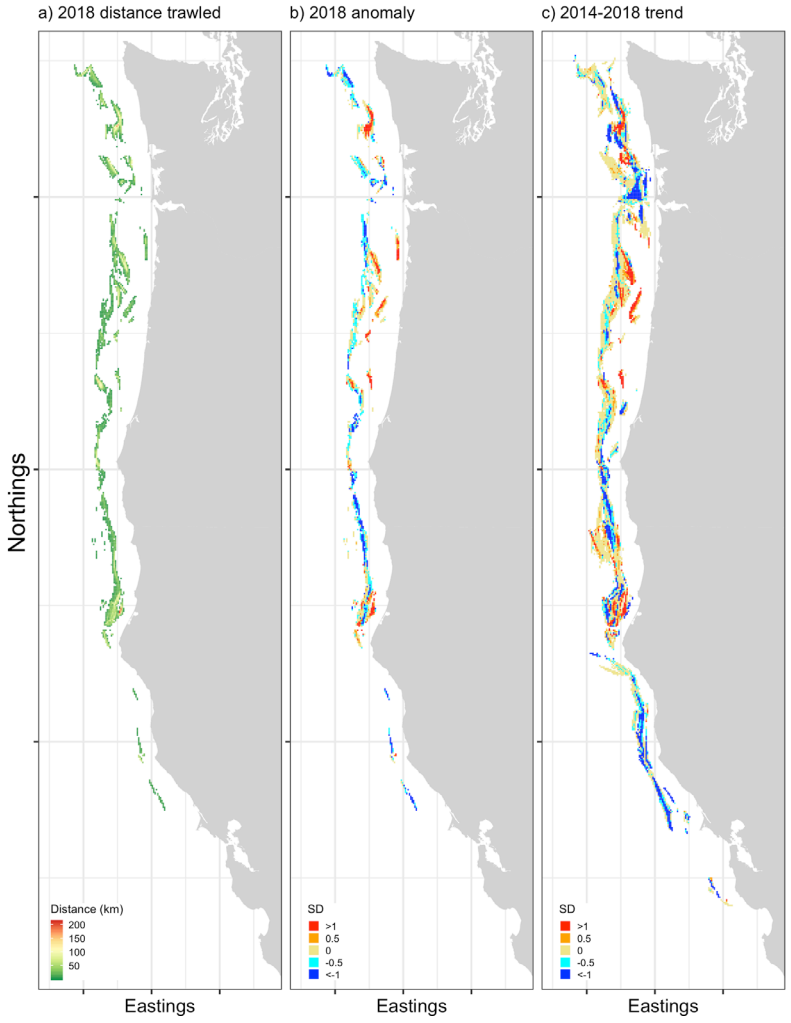

Figure 5.2.1 Analysis of distances trawled using bottom trawl gear in 2x2 km grid cells from 2002–2018. Left: Total distances trawled in 2018. Middle: Anomalies in 2018 relative to the long-term mean. Right: Normalized trend values for the most recent five-year period (2014–2018). Grid cell values >1 (red) or <-1 (blue) represent a cell in which the anomaly or 5-year trend was at least 1 s.d. away from the long-term mean of that cell.

6 HUMAN WELLBEING

6.1 SOCIAL VULNERABILITY

Coastal community vulnerability indices are generalized socioeconomic vulnerability metrics for communities. The Community Social Vulnerability Index (CSVI) is derived from social vulnerability data (demographics, personal disruption, poverty, housing, labor force structure, etc.; Jepson and Colburn 2013). We monitor CSVI in communities that are highly reliant upon fishing.

The commercial fishing reliance index reflects *per capita* engagement in commercial fishing (e.g., landings, revenues, permits, and processing) in 1140 West Coast communities. Figure 6.1.1 plots CSVI updated through 2017 against commercial fishery reliance for communities that are most reliant on commercial fishing along the West Coast. Communities above and to the right of the dashed lines are those with above average levels of CSVI (horizontal dashed line) and commercial fishing reliance (vertical dashed line). For example, Westport and Port Orford have fishing reliance (14.3 and 2.1 s.d. above average, respectively) and high CSVI (3.4 and 6.7 s.d. above average) compared to other coastal fishing communities. Coastal fishing communities that are outliers in both indices may be especially socially vulnerable to downturns in commercial fishing. Additional findings on these relationships are in Appendix M.

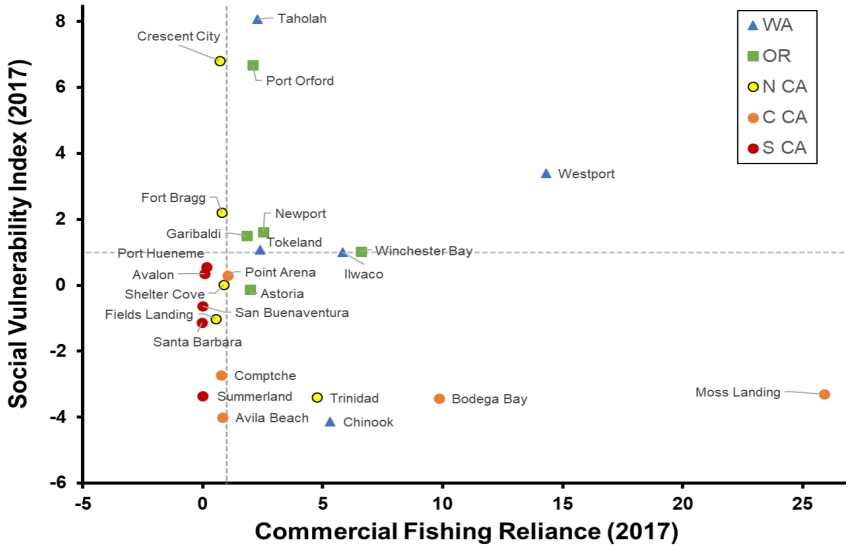

Figure 6.1.1 Commercial fishing reliance and social vulnerability scores as of 2017, plotted for twenty-five communities from each of the 5 regions of the California Current: WA, OR, Northern, Central, and Southern California. The top five highest scoring communities for fishing reliance were selected from each region.

In last year's report, we also compared CSVI with recreational fishing reliance, which reflects *per capita* recreational fishing engagement (e.g., number of boat launches, number of charter boat and fishing guide license holders, number of charter boat trips, bait and tackle shops, etc.). Unfortunately, the data used in last year's report were available only through 2016 and have not been updated since; we will have to identify alternate indices of recreational engagement for future reports.

6.2 DIVERSIFICATION OF FISHERY REVENUES

According to the Effective Shannon Index (ESI) that we use to measure diversification of revenues across different fisheries (see Appendix N), the fleet of 28,000 vessels that fished the West Coast and Alaska in 2018 was essentially unchanged from 2017, but was less diverse on average than at any time in the prior 37 years (Figure 6.2.1a). Diversification rates for most categories of vessels fishing on the West Coast have been trending down for several years, but there was little change over the last year for most vessels (Figure 6.2.1b-d). The California fleet had a slight increase in diversification in recent years while diversification of the Washington and Oregon fleets continued to decline. The long-term declines are due both to entry and exit of vessels and changes for individual vessels. Less

diversified vessels have been more likely to exit; vessels that remain in the fishery have become less diversified, at least since the mid-1990s; and newer entrants have generally been less diversified than earlier entrants. Within the average trends are wide ranges of diversification levels and strategies, and some vessels remain highly diversified. Additional port-level results are presented in Appendix N.

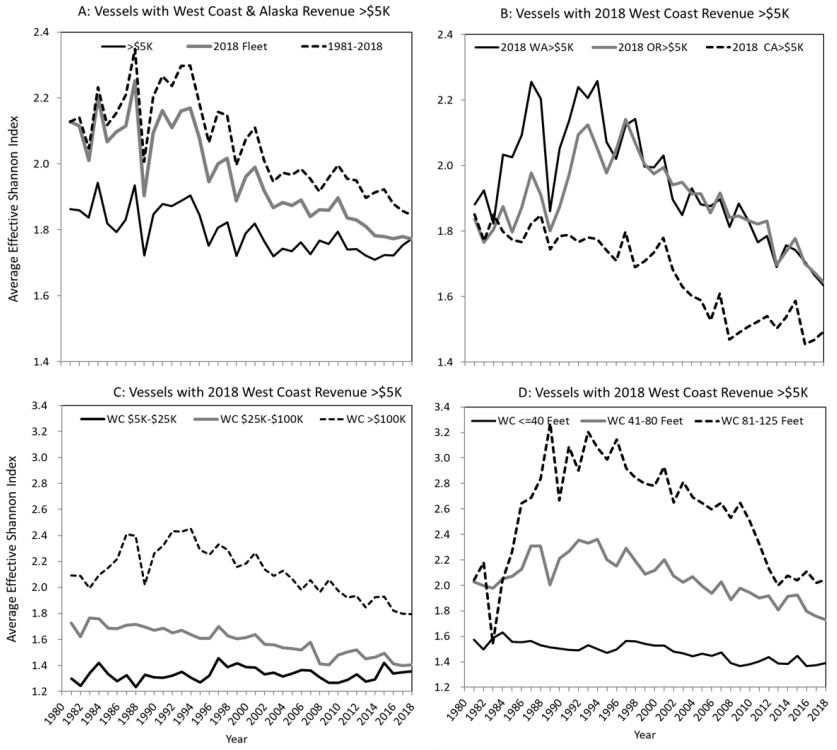

Figure 6.2.1 Average diversification for US West Coast and Alaskan fishing vessels with >$5K in average revenues (top left) and for vessels in the 2018 West Coast Fleet with >$5K in average revenues, grouped by state (top right), average gross revenue classes (bottom left) and vessel length classes (bottom right).

6.3 Revenue Consolidation

At the request of Council advisory bodies, we are working to develop indicators relevant to National Standard 8 (NS-8) of the Magnuson-Stevens Act. NS-8 states that fisheries management measures should "provide for the sustained participation of [fishing] communities" and "minimize adverse economic impacts on such communities." With guidance from economists in the NOAA IEA network, we chose ex-vessel revenue as a potential indicator of progress toward NS-8.

We plotted port-specific commercial revenue as a proportion of total West Coast commercial revenue over time to see if trends existed. Figure 6.3.1 shows the proportion of total revenue from all commercial fishery landings at the top 16 ports (by revenue) from 1982-2018. While many ports have received fairly stable proportions of total revenue over the long term, some have showed clear increases since the early 1980s (Westport, Newport, Astoria) while others have decreased (Bellingham, San Pedro, Terminal Island). This may indicate some consolidation of total commercial revenue. All ports have experienced interannual variability, of varying magnitude. FMP-specific plots are available in Appendix O.

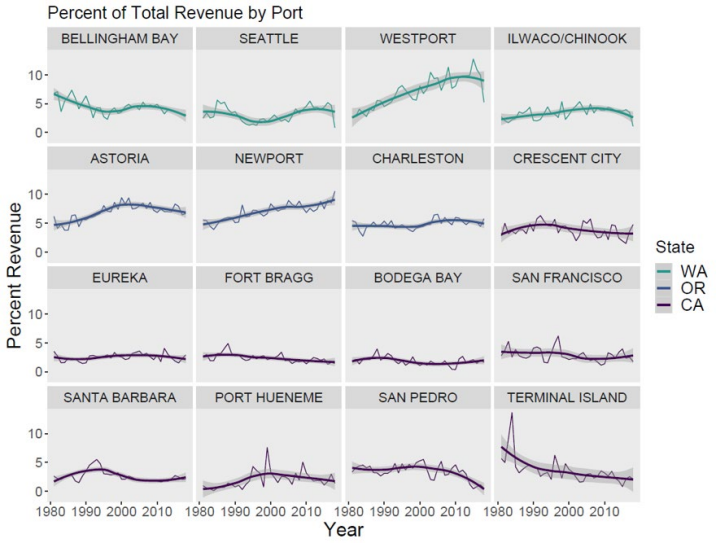

Figure 6.3.1 Port-specific percentages of total commercial fishing revenue, 1982-2018, for the top 16 ports by revenue during this period. Data are based on port-specific revenue share relative to coastwide revenue in a given year. Heavy line is LOESS model fit with 95% confidence interval.

We stress that this analysis is preliminary (see Appendix O), and presented for the purpose of initiating discussion on how to proceed with development of this indicator. We have not attempted to interpret findings with respect to NS-8, or to link changes to specific causes. We will work with the Council and advisory bodies to develop recommendations for further analyses.

7 SYNTHESIS

7.1 SUMMARY OF RECENT CONDITIONS

The CCE was strongly and negatively affected in 2014-2016 by a marine heatwave (the "Blob"), with impacts such as poor productivity, a major HAB event, shifts in species distributions, and lost fishing opportunities. A positive sign was high production of juvenile groundfish, supporting ongoing recovery of many groundfish stocks. In 2017-2018, the system exhibited some recovery from the marine heatwave: physical conditions were largely (but not entirely) similar to long-term averages, and many species showed signs of increased productivity, particularly anchovy. Yet, the system also showed lingering effects from the heatwave, including subsurface heat, high concentrations of pyrosomes, and whale entanglements in fishing gear. Other concerning signs included persistently low NPGO, widespread hypoxia, episodes of north Pacific warming, and loss of fishery diversification.

In 2019, environmental conditions for the CCE were largely consistent with poorer production, including a weak El Niño event in the first half of the year, persistence of the weak NPGO, and a large, surface-oriented marine heatwave in the second half of the year (see Section 7.2). Ecological responses that could possibly be connected to these poor conditions were mostly in northern and central California waters, and included poor production of krill, declines in other forage such as juvenile rockfishes, increases in pyrosomes, and poor production and high mortality at seabird colonies in central and northern California. Ecological indicators off Washington and Oregon (e.g., copepod community composition, juvenile salmon catches, seabird productivity, disappearance of pyrosomes) and Southern California (e.g., anchovy abundance, sea lion pup production) were more favorable, although there is some evidence that the productive season in the northern CCE was truncated in late summer.

7.2 THE 2019 MARINE HEATWAVE: TIMELINE AND "HABITAT COMPRESSION"

We close this year's main report with an assessment of the northeast Pacific marine heatwave that occurred in 2019. We reserved this assessment for the end of the report because the 2019 heatwave occurred later in the year, after many surveys had already been completed. Thus, it is difficult to conclude what ecological and socioeconomic impacts it may have had on the CCE, and we hoped to avoid the perception of direct attribution. However, due to the magnitude of this event, it deserves mention, particularly given the recent history of marine heatwaves in the CCE.

As described in Section 3.1.1, high SST anomalies over large portions of the northeast Pacific in summer and fall of 2019 marked the appearance of a large marine heatwave, similar in many respects to the Blob of 2013-2016. The 2019 event began offshore in late May (Figure 7.2.1, left), and by July 13th the feature intersected coastal Washington (Figure 7.2.1). The feature peaked in size and intensity in August and September 2019, when it reached an area >8 x 10^6 km^2 and an average intensity of >4°C above normal, which rivaled the Blob in size and intensity (Appendix D.2). At that time, the 2019 feature intersected the coast for all of Washington, Oregon and northern California (Figure 7.2.1). After that point, the feature receded from the coast and weakened, thus reducing its potential impacts on the coastal CCE. This continued until by mid January 2020, the feature no longer met the criteria for being a marine heatwave, although SST was still warmer than normal for a large offshore region of the northeast Pacific (Figure 7.2.1, right). Compared to the 2013-2016 event, the 2019 marine heatwave did not penetrate as deeply into the water column. However, there remains a large amount of stored heat in the north Pacific water column following the heatwaves of 2013-2016,

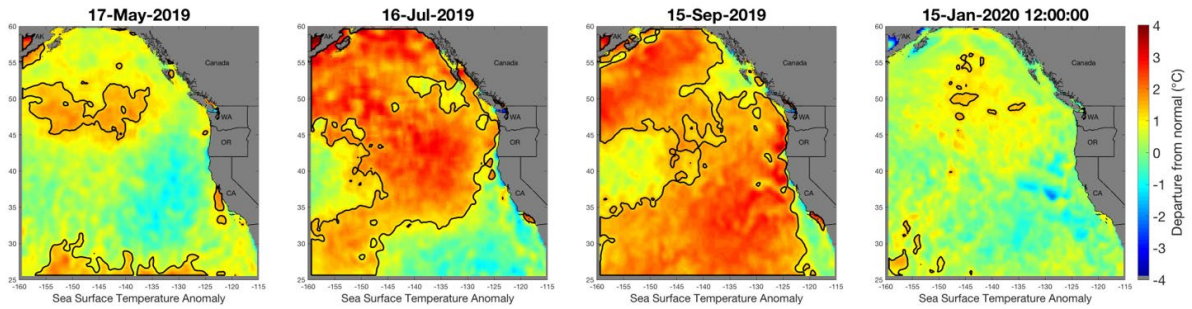

Figure 7.2.2 Standardized SSTa across the Pacific Northeast for May, July, and September 2019, and January 2020. Dark contours denote regions that meet the criteria of a marine heat wave (see text and Appendix D.2). The standardized SSTa is defined as SSTa divided by the standard deviation of SSTa at each location calculated over 1982-2019, thus taking into account spatial variance in the normal fluctuation of SSTa.

2018, and now 2019. Further details on this event, how it compared to the Blob, and our analytical methods are provided in Appendix D.2.

A concept emerging from these warming events is "habitat compression." The large-scale warming in the northeast Pacific over the past 7 years mostly occurred offshore, while much of the nearshore region experienced average temperatures due to upwelling. However, this relatively cool upwelling habitat was restricted to a narrow band along the coast by the warm offshore conditions. This compressed the cool upwelling habitat and consequently altered pelagic species composition and distribution, from forage species to top predators. Habitat compression led to severe impacts such as those associated with whale entanglements in fixed fishing gear, and may have contributed to poor conditions experienced by a number of species off central and northern California in 2019. Santora et al. (2020) developed a Habitat Compression Index (HCI) to track changes in the extent of cold upwelled surface waters, how far that habitat extends offshore, and its latitudinal variability (Figure 7.2.2). The HCI is defined as the area of cool (≤12°C) monthly averaged surface temperatures in a region extending from the coast to 150 km offshore between 35.5°N-40°N (roughly from Morro Bay to Cape Mendocino). Figure 7.2.2 demonstrates the strong shift in compression that occurred in 2014, and has continued since then, especially in winter.

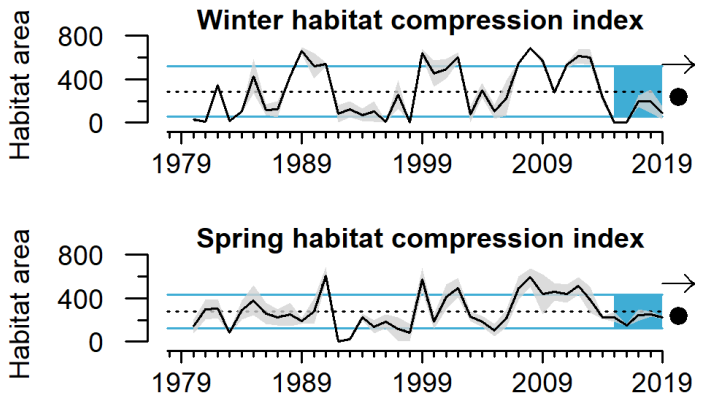

Figure 7.2.1 Mean winter (Jan - March) and spring (April - June) habitat compression index (SST < 12C, x100 km²) for 1980-2019. Error envelope indicates ± 1.0 s.e. Lines, colors, and symbols are as in Fig. 1.

The HCI provides a new regional metric for assessing the impact of warming events on coastal upwelling conditions and should be combined with other marine heatwave diagnostics. Similar levels of compression have been observed in earlier years (Figure 7.2.2), and we will continue to study this metric in relation to other indicators in hopes of understanding why coastal impacts in recent years have been so severe.

SUPPLEMENTARY MATERIALS TO THE CALIFORNIA CURRENT INTEGRATED ECOSYSTEM ASSESSMENT (CCIEA) CALIFORNIA CURRENT ECOSYSTEM STATUS REPORT, 2020

Appendix A LIST OF CONTRIBUTORS TO THIS REPORT, BY AFFILIATION

NWFSC, NOAA Fisheries
Mr. Kelly Andrews
Ms. Katie Barnas
Dr. Richard Brodeur
Dr. Brian Burke
Dr. Jason Cope
Dr. Correigh Greene
Dr. Thomas Good
Dr. Chris Harvey (co-lead editor)
Dr. Daniel Holland
Dr. Kym Jacobson
Dr. Stephanie Moore
Dr. Stuart Munsch
Dr. Karma Norman
Dr. Jameal Samhouri
Dr. Nick Tolimieri (co-editor)
Ms. Margaret Williams
Dr. Jeannette Zamon

Pacific States Marine Fishery Commission
Ms. Amanda Phillips
Mr. Gregory Williams (co-editor)

Oregon State University
Ms. Jennifer Fisher
Ms. Cheryl Morgan
Ms. Samantha Zeman

AFSC, NOAA Fisheries
Dr. Stephen Kasperski
Dr. Sharon Melin

NOAA Fisheries West Coast Region
Mr. Dan Lawson

Farallon Institute
Dr. William Sydeman

Point Blue Conservation Science
Dr. Jaime Jahncke

University of Washington
Dr. Julia Parrish

Scripps Institute of Oceanography
Dr. Dan Rudnick

SWFSC, NOAA Fisheries
Dr. Eric Bjorkstedt
Dr. Steven Bograd
Ms. Lynn deWitt
Dr. John Field
Dr. Newell (Toby) Garfield (co-lead editor)
Dr. Elliott Hazen
Dr. Michael Jacox
Dr. Andrew Leising
Dr. Nate Mantua
Mr. Keith Sakuma
Dr. Jarrod Santora
Dr. Andrew Thompson
Dr. Brian Wells
Dr. Thomas Williams

University of California-Santa Cruz
Ms. Rebecca Miller
Dr. Barbara Muhling
Dr. Isaac Schroeder

Humboldt State University
Ms. Roxanne Robertson

California Department of Public Health
Ms. Christina Grant
Mr. Duy Trong
Ms. Vanessa Zubkousky-White

California Department of Fish and Wildlife
Ms. Christy Juhasz

CA Office of Env. Health Hazard Assessment
Dr. Rebecca Stanton

Oregon Department of Fish and Wildlife
Dr. Caren Braby
Mr. Matthew Hunter

Oregon Department of Agriculture
Mr. Alex Manderson

Washington Department of Health
Mr. Jerry Borchert
Ms. Audrey Coyne

Appendix B LIST OF FIGURE AND DATA SOURCES FOR THE MAIN REPORT

Figure 3.1.1: Oceanic Niño Index data are from the NOAA Climate Prediction Center (http://www.cpc.ncep.noaa.gov/products/analysis_monitoring/ensostuff/ONI_change.shtml). PDO data are from N. Mantua, NMFS/SWFSC, derived from the University of Washington Joint Institute for the Study of the Atmosphere and Ocean (JISAO; http://research.jisao.washington.edu/pdo/). North Pacific Gyre Oscillation data are from E. Di Lorenzo, Georgia Institute of Technology (http://www.o3d.org/npgo/).

Figure 3.1.2: Sea surface temperature maps are optimally interpolated remotely-sensed temperatures (Reynolds et al. 2007). The daily optimal interpolated AVHRR SST can be downloaded using ERDDAP (http://upwell.pfeg.noaa.gov/erddap/griddap/ncdcOisst2Agg.html).

Figure 3.1.3: Newport Hydrographic (NH) line temperature data from J. Fisher, NMFS/NWFSC, OSU. CalCOFI data from https://calcofi.org. CalCOFI data before 2019 are from the bottle data database, while 2019 data are preliminary from the recent conductivity, temperature, and depth (CTD) database.

Figure 3.2.1: Daily 2019 values of BEUTI and CUTI are provided by M. Jacox, NMFS/SWFSC; detailed information about these indices can be found at https://mjacox.com/upwelling-indices/.

Figure 3.3.1: Newport Hydrographic (NH) line dissolved oxygen data are from J. Fisher, NMFS/NWFSC, OSU. CalCOFI data from https://calcofi.org. CalCOFI data before 2019 are from the bottle data database, while 2019 data are preliminary from the recent CTD database.

Figure 3.4.1: Domoic acid concentrations in razor clams and Dungeness crab from Washington are compiled by the Washington State Department of Health from tests conducted by tribal, state, and county partners on Washington beaches. Oregon domoic acid data are compiled by Oregon Department of Fish and Wildlife (ODFW) from samples collected from sites across the Oregon coast by Oregon Department of Agriculture and ODFW staff. California data are compiled by the California Department of Public Health from samples collected by local, tribal, and state partners.

Figure 3.5.1: Snow-water equivalent data were derived from the California Department of Water Resources snow survey (http://cdec.water.ca.gov/) and the Natural Resources Conservation Service's SNOTEL sites in WA, OR, CA and ID (http://www.wcc.nrcs.usda.gov/snow/).

Figure 3.5.2: Minimum and maximum streamflow data were provided by the US Geological Survey (http://waterdata.usgs.gov/nwis/sw).

Figure 4.1.1: Copepod biomass anomaly data were provided by J. Fisher, NMFS/NWFSC, OSU.

Figure 4.1.2. Krill data were provided by E. Bjorkstedt, NMFS/SWFSC and Humboldt State University (HSU), and R. Robertson, Cooperative Institute for Marine Ecosystems and Climate (CIMEC) at HSU.

Figure 4.2.1: Pelagic forage data from the Northern CCE from B. Burke, NMFS/NWFSC and C. Morgan, OSU/CIMRS. Data are derived from surface trawls taken during the NWFSC Juvenile Salmon & Ocean Ecosystem Survey (JSOES; https://www.nwfsc.noaa.gov/research/divisions/fe/estuarine/oeip/kb-juvenile-salmon-sampling.cfm).

Figure 4.2.2: Pelagic forage data from the Central CCE were provided by J. Field and K. Sakuma, NMFS/SWFSC, from the SWFSC Rockfish Recruitment and Ecosystem Assessment Survey (https://swfsc.noaa.gov/textblock.aspx?Division=FED&ParentMenuId=54&id=20615).

Figure 4.2.3: Pelagic forage larvae data from the Southern CCE were provided by A. Thompson, NMFS/SWFSC, and derived from spring CalCOFI surveys (https://calcofi.org/).

Figure 4.3.1: Chinook salmon escapement data were derived from the California Department of Fish and Wildlife (https://www.dfg.ca.gov/fish/Resources/Chinook/CValleyAssessment.asp), PFMC pre-season reports (https://www.pcouncil.org/salmon/stock-assessment-and-fishery-evaluation-safe-documents/review-of-2018-ocean-salmon-fisheries/), and the NOAA NWFSC's "Salmon Population Summary" database (https://www.webapps.nwfsc.noaa.gov/sps), with data provided directly from the Nez Perce Tribe, the Yakama Nation Tribe, and from Streamnet's Coordinated Assessments database (cax.streamnet.org), with data provided by the Oregon Department of Fish and Wildlife, Washington Department of Fish and Wildlife, Idaho Department of Fish and Game, Confederated Tribes and Bands of the Colville Reservation, Shoshone-Bannock Tribes, Confederated Tribes of the Umatilla Indian Reservation, and U.S. Fish and Wildlife Service.

Figure 4.3.2: Data for at sea juvenile salmon provided by B. Burke, NMFS/NWFSC, with additional calculations by C. Morgan, OSU/CIMRS. Derived from surface trawls taken during the NWFSC Juvenile Salmon and Ocean Ecosystem Survey (JSOES) cruises.

Figure 4.4.1: Groundfish stock status data provided by J. Cope, NMFS/NWFSC, derived from NOAA Fisheries stock assessments.

Figure 4.6.1: California sea lion data provided by S. Melin, NMFS/AFSC.

Figure 4.6.2: Whale entanglement data provided by D. Lawson, NMFS/WCR.

Figure 4.7.1: Seabird fledgling production data at nesting colonies on Southeast Farallon provided by J. Jahncke, Point Blue Conservation Science.

Figure 5.1.1: Data for commercial landings are from PacFIN (http://pacfin.psmfc.org). Data for recreational landings are from RecFIN (http://www.recfin.org/).

Figure 5.2.1: Data for total distance trawled by federally managed bottom-trawl fisheries were provided by J. McVeigh, NMFS/NWFSC, West Coast Groundfish Observer Program. Figures created by K. Andrews, NMFS/NWFSC.

Figure 6.1.1: Community social vulnerability index (CSVI) and commercial fishery reliance data provided by K. Norman, NMFS/NWFSC, and A. Phillips, PSMFC, with data derived from the US Census Bureau's American Community Survey (ACS; https://www.census.gov/programs-surveys/acs/) and PacFIN (http://pacfin.psmfc.org), respectively.

Figure 6.2.1: Fishery diversification estimates were provided by D. Holland, NMFS/NWFSC, and S. Kasperski, NMFS/AFSC.

Figure 6.3.1: Commercial revenue data compiled by A. Phillips and K. Norman, NMFS/NWFSC, and derived from PacFIN (http://pacfin.psmfc.org).

Figure 7.2.1.: Standardized SSTa plots were created by A. Leising, NMFS/SWFSC, using SST data from NOAA's Optimum interpolation Sea Surface Temperature analysis (OISST; https://www.ncdc.noaa.gov/oisst), with the SST anomaly calculated using climatology from NOAA's AVHRR-only OISST dataset.

Figure 7.2.2.: Compression index estimates developed and provided by J. Santora, NMFS/SWFSC and I. Schroeder, NMFS/SWFSC, UCSC.

Table 4.3.1: Stoplight table of indicators and projected 2019 salmon returns courtesy of B. Burke and K. Jacobson, NMFS/NWFSC; J. Fisher, C. Morgan, and S. Zeman, OSU/CIMRS.

Table 4.3.2: Table of indicators and qualitative outlook for 2020 Chinook salmon returns to the Central Valley courtesy of N. Mantua, NMFS/SWFSC.

Appendix C CHANGES IN THIS YEAR'S REPORT

Below we summarize major changes and improvements in the 2020 Ecosystem Status Report, in response to the requests and suggestions received from the Council and advisory bodies under FEP Initiative 2, "Coordinated Ecosystem Indicator Review" (March 2015, Agenda Item E.2.b). We also note other new items we have added and information gaps that we have filled since last year's report.

Request/Need	Response/Location in document
Description of marine heatwave and habitat compression along the West Coast, in relation to other basin-scale climate indicators, upwelling, and habitat suitability for key species	Because marine heatwaves have been a recurring feature in the California Current from 2014-2016, 2018, and 2019, we dedicated space in the main body (Section 7.2) and the Supplement (Appendix D.2). These sections feature both analyses of marine heatwave physical characteristics (reviewed previously by the SSC), and of compression of cool-water, upwelled habitat along the coast (Figure 7.2.2).
In 2019, we included harmful algal bloom (HAB) data in the report for the first time, but data were limited to Washington razor clams. Several Council bodies requested coastwide HAB indicator data.	In this year's report, we include domoic acid levels in razor clams and Dungeness crabs from multiple sites in Washington, Oregon and California, as well as spiny lobster and rock crab in southern California. Plots and text are in the main body (Section 3.4) and Supplement (Appendix E).
In 2018, the Ecosystem Advisory Subpanel requested that the IEA team develop indicators of community-level fishery participation and economic status, as related to National Standard 8 (NS-8) under the Magnuson-Stevens Act.	This year we introduce indicators of the proportion of commercial fishing revenue brought in by the top 16 ports in terms of total revenue and FMP-specific revenue. Total revenue is presented in the main body (Section 6.3) and FMP-specific revenue is in the Supplement (Appendix O).
Several Council bodies have requested "stoplight" tables of indicators related to returns of salmon from central California, similar to the table for salmon returns to the Columbia River and Oregon coast.	This year we introduce a fairly simple indicator summary table that relates ecosystem indicators to Central Valley fall Chinook salmon returns. The table is in the main body (Section 4.3).
In 2019, the Coastal Pelagic Species Advisory Subpanel requested that dissolved oxygen and ocean acidification data broadly reflect conditions from different regions of the West Coast	In the main body, Figure 3.3.1, we now include dissolved oxygen time series from both Newport, Oregon and CalCOFI line 93 in Southern California, with additional time series from both sites and broader dissolved oxygen maps in the Supplement (Appendix D.3). We are unaware of time series of dissolved oxygen transects in the region from Cape Mendocino to Point Conception. In this year's report, we put all ocean acidification information in Appendix D.3, for space considerations and lack of clear mechanistic links to broad ecosystem impacts at this time. All data are from off Newport, Oregon; we are unaware of other time series of aragonite saturation state along the coast.

Request/Need	Response/Location in document
In 2019, the Ecosystem Workgroup requested additional indicators of krill from the northern portion of the system	In the Supplement (Appendix G.1), we add maps of krill densities from spring surveys over most of the past decade, off the coast of Oregon and Washington. We will work to identify additional time series from this portion of the coast.
In 2019, the Habitat Committee recommended that the Gear Contact with Seafloor indicator be reviewed by the SSC-ES, to ensure the analytical methods were supported and that the indicator would be suitable for capturing changes in bottom trawling activity related to Groundfish FMP Amendment 28.	The SSC-ES reviewed this analysis in September 2019, and the plots shown in the main body (Section 5.2) (Appendix L) incorporate recommendations from that review. Specifically: in Figure 5.2.1, we replaced the 5-year mean panel with a panel showing the raw, annual data, which shows the magnitude of bottom contact occurring most recently, while retaining an indicator of the historical status (anomaly panel) and trend (5-yr trend). The new raw, annual data panel should provide a rapid assessment of changes in bottom trawl gear contact in the newly opened and closed areas associated with Amendment 28. The SSC-ES suggested that we incorporate VMS data into this indicator in order to capture the path of the trawling vessel in between the set and haul-back coordinates more accurately. We have not incorporated this yet as we are waiting for the development of a "Best Practices Methodology" for processing, standardizing, matching to fish ticket data and increased accessibility that is being funded by the Fisheries Information System Program and carried out by researchers across the U.S. West Coast in 2020.
In March 2019, the SSC stated, “For the first time there are numerical forecasts of salmon returns included in the Status Report…These forecasts are not comparable to the forecasts used by the Salmon Technical Team (STT) for salmon management. The SSC will work with the CCIEA team to review these forecasts and determine how best to communicate this information in future CCIEA reports.”	In September 2019, the SSC-ES reviewed the approaches used in the figures in question in a pre-Council advisory body meeting with IEA scientists. The general approach was acceptable but the SSC-ES made some recommendations, including that the term “forecasts” not be used to avoid confusion; we have taken this guidance where these figures and text are presented in this year’s Supplement (Appendix H.3). The SSC-ES recommended that we expand the approach to stocks over which the Council has greater management responsibility. This recommendation will require additional research and staff time that we currently do not have, but will look to address in future years. Finally, unlike last year the projections in Figure H.3.2 this year do not include a coho projection, due to poor model performance and lack of staff time.

Request/Need	Response/Location in document
Including recreational fishing reliance and engagement in Human Wellbeing section	At the request of various advisory bodies, last year we introduced community-level estimates of recreational fishing reliance and engagement into the Human Wellbeing section (Section 7 of the main document and Appendix M of the Supplement). Those data have not been updated since last year's report and the most recent data go back to 2016; thus, we have not repeated them in this year's report, for space considerations.
At the 2019 March Council meeting, we received feedback that the seabird indicators in the main body of the report (i.e., indicators of at-sea density of birds) were not particularly relevant to foraging conditions in the different regions.	In this year's report, we put indicators of seabird colony production (species-specific fledgling production) in the main report (Section 4.7). Productivity measures like these connect more closely to other indicators of regional forage availability. At-sea densities of seabirds and other seabird indicators are in the Supplement, Appendix J.

Appendix D CLIMATE AND OCEAN INDICATORS

Section 3 of the Main Body describes indicators of basin-scale and region-scale climate and ocean drivers. Here we present additional plots to allow a more complete picture of these indicators.

D.1 BASIN-SCALE CLIMATE/OCEAN INDICATORS AT SEASONAL TIME SCALES

These plots show seasonal averages, short-term trends, and short-term averages of the three basin-scale climate forcing indicators shown in the main report in Figure 3.1.1. Notable outcomes include: both winter and summer Ocean Niño Index (ONI) have declining trends, illustrating the strength of the 2016 El Niño (and the relative weakness of the 2019 El Niño, shown in Figure D.1.1, top); summer and winter PDO have negative trends since 2015 (Figure D.1.2), illustrating the strength of the 2013-2016 marine heatwave (the "Blob"); winter PDO has been above average over the past 5 years (Figure D.1.2, top), illustrating that the system continues to be warmer than normal in the aftermath of the Blob; winter NPGO has a decreasing 5-year trend (Figure D.1.3, top); and summer NPGO has been below average over the past 5 years, and has the lowest values in the time series (Figure D.1.3, bottom).

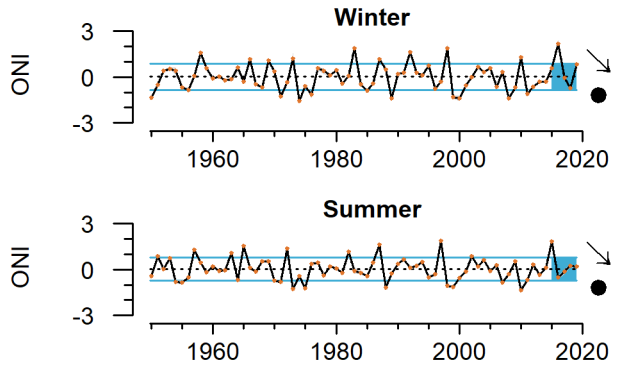

Figure D.1.1 Winter (top, Jan-Mar) and Summer (bottom, July-Sep) values of the Ocean Nino Index from 1950-2019. Lines, colors, and symbols are as in Fig. 1.

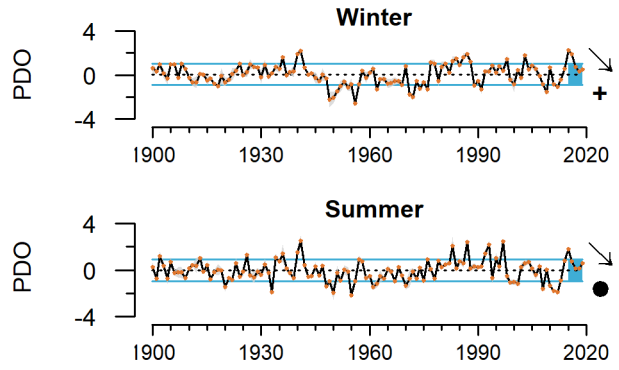

Figure D.1.2 Winter (top, Jan-Mar) and Summer (bottom, July-Sep) values of the Pacific Decadal Oscillation Index 1900-2019. Lines, colors, and symbols are as in Fig. 1.

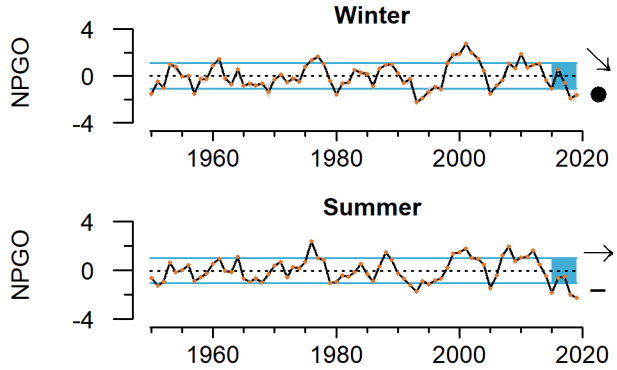

Figure D.1.3 Winter (top, Jan-Mar) and Summer (bottom, July-Sep) values of the North Pacific Gyre Oscillation Index from 1950-2019. Lines, colors, and symbols are as in Fig. 1.

D.2 ASSESSING THE 2019 MARINE HEATWAVE

There is increased recognition that marine heatwaves can have immediate short-term impacts on the ecosystem, as well as an indication of stock displacements that may occur with long-term climate warming. For these reasons, monitoring marine heatwaves and developing robust indices of these features are important for management. As noted in Section 3.1 and Section 7.2 of the main body of the report, a large marine heatwave emerged in the northeast Pacific Ocean in the second half of 2019, similar in size and intensity to the 2013-2016 northeast Pacific marine heatwave known as the "Blob." Here we describe additional analysis related to this event and compare its progression to that of the Blob.

Based on an analysis of sea surface temperature anomalies (SSTa) from 1982–2019, a marine heatwave has the potential to cause impacts in the CCE that are comparable to those from the 2013–2016 event if the anomalous feature: 1) has statistically normalized SSTa >1.29 s.d. (90th percentile) of the long-term SSTa time series at a location; 2) is ≥3.5 x 10^6 km^2 in area; 3) lasts for >5 days; and 4) comes within 500 km of the coast (Hobday et al. 2016; Leising in prep). Events in both 2018 and 2019 surpassed these thresholds (Figure D.2.1, Figure D.2.2). In the case of the 2019 event, because it only encroached on coastal waters from July to September, it is too early to determine the impacts of the event on the CCE.

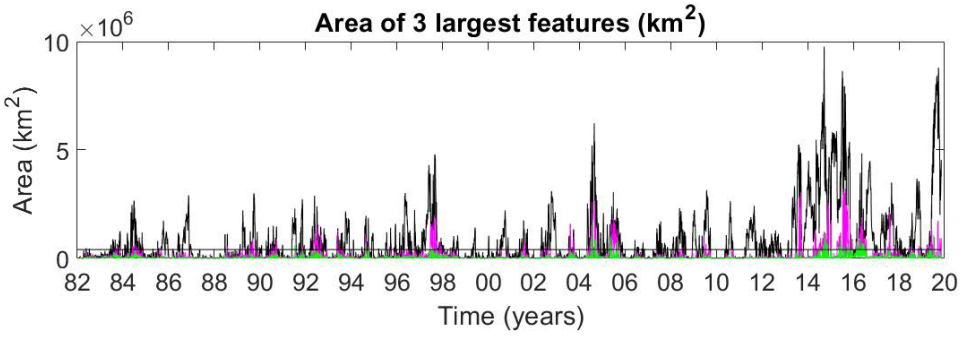

Figure D.2.1 Area of North Pacific warm SST anomalies >2 s.d. from 1982-2019. Because multiple anomalies can be present, black is the largest anomaly, magenta is the second largest and green is the third largest. The horizontal line represents 500,000 km², the area threshold for features likely to impact the coastal region of the CCE. Data courtesy of Dr. Andrew Leising (NMFS/SWFSC).

The 2019 heatwave was preceded by a fairly large heatwave during the fall of 2018, which also began during the middle of the year and continued until early December. However, there was no surface expression of a marine heatwave from December 2018 until early May 2019. In May 2019, the new marine heatwave rapidly developed, reaching a peak by August (Figure D.2.2). Its peak conditions rivaled the 2014 event in terms of size and intensity (Figure D.2.1). It is unclear if the 2018 event should be considered a precursor or separate event from the 2019 event, although an ongoing analysis of subsurface temperature anomalies may determine if there was a linkage.

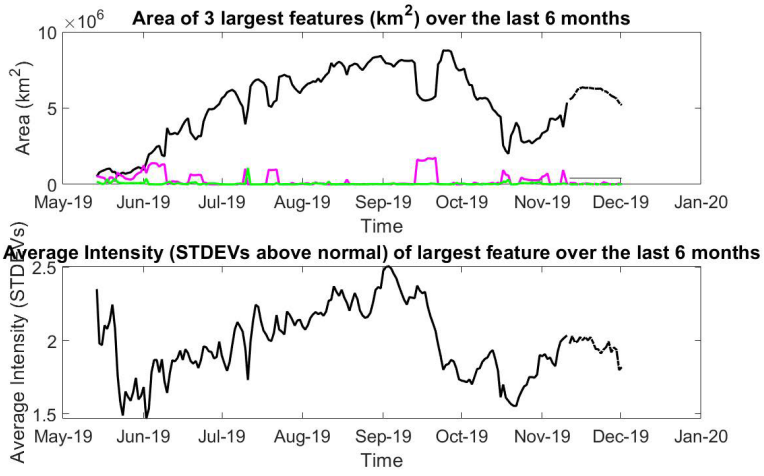

Figure D.2.2. Companion figure to Fig. D.2.1, focusing on the size and intensity of northeast Pacific marine heatwaves that were present from May to December 2019. Data courtesy of Dr. Andrew Leising (NMFS/SWFSC).

The 2019 heatwave had some similarities, but also some important differences from the 2013-2016 "Blob" event. The Blob began in the far offshore region during mid 2013, grew and moved closer to the coast, showed a slight recession during the winter of 2013-2014, but then steadily gained strength throughout 2014, with a peak intensity that year during September (Figure D.2.3). The anomalous warming persisted into the winter of 2014-2015 (Figure D.2.3, right). The 2019 event (Figure 7.2.1) evolved much more rapidly to its maximum size than the Blob during the similar time period in 2014. By mid October 2019, the recent heatwave showed signs of recession, decreasing in size and intensity, such that by early January 2020, it no longer met the marine heatwave criteria outlined above (Figure 7.2.1). Thus, unlike the Blob, both the 2018 and 2019 events have failed to persist into winter. However, a significant pool of warmer than normal water remained in the far offshore region. Since a similar buildup and then recession occurred during 2013-2014, and we continue to observe anomalously warm water far offshore and retention of heat by deeper waters, it is unclear if we may see a resurgence of another heatwave in the summer of 2020.

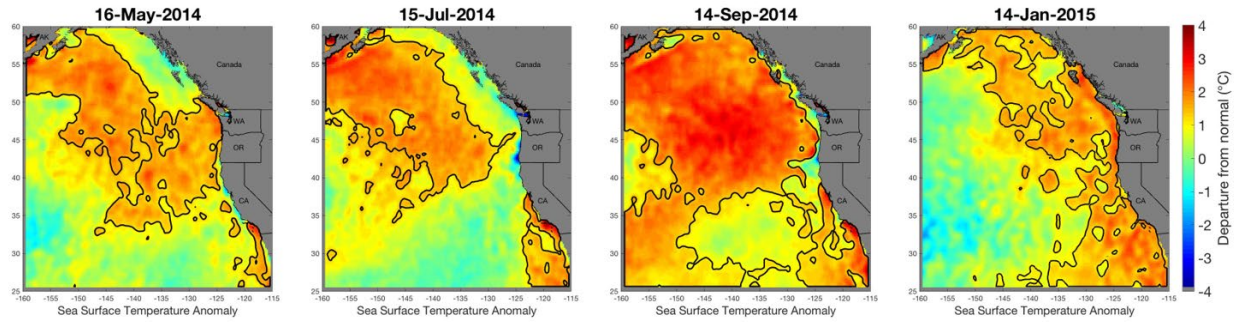

Figure D.2.3 Progression of standardized sea surface temperature (SST) anomalies in 2014-2015, the time period when the 2013-2016 large marine heatwave (the "Blob") first expanded into California Current waters and intersected coastal waters. Dark contours denote regions that meet the criteria of a marine heat wave (see text). Compare with progression of images for the 2019 marine heatwave shown in Figure 7.2.1. Plots were created by A. Leising, NMFS/SWFSC, using SST data from NOAA's Optimum interpolation Sea Surface Temperature analysis (OISST; https://www.ncdc.noaa.gov/oisst).

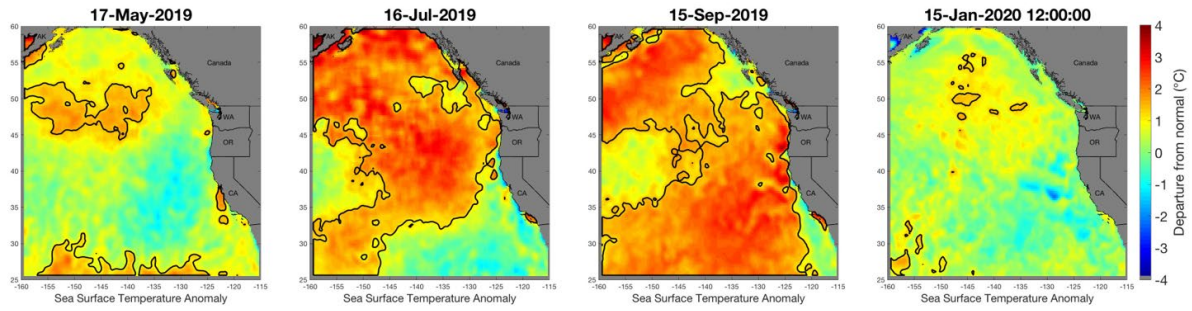

Copy of Figure 7.2.6 for comparison with Figure D.2.3. Standardized SSTa across the Pacific Northeast for May, July, and September 2019, and January 2020.

The above plots and analyses focus on sea surface temperatures. Subsurface temperature data from autonomous glider transects provide additional information. The northeast Pacific Ocean has remained anomalously warm since the 2014 marine heatwave and 2015 El Niño (Figure D.2.4). Time series of glider data from CalCOFI line 90 (off Dana Point in the Southern California Bight) at 10-m and 50-m depths from the shore to a distance 500 km offshore illustrate the dramatic subsurface temperature change that occurred in 2014 and continues through the end of 2019.

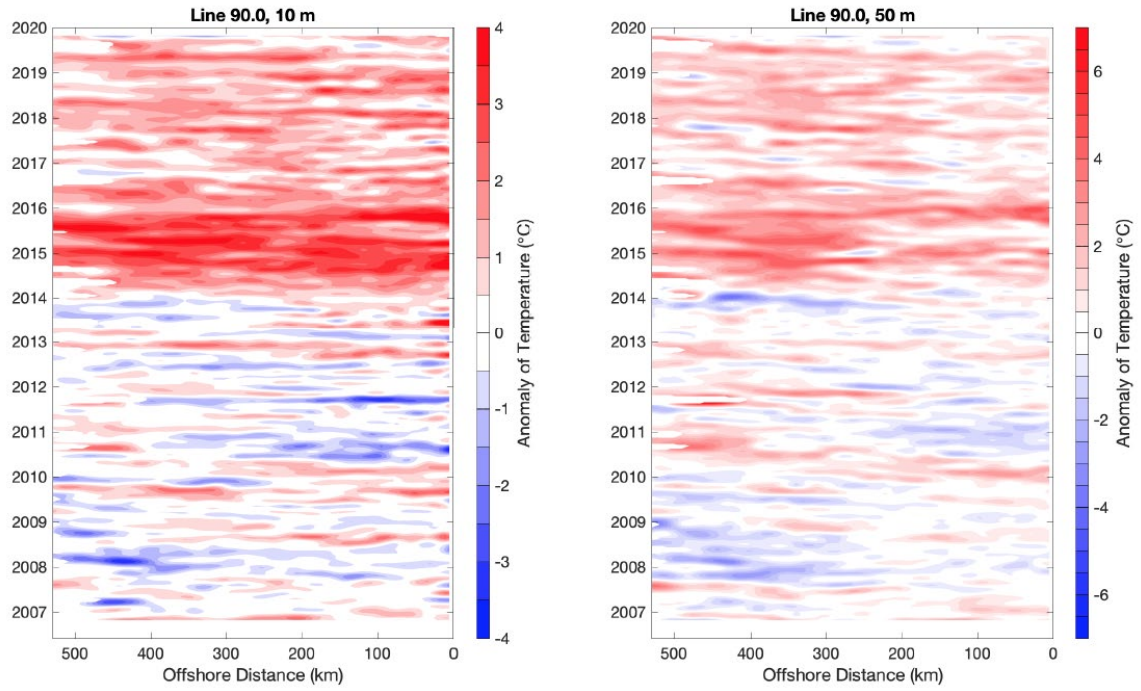

Figure D.2.6 Temperature anomalies at depths of 10 m (left) and 50 m (right) along CalCOFI line 90, extending from the coast to 500 km offshore, 2007-2019. Conditions from 2007 to 2014 oscillated about the mean while from 2014 to the end of 2019, positive temperature anomalies have been consistent. The large anomaly starting in 2014 is the marine heatwave of 2014-2016. Conditions have remained warmer than average ever since. Data from the California Underwater Glider Network are provided by Dr. Dan Rudnick, Scripps Institute of Oceanography Instrument Development Group (doi: 10.21238/S8SPRAY1618).

Note that prior to 2014 the CalCOFI subsurface temperature indices at both 10-m and 50-m depths tracked closely with the ONI index (Figure D.2.5), consistent with the finding that the El Niño Southern Oscillation was the major source of variability in the CCLME for the majority of this time series (Jacox et

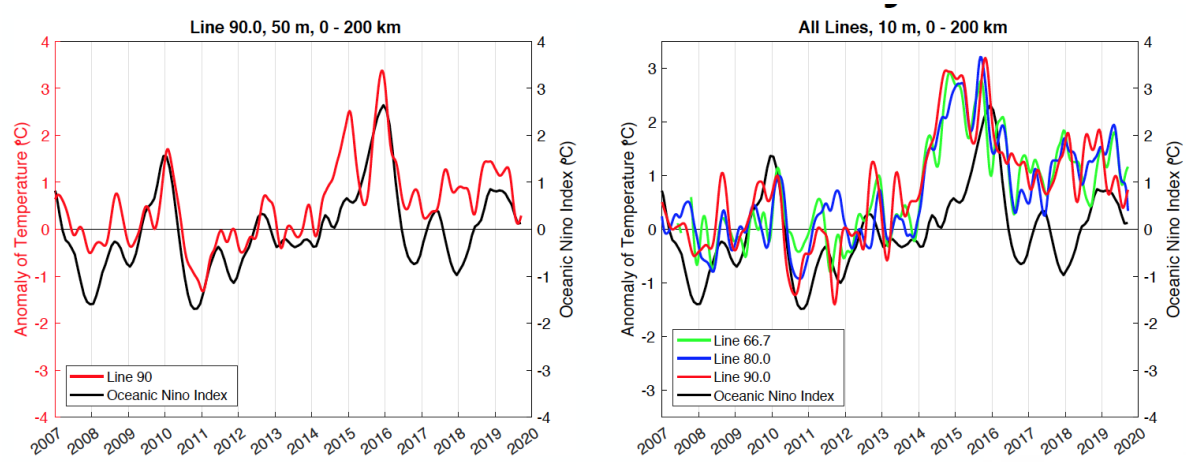

Figure D.2.5 CalCOFI temperature indices for CalCOFI lines 66.7, 80, and 90 (Figure 2.1) compared to the ONI index. The CalCOFI temperature indices are the temperature at the indicated depth averaged from the shore to 500 km offshore. ONI data are from the NOAA Climate Prediction Center. Data from the California Underwater Glider Network are provided by Dr. Dan Rudnick, Scripps Institute of Oceanography Instrument Development Group (doi: 10.21238/S8SPRAY1618).

al. 2016). In 2014, the CalCOFI temperature indices on three separate glider lines (Line 67 off Monterey Bay; Line 80 off Point Conception; Line 90 off Dana Point) show the temperature increase began prior to the major 2015-2016 El Niño, but did not return to normal following the end of the El Niño in 2016. The glider trends increase with the mild 2018-2019 El Niño, but still remain anomalously high. These data agree with the anomaly contours of CalCOFI 93.3 in Figure 3.1.3, demonstrating that southern and central California remain warm due to the marine heatwave, and experienced some additional influence from the recent El Niño events.

Data from the glider surveys suggest further changes in the water column, in particular changes in subsurface salinity. A major salinity anomaly can be seen along CalCOFI Line 90 at 10-m and 50-m depths starting in 2018 (Figure D.2.6). These represent some of the largest and most extensive positive anomalies of the available time series. The anomalies suggest that the Southern California Bight temperatures since 2018 may be due to the influx of a warmer, saltier water into the region.

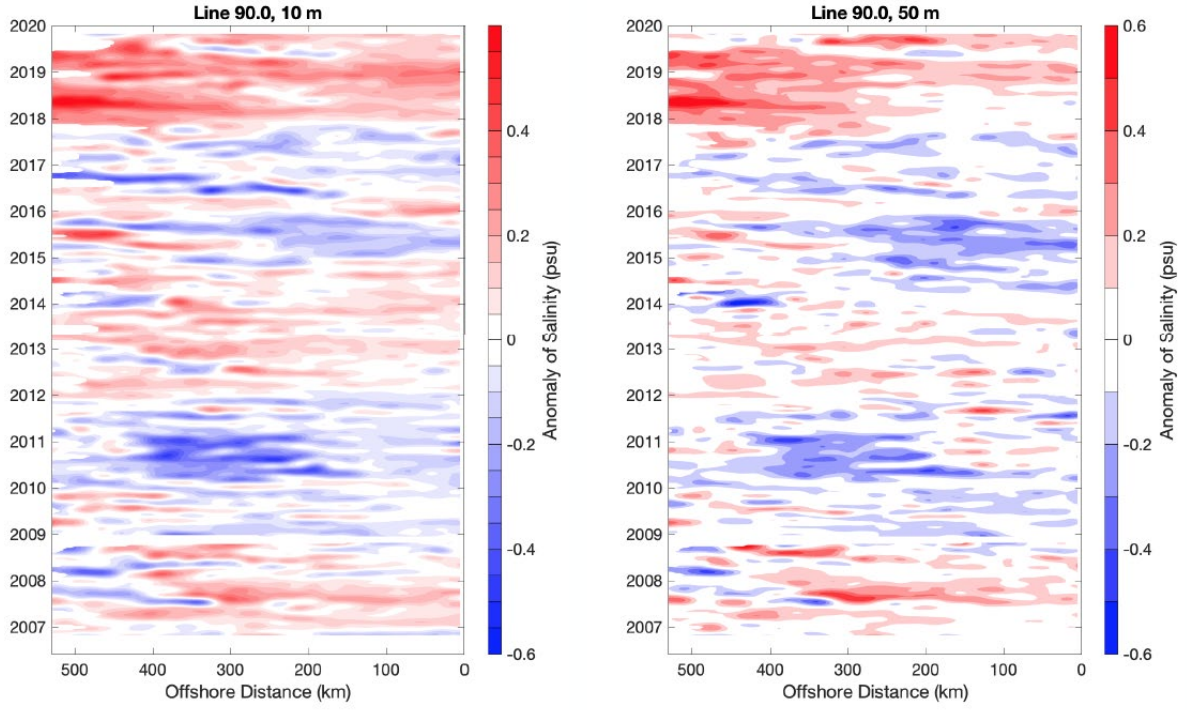

Figure D.2.7 Salinity anomalies at depths of 10 m (left) and 50 m (right) along CalCOFI Line 90 from the coast out 500 km, 2007-2019. Data from the California Underwater Glider Network are provided by Dr. Dan Rudnick, Scripps Institute of Oceanography Instrument Development Group (doi: 10.21238/S8SPRAY1618).

D.3 SEASONAL AND SPATIAL DISSOLVED OXYGEN AND OCEAN ACIDIFICATION INDICATORS

The first series of plots in this section shows summer and winter averages for dissolved oxygen (DO) data off Newport, OR (stations NH05 and NH25, 5 and 25 nautical miles off the coast respectively) and in the Southern California Bight (stations CalCOFI 90.90 and CalCOFI 93.30). In 2019, winter DO concentrations were consistently above the hypoxia threshold (1.4 ml O_2 per L water) at each of the stations, as is typical for the entirety of the winter time series (Figure D.3.1). Summer DO concentrations in 2019 were also above the hypoxia threshold at each station (Figure D.3.2); notable is that DO concentrations in summer 2019 were improved over summer 2018 at station NH05.

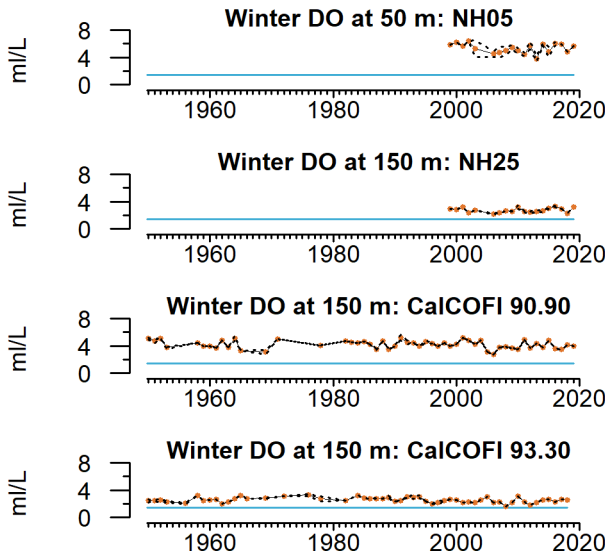

Figure D.3.1 Winter (Jan-Mar) dissolved oxygen (DO) at 150 m depth off of Oregon, 1999-2019 and southern California, 1950-2019. Stations NH25 and 93.30 are < 50 km from the shore; station 90.90 is >300 km from shore. Blue line indicates hypoxic threshold of 1.4 ml O2 per L. Lines, colors, and symbols are as in Fig. 1.

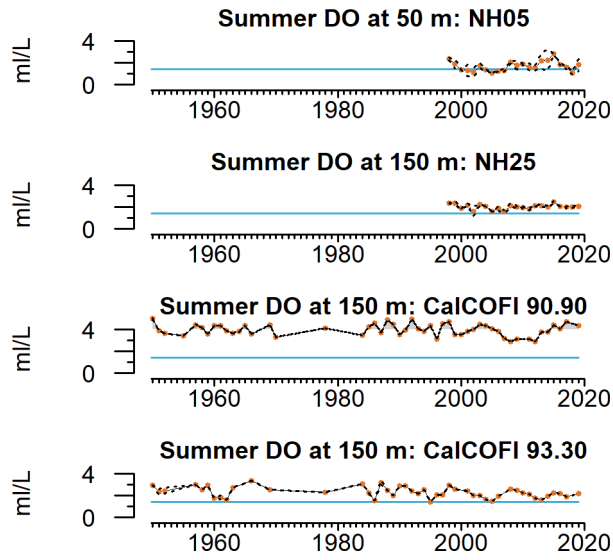

Figure D.3.2 Summer (Jul-Sep) dissolved oxygen (DO) at 50-m and 150 m depth off of Oregon, 1999-2019 and southern California, 1950-2019. Stations NH05, NH25 and 93.30 are < 50 km from the shore; station 90.90 is >300 km from shore. Blue line indicates hypoxic threshold of 1.4 ml O2 per L. Lines, colors, and symbols are as in Fig. 1.

The next figure (Figure D.3.3) shows interpolated estimates of DO at different depths from the summer 2019 CalCOFI survey of the Southern California Bight. Summer DO values displayed strong inshore-offshore and depth gradients, with higher values measured farther offshore and lower values measured at depth. The southern CCE DO levels in the upper 150 m measured during the summer 2019 CalCOFI survey had levels above the hypoxic threshold (Figure D.3.3, left and middle). The DO measured during the summer cruise was average, with all stations having DO values near the long-term mean. DO values at 500 m depths were well below the 1.4 ml/L hypoxic threshold, although this is typical. In the area around the Channel Islands and for stations adjacent to shore, DO values near the seafloor were above the hypoxic threshold (Figure D.3.3, right). (We will also hope to have figures of on-bottom DO from the 2019 NMFS groundfish bottom trawl survey by the time of the March PFMC meeting.)

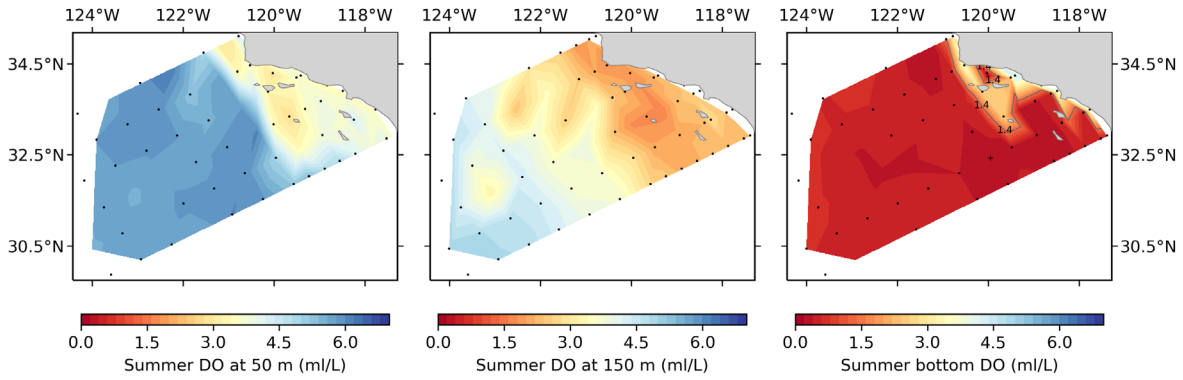

Figure D.3.3 Summer 2019 dissolved oxygen (DO) concentrations during the summer CalCOFI survey of the southern CCE at 50m (left), 150 m (middle), and on the bottom of the hydrographic cast (right) in the CalCOFI survey area. DO was sampled at stations marked by black dots; hydrographic casts extended to near bottom or to a maximum depth of 500 m; only a small number of stations, typically near the coastline or near islands, have depths <500 m. Dots were changed to a + or a – sign if the measured value was more than 1 s.d. above / below the long-term mean. The 1.4 ml/L contour (indicating the hypoxia threshold) is labeled in the right panel.

The final set of plots shows aragonite saturation state (an ocean acidification indicator) off Newport, Oregon. First are time series of seasonal aragonite saturation from near bottom at stations NH05 and NH25. Winter saturation state was consistently above the threshold of 1.0 at station NH05, but indicated generally corrosive conditions at station NH25 for most of the time series, including 2019 (Figure D.3.4). Summer aragonite saturation states indicated corrosive waters near bottom at both stations for most of the time series, including 2019 (Figure D.3.5). Saturation horizon depth profiles at NH05 and NH25 are shown in Figure D.3.6. They show that more of the water column was saturated (i.e., aragonite saturation state ≥1.0) in 2019 than in 2018, but overall was consistent with long-term expectations.

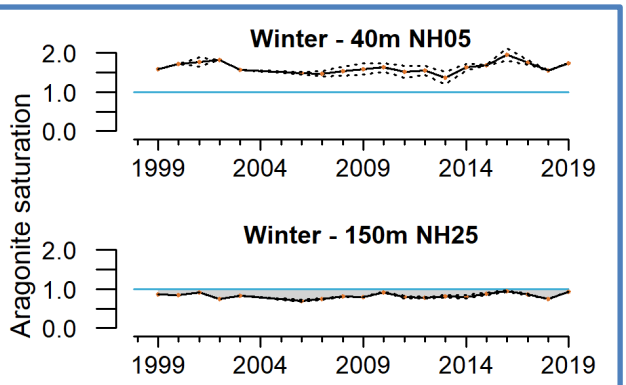

Figure D.3.4 Winter (Jan-Mar) aragonite saturation values at two stations off of Newport, OR, 1999-2019. The blue line indicates aragonite saturation state = 1.0. Dotted lines indicate ± 1.0 s.e. Lines, colors, and symbols are as in Fig. 1.

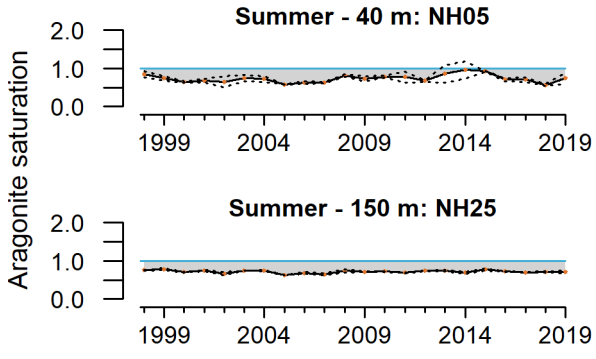

Figure D.3.5 Summer (Jul-Sep) aragonite saturation values at two stations off of Newport, OR, 1998-2019. The blue line indicates aragonite saturation state = 1.0. Dotted lines indicate ± 1.0 s.e. Lines, colors, and symbols are as in Fig. 1.

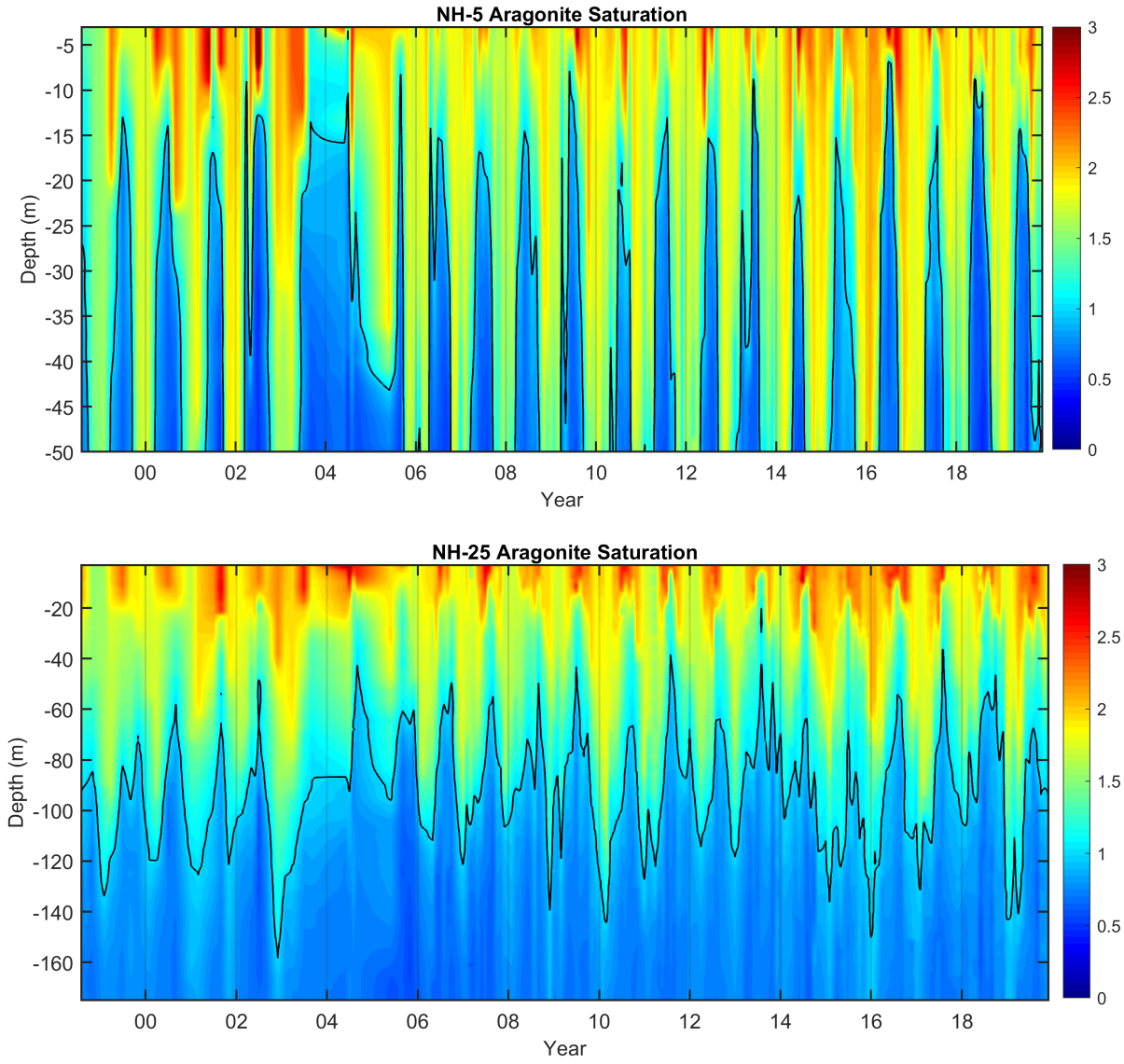

Figure D.3.6 Aragonite saturation horizon profiles for stations NH05 and NH25 off of Newport, OR. Black line indicates the depth at which aragonite saturation state = 1.0, which is considered a biological threshold below which seawater can be especially corrosive to shell-forming organisms. Station NH05 and NH25 are 5 and 25 nautical miles offshore, respectively.

Appendix E DOMOIC ACID ON THE WEST COAST

Harmful algal blooms (HABs) of diatoms in the genus *Pseudo-nitzschia* have been of particular concern along the West Coast in recent years. Certain species of *Pseudo-nitzschia* produce the toxin domoic acid that can accumulate in filter feeders and extend through food webs to cause harmful or lethal effects on people, marine mammals, and seabirds (Lefebvre et al. 2002, McCabe et al. 2016). To protect human health, fisheries that target shellfish (including razor clam, Dungeness crab, rock crab, and spiny lobster) are closed or operate under a health advisory in the recreational sector when concentrations of domoic acid exceed regulatory thresholds for human consumption. Domoic acid levels at or exceeding the Federal Drug Administration (FDA) action level of 20 parts per million (ppm) trigger closures of razor clam harvests. The FDA action level for domoic acid in Dungeness crab is >30 ppm for the viscera and >20 ppm for the meat tissue. In Oregon, Dungeness crab can be landed when the viscera exceeds the FDA alert level but the meat tissue does not if the crab are eviscerated by a licensed processor. In southern California, rock crab and spiny lobster are monitored for domoic acid.

Fishery closures can cause tens of millions of dollars in lost revenue and a range of sociocultural impacts in fishing communities (Dyson and Huppert 2010, NMFS 2016, Ritzman et al. 2018), and can also cause "spillover" of fishing effort into other fisheries. Extremely toxic HABs of *Pseudo-nitzschia* are influenced by ocean conditions and have been documented in 1991, 1998-99, 2002-03, 2005-06, and 2015-19. In the northern CCE, they have been found to coincide with or closely follow El Niño events or positive PDO regimes and track regional anomalies in southern copepod species (McCabe et al. 2016, McKibben et al. 2017). The largest and most toxic HAB of *Pseudo-nitzschia* ever recorded on the West Coast coincided with the 2014-16 Northeast Pacific marine heatwave and caused extensive closures and delays in the opening of crab fisheries, resulting in the appropriation of over $25M in federal disaster relief funds (McCabe et al. 2016).

In 2019, low levels of domoic acid detected in Washington razor clams and Dungeness crab did not trigger any fisheries closures (Figure E.1).

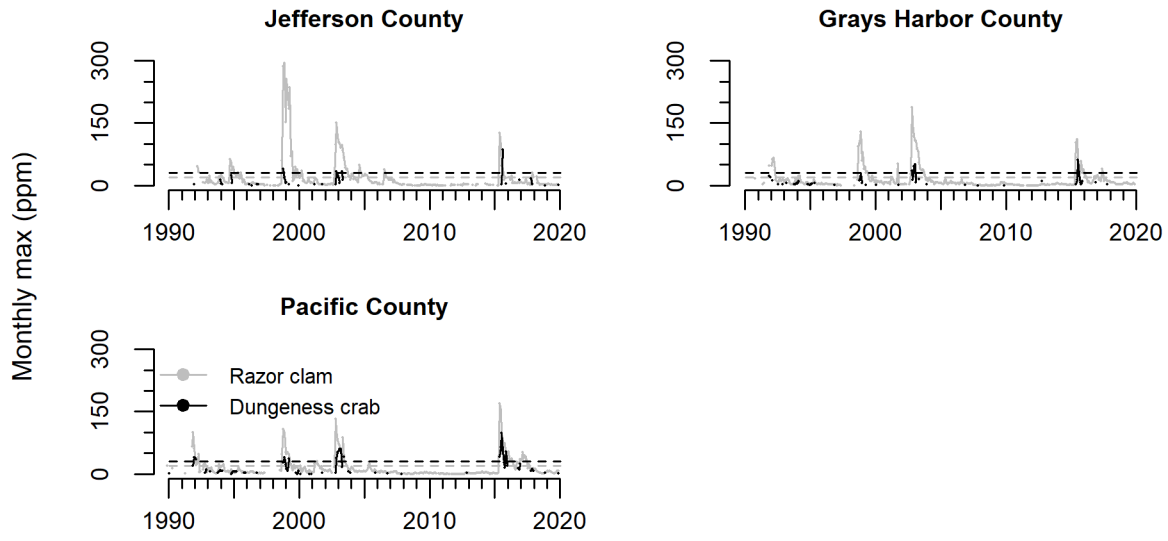

Figure E.1 Monthly maximum domoic acid concentration (ppm) in razor clams (gray) and Dungeness crab viscera (black) through 2019 by coastal counties in Washington State (north to south). Horizontal dashed lines are the management thresholds of 20 ppm (clams, in gray) and 30 ppm (crab viscera, in black). Data compiled by the Washington Department of Health (WDOH) from samples collected and analyzed by a variety of local, tribal, and state partners.

An extended closure of the razor clam fishery due to domoic acid in southern Oregon began in August 2014, but was lifted in September 2019. It was then reinstated in October 2019 (Figure E.2). On December 13, 2019 the entire Oregon coast was closed for razor clams due to domoic acid. A delay in the opening of the 2018-2019 Oregon commercial Dungeness crab fishery due to low meat quality extended into 2019; the fishery opened on January 4, 2019 but was delayed in southern Oregon (Cape Arago to the California border) until January 31, 2019 due to a combination of low meat quality and domoic acid.

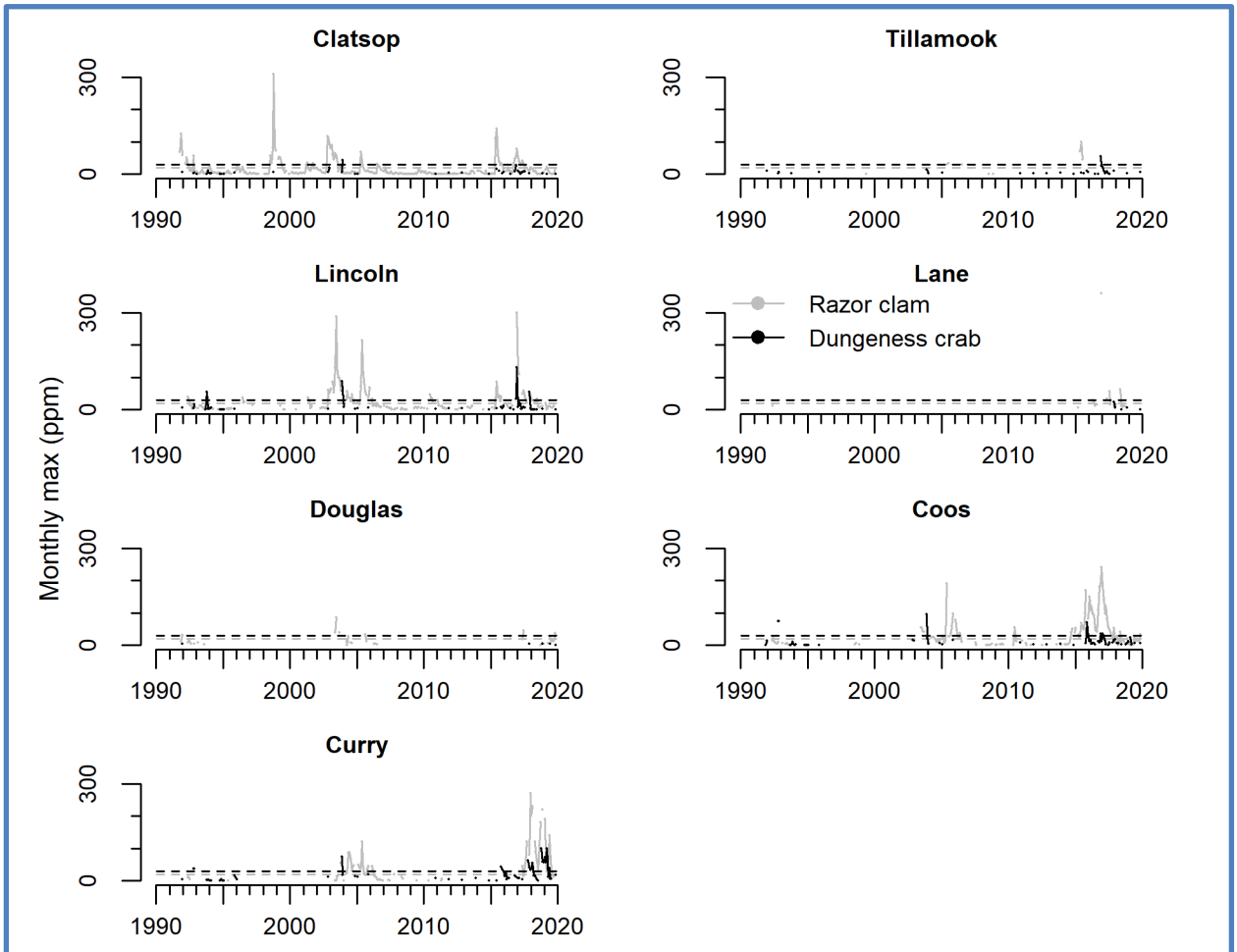

Figure E.2 Monthly maximum domoic acid concentration (ppm) in razor clams (gray) and Dungeness crab viscera (black) through 2019 by coastal counties in Oregon State (north to south). Horizontal dashed lines are the management thresholds of 20 ppm (clams, in gray) and 30 ppm (crab viscera, in black). Razor clam tissue sampling is conducted twice monthly from multiple sites across the Oregon coast, year-round, and domoic acid concentrations are determined from analyses conducted by the Oregon Department of Agriculture (ODA) using High Pressure Liquid Chromatography (HPLC).

In northern California, the razor clam fishery remained closed throughout 2019, extending a closure that began in 2016. Northern California also experienced a delay in the opening of the 2018-2019 commercial Dungeness crab fishery due to low meat quality. Even after the crab filled out, the delay extended until January 25, 2019 for Del Norte and northern Humboldt counties due to domoic acid. Across California, the 2018-2019 commercial Dungeness crab season was closed early on April 15, 2019 to avoid marine life entanglements (Figure E.3). The openings of the 2019-2020 commercial Dungeness crab fisheries were delayed in northern California due to low meat quality, and in central California to avoid marine

life entanglements, respectively; however, exceedances of domoic acid were also observed in Dungeness crab from some regions of California that eventually cleared prior to these delayed start dates.

Domoic acid can also affect California fisheries that target rock crab and spiny lobster. In Southern California, there were no domoic acid-related closures of spiny lobster or rock crab in 2019 (Figure E.3). However, the northern rock crab fishery is still closed in two areas due to domoic acid concerns (data not shown; see https://wildlife.ca.gov/Fishing/Ocean/Health-Advisories), and these areas have not been open since November of 2015.

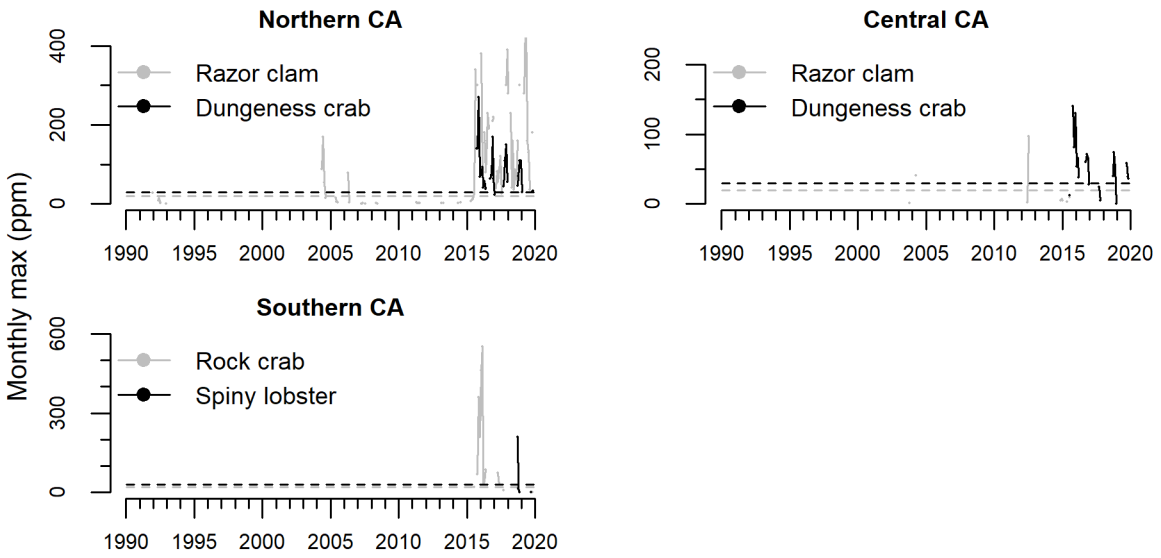

Figure E.3 Monthly maximum domoic acid concentration (ppm) in razor clams (gray) and Dungeness crab viscera (black) through 2019 in northern California (NCA; Del Norte south to Humboldt counties) and central California (CCA; Sonoma south to San Luis Obispo counties). Few to no razor clams or Dungeness crab occur in southern CA (SCA), where rock crab (gray) and spiny lobster (black) are typically monitored for domoic acid. Horizontal dashed lines are the management thresholds of 20 ppm (clams, in gray) and 30 ppm (crab viscera, in black). Data compiled by the California Department of Public Health (CDPH) from samples collected by a variety of local, tribal, and state partners and analyzed by CDPH's Food and Drug Laboratory Branch using High Pressure Liquid Chromatography (HPLC).

Appendix F SNOW-WATER EQUIVALENT, STREAMFLOW, AND STREAM TEMPERATURE

Development of habitat indicators in the CCIEA has focused on freshwater habitats. All habitat indicators are reported based on a hierarchical spatial framework. This spatial framework facilitates comparisons of data at the right spatial scale for particular users, whether this be the entire California Current, ecoregions within these units, or smaller spatial units. The framework we use divides the region encompassed by the California Current ecosystem into ecoregions (Figure 2.1b), and ecoregions into smaller physiographic units. Freshwater ecoregions are based on the biogeographic delineations in Abell et al. (2008; see also www.feow.org), who define six ecoregions for watersheds entering the California Current, three of which comprise the two largest watersheds directly entering the California Current (the Columbia and the Sacramento-San Joaquin Rivers). Within ecoregions, we summarized data using evolutionary significant units and 8-field hydrologic unit classifications (HUC-8). Status and trends for all freshwater indicators are estimated using space-time models (Lindgren and Rue 2015), which account for temporal and spatial autocorrelation.

Snow-water equivalent (SWE) is measured using two data sources: a California Department of Water Resources snow survey program (data from the California Data Exchange Center http://cdec.water.ca.gov/) and The Natural Resources Conservation Service's SNOTEL sites across Washington, Oregon, California and Idaho, http://www.wcc.nrcs.usda.gov/snow/). Snow data (Figure F.1) are converted into SWEs based on the weight of samples collected at regular intervals using a standardized protocol. Measurements at April 1 are considered the best indicator of maximum extent of SWE; thereafter snow tends to melt rather than accumulate. Data for each freshwater ecoregion are presented in Section 3.5 of the main report.

The outlook for snowpack in 2020 is limited to examination of current SWE, an imperfect correlate of SWE in April due to variable atmospheric temperature and precipitation patterns. SWE as of February 1, 2020 was below the long-term median throughout much of the region, although parts of eastern Washington, eastern Oregon, northern and southern Idaho, and northeastern California are above the median, as are several individual sites in the Cascades and the Olympic Peninsula (Figure F.1). Stations in interior central California are mostly below the median. The April 1, 2020 SWE measurements will be presented in next year's report.

Figure F.1 Snow water equivalent relative to 1981-2010 median value as of February 1, 2020. Data are from the Natural Resource Conservation Service SNOTEL database. Open circles are stations that either lack current data or long-term median data.

Mean maximum temperatures in August were determined from 446 USGS gages with temperature monitoring capability. While these gages did not necessarily operate simultaneously throughout the period of record, at least two gages provided data each year in all ecoregions. Stream temperature records are limited in California, so two ecoregions were combined. Maximum temperatures continued to exhibit strong ecoregional differences (for example, the Salish Sea / Washington Coast streams were much cooler on average than California streams). The most recent 5 years have been marked by largely average values region-wide with the exception of the Salish Sea and Washington Coast, which has much higher temperatures in the last five years compared to the period of record (Figure F.2). Recent trends in maximum August stream temperatures have been relatively stable; the recent decline in Sacramento-San Joaquin and Southern California streams is not statistically significant.

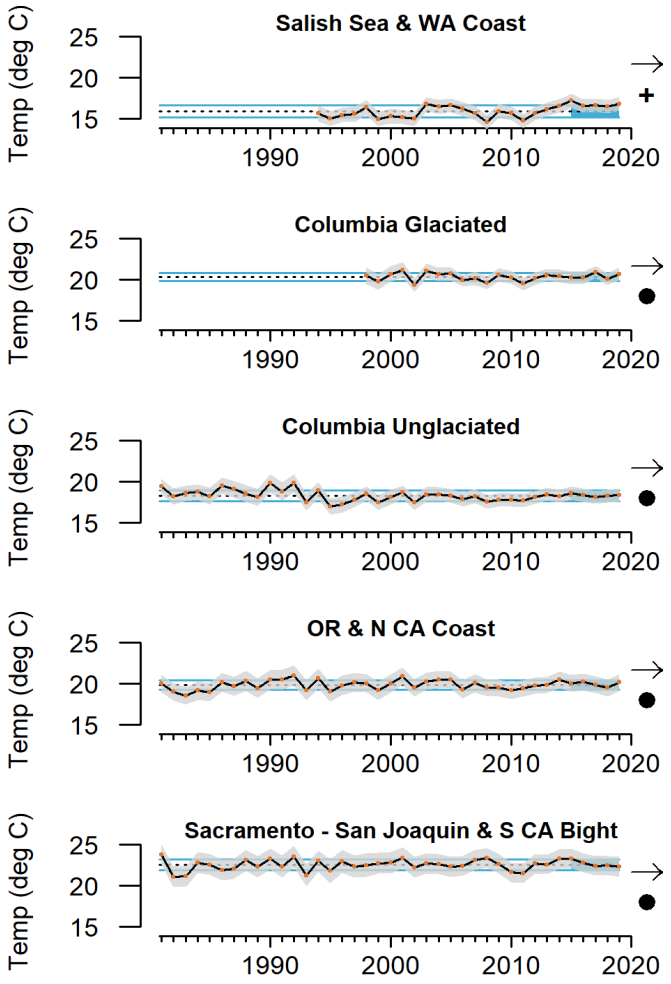

Figure F.2 Mean maximum stream temperature in August measured at 466 USGS gauges in six ecoregions from 1981-2019. Gages include both regulated (subject to hydropower operations) and unregulated systems, although trends were similar when these systems were examined separately. Error envelopes represent the 2.5% and 97.5% upper and lower credible intervals. Symbols to the right follow those in Fig. 1, but were evaluated based on whether the credible interval overlapped zero (slope of the 5-year trend) or the long-term mean (5-year mean).

Streamflow is measured using active USGS gages with records that meet or exceed 30 years in duration. Average daily values from 213 gages were used to calculate both annual 1-day maximum and 7-day minimum flows. These indicators correspond to flow parameters to which salmon populations are most sensitive. We use standardized anomalies of streamflow time series from individual gages. Across ecoregions of the California Current, both minimum and maximum streamflow anomalies have exhibited some variability in the most recent five years. At the ecoregion scale, minimum stream flows were below average with no significant trend over the past 5 years in the two northernmost ecoregions (Figure F.3, see Figure F.5 for flows by ESU). Minimum flow increased over the past 5 years for the Columbia Unglaciated, Oregon/California Coast and Sacramento/San Joaquin ecoregions, possibly reflecting the 5-year increasing trend in SWE shown in Figure 3.5; correspondingly, central and inland Chinook salmon ESUs also exhibited short-term increases in minimum flow (Figure F.5). Minimum flow in the Southern California Bight was stable over the last 5 years, and has been among the ecoregion's lowest on record for many years.

Because high rates of maximum late-winter flow are generally beneficial for juvenile salmon in inland regions but detrimental to northern coastal populations, flow conditions during egg incubation (after spawning) may have been good across a wide range of the Pacific Coast. The Salish Sea / WA coast and Columbia Glaciated ecoregions experienced downturns in maximum flow in 2019, and the Salish Sea /

WA Coast has experienced a negative short-term trend (Figure F.4; see Figure F.6 for flows by ESU). Maximum flow in most other ecoregions has been trending higher since 2015. Recent 5-year averages in maximum flow were not significantly different from long-term averages at the ecoregional level, although several ESUs—most notably Klamath, Sacramento and Central Valley, and Upper Columbia ESUs—exhibited recent 5-year averages that were greater than long-term averages (Figure F.6).

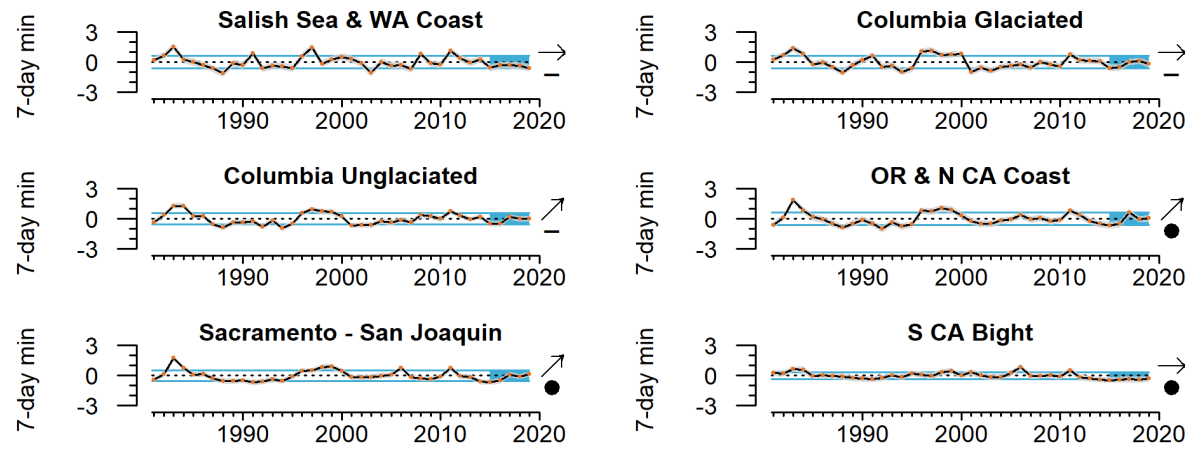

Figure F.3 Anomalies of the 7-day minimum streamflow measured at 213 gauges in six ecoregions for 1981-2019. Gages include both regulated (subject to hydropower operations) and unregulated systems, although trends were similar when these systems were examined separately. Error envelopes represent the 2.5% and 97.5% upper and lower credible intervals. Symbols to the right follow those in Fig. 1, but were evaluated based on whether the credible interval overlapped zero (slope of the 5-year trend) or the long-term mean (5-year mean).

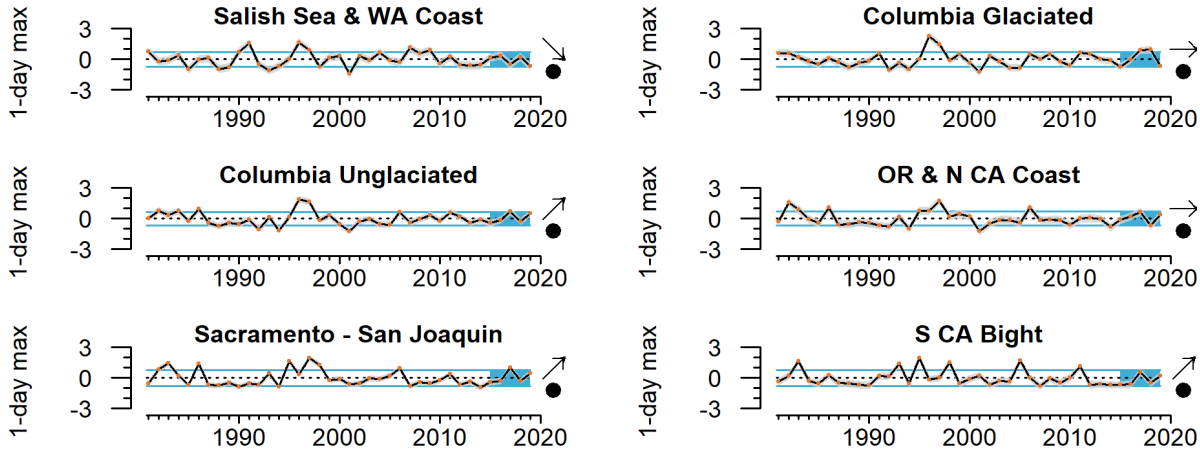

Figure F.4 Anomalies of the 1-day maximum streamflow measured at 213 gauges in six ecoregions for 1981-2019. Gages include both regulated (subject to hydropower operations) and unregulated systems, although trends were similar when these systems were examined separately. Error envelopes represent the 2.5% and 97.5% upper and lower credible intervals. Symbols to the right follow those in Fig. 1, but were evaluated based on whether the credible interval overlapped zero (slope of the 5-year trend) or the long-term mean (5-year mean).

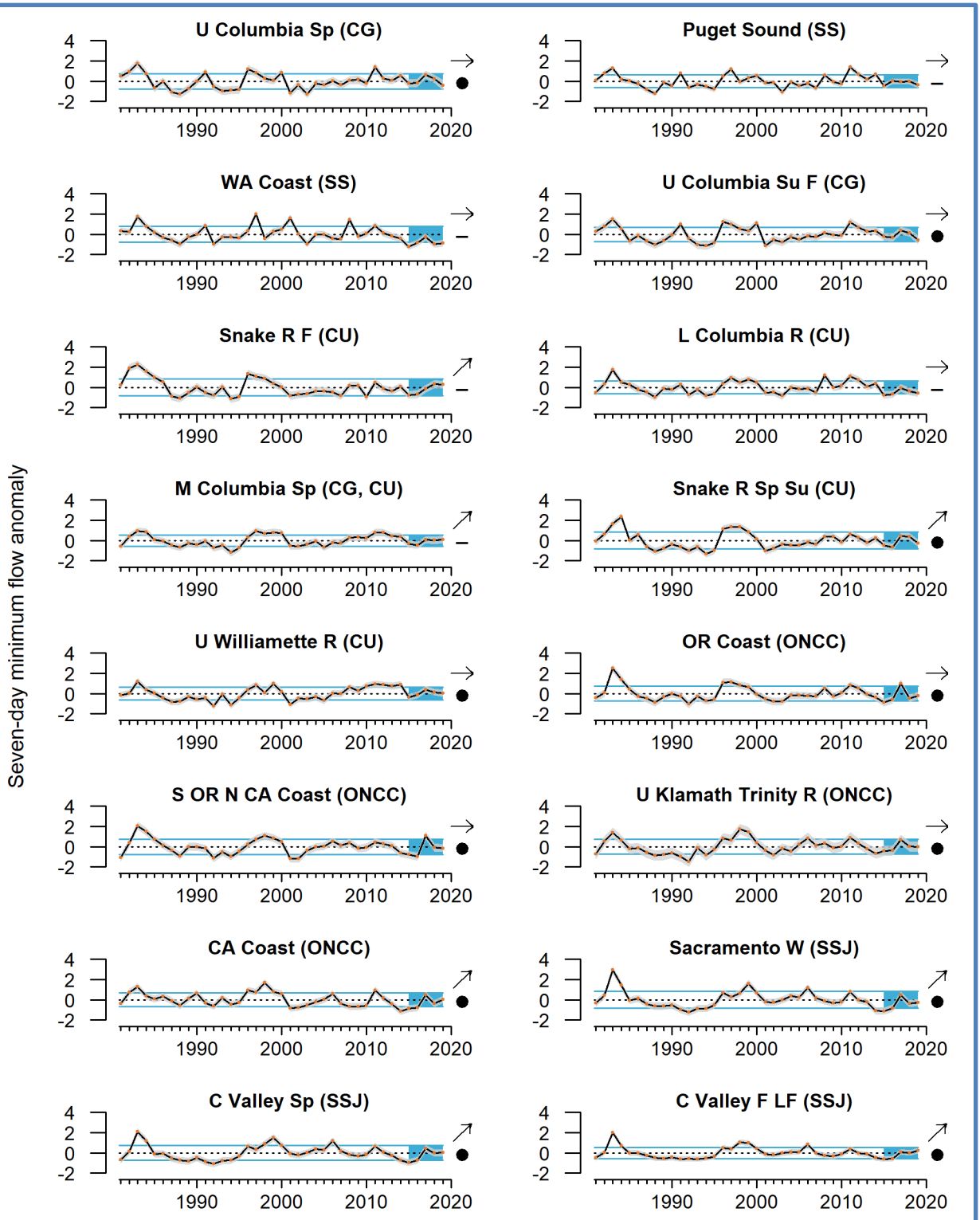

Figure F.5 Anomalies of the 7-day minimum streamflow measured at 213 gauges in 16Chinook salmon ESUs for 1981-2019. Gages include both regulated (subject to hydropower operations) and unregulated systems, although trends were similar when these systems were examined separately. Error envelopes represent the 2.5% and 97.5% upper and lower credible intervals. Symbols to the right follow those in Fig. 1, but were evaluated based on whether the credible interval overlapped zero (slope of the 5-year trend) or the long-term mean (5-year mean).

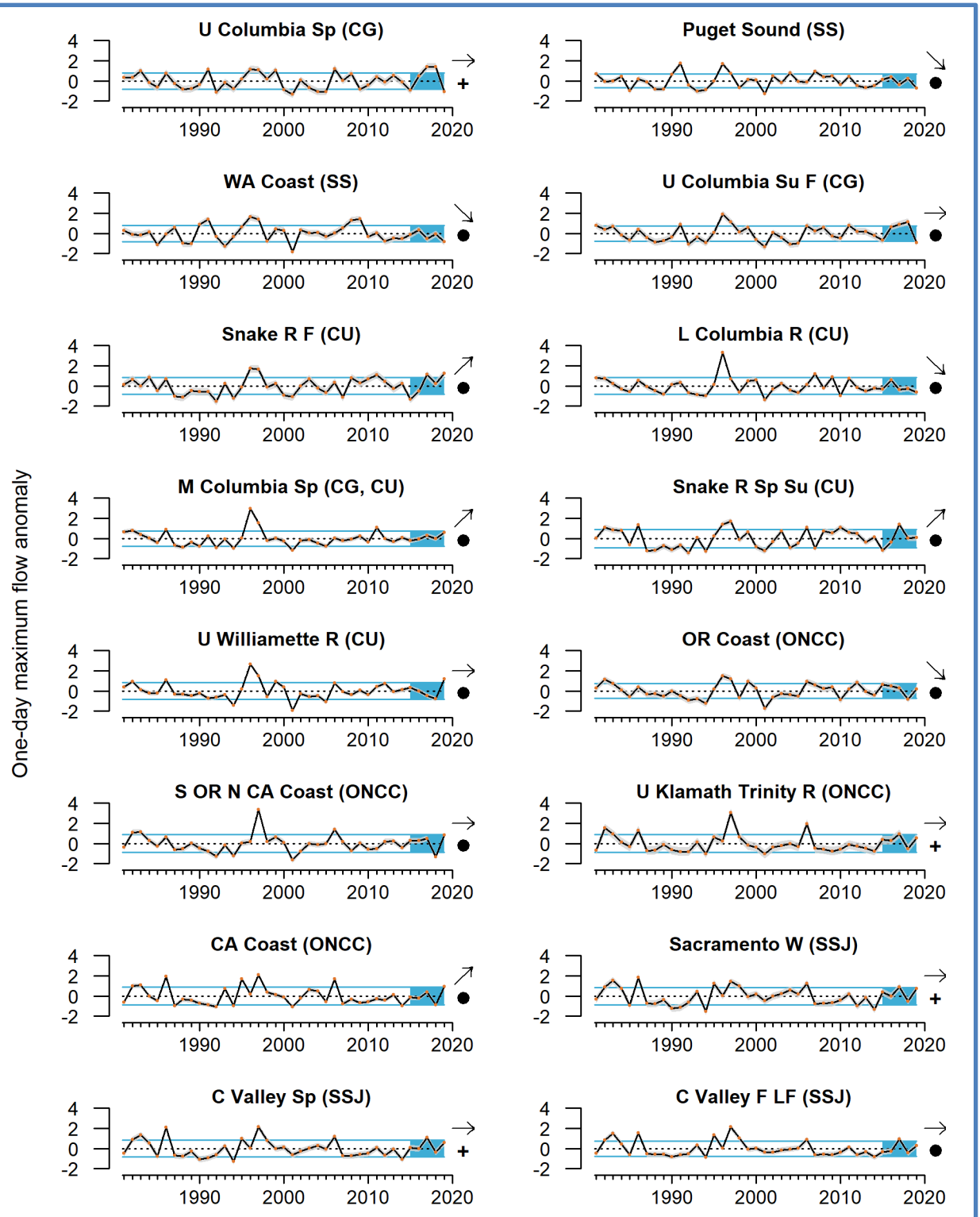

Figure F.6 Anomalies of the 1-day maximum streamflow measured at 213 gauges in 16Chinook salmon ESUs for 1981-2019. Gages include both regulated (subject to hydropower operations) and unregulated systems, although trends were similar when these systems were examined separately. Error envelopes represent the 2.5% and 97.5% upper and lower credible intervals. Symbols to the right follow those in Fig. 1, but were evaluated based on whether the credible interval overlapped zero (slope of the 5-year trend) or the long-term mean (5-year mean).

Appendix G REGIONAL FORAGE AVAILABILITY

Regional trends in forage availability are presented in Section 4.2 of the main body, using a cluster analysis method. Here we present the time series that were used in the cluster analyses, along with some additional species that are associated with the forage community.

G.1 NORTHERN CALIFORNIA CURRENT FORAGE

The Northern CCE survey (known as the "Juvenile Salmon Ocean Ecology Survey") occurs in June and targets juvenile salmon in surface waters off Oregon and Washington, but also collects adult and juvenile (age 1+) pelagic forage fishes, market squid, and gelatinous zooplankton with regularity. The gear is fished during daylight hours in near-surface waters, which is appropriate for targeting juvenile salmon.

In 2019, catches of juvenile Chinook, coho and sockeye salmon were close to average and had non-significant 5-year trends (Figure G.1.1). Chum salmon catches were above average in 2019 and

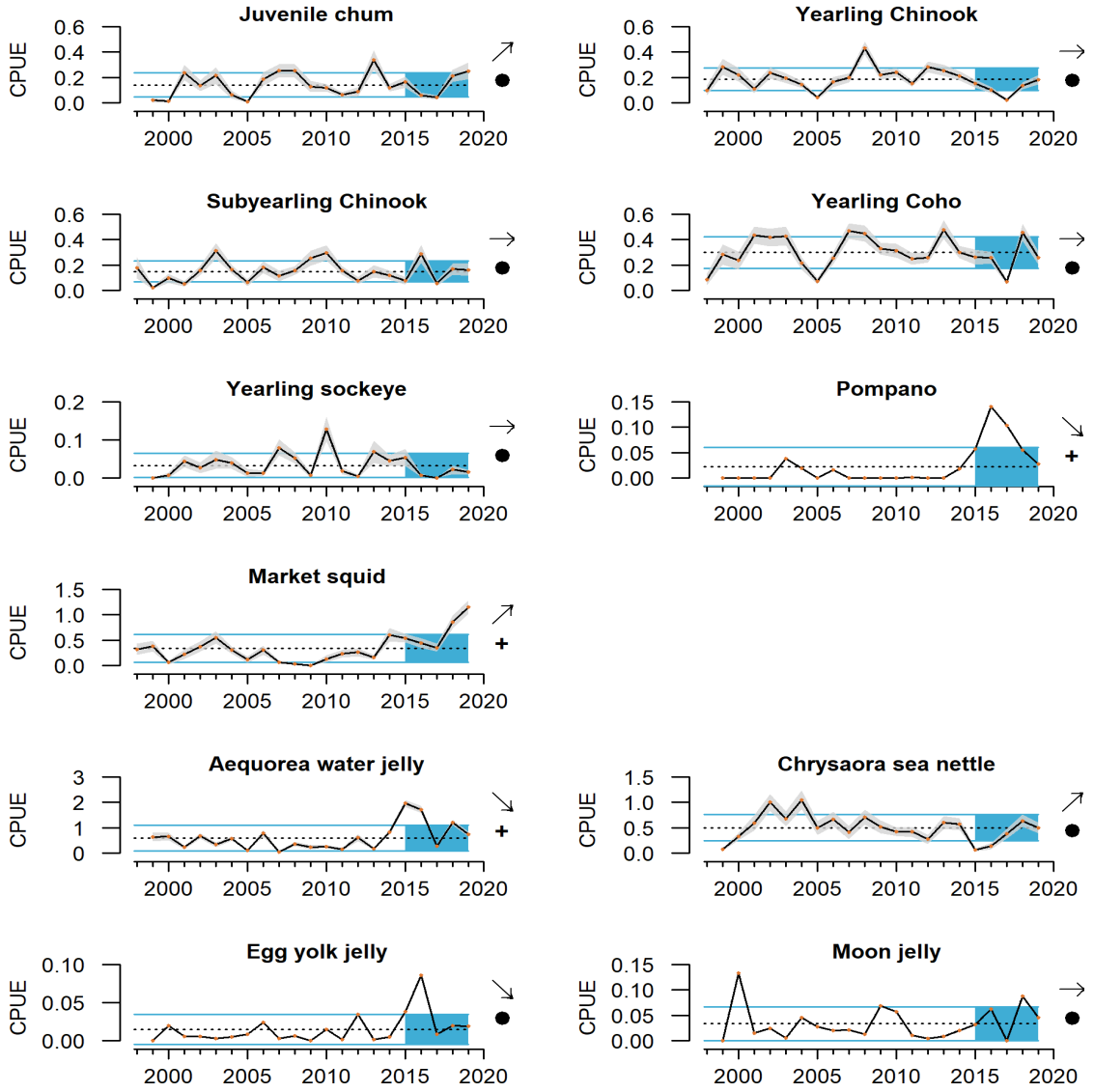

Figure G.1.1 Geometric mean CPUEs (Log$_{10}$(no/(km + 1))) of key forage groups in the Northern CCE, from surface trawls conducted as part of the NMFS Juvenile Salmon Ocean Ecology Survey, 1998-2019. Lines, colors, and symbols are as in Fig. 1.

contributed to a positive 5-year trend. Catches of market squid in 2019 were the highest on record; high catches in both 2018 and 2019 contributed to an increasing trend. Catches of *Chrysaora* jellyfish (sea nettles) have been increasing since the low in 2015 following the marine heatwave, and are near average values. Contrastingly, catches of pompano (butterfish), egg yolk jelly, and water jelly *Aequorea*, all of which peaked during the marine heatwave in 2015 and 2016, have declined.

Some prominent forage species like anchovy, sardine, herring and mackerels are caught by this survey, but not very efficiently because they tend to be deeper in the water column during daylight hours. Thus, we do not report catch-per-unit-effort (CPUE) of such species. However, researchers have tracked the proportion of hauls in which at least one individual of a given species is captured in order to get a general sense of their prevalence (see Thompson et al. 2019b, their Figure 29). In 2018-2019, the prevalence data reflect a community composed of juvenile salmon and market squid, and relatively high occurrence of herring, while warmer-water species like mackerel, water jellies and pyrosomes have declined in occurrence relative to 2015-2017.

Finally, limited krill data are available for the northern CCE from a related survey (which has been operating since 2011 as a northern extension of the forage sampling in the central CCE, described in the next section). This survey covers offshore waters from approximately Willapa Bay, Washington to the Oregon/California border. In 2019, krill densities within the survey area were ~400 individuals per tow (Figure G.1.2). Krill densities within the survey areas have been low since 2015, following the onset of coastal impacts of the 2013-2016 marine heatwave; densities prior to that were several orders of magnitude higher than at present.

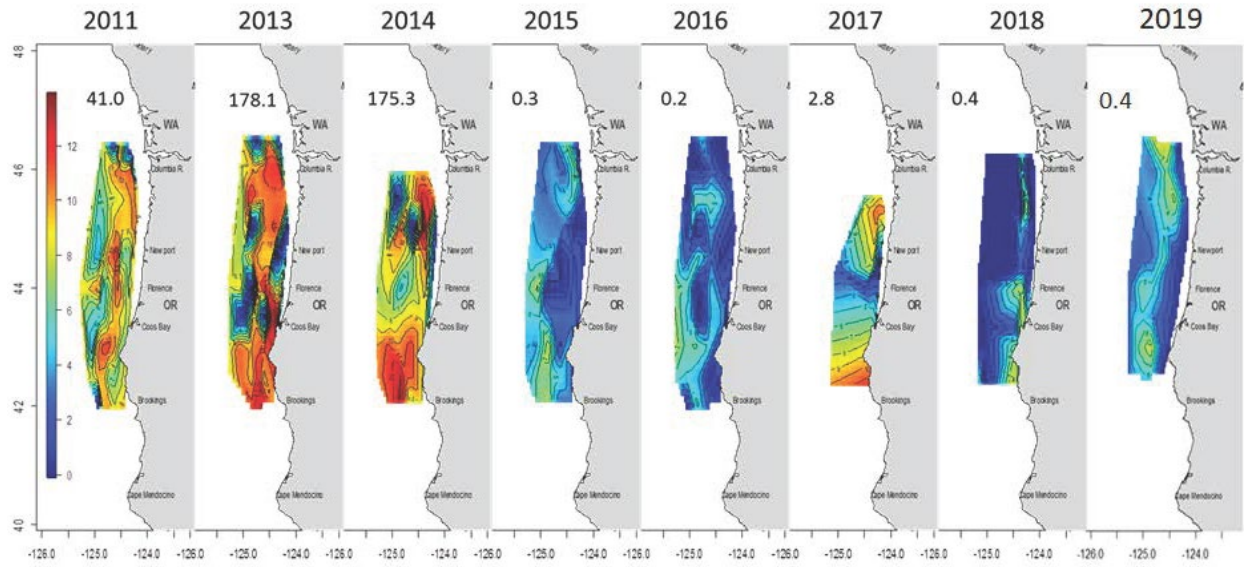

Figure G.1.2 Spatiotemporal distributions of krill off of Oregon and Washington from May/June 2011-2019 (no data from 2012). Colors represent catch per unit effort in units of thousands of krill per standardized tow. Data provided by R. Brodeur, NMFS/NWFSC.

G.2 CENTRAL CALIFORNIA CURRENT FORAGE

The Central CCE forage survey (known as the "Rockfish Recruitment and Ecosystem Assessment Survey" or RREAS) samples this region using midwater trawls, which not only collect young-of-the-year (YOY) rockfish species, but also a variety of other YOY and adult forage species, market squid, adult krill, and gelatinous zooplankton. Time series presented here are from the "Core Area" of that survey (see Figure 2.1c in the Main Report). In 2019, catches of adult anchovy increased remarkably for a second straight year, and there were also increases in adult sardine (Figure G.2.2). Market squid catches were above average for a third straight year. In contrast, there were decreases in YOY anchovy, YOY sardine, YOY hake, YOY rockfish, YOY sanddabs, and krill in 2019, and overall over the past 5 years. Krill catches in 2019 were among the lowest of the time series. Catches of jellyfish (*Aurelia* sp., *Chrysaora*) were average, and lower than the dramatic catches in 2018. Pyrosome catches were above average, after dipping to average in 2018.

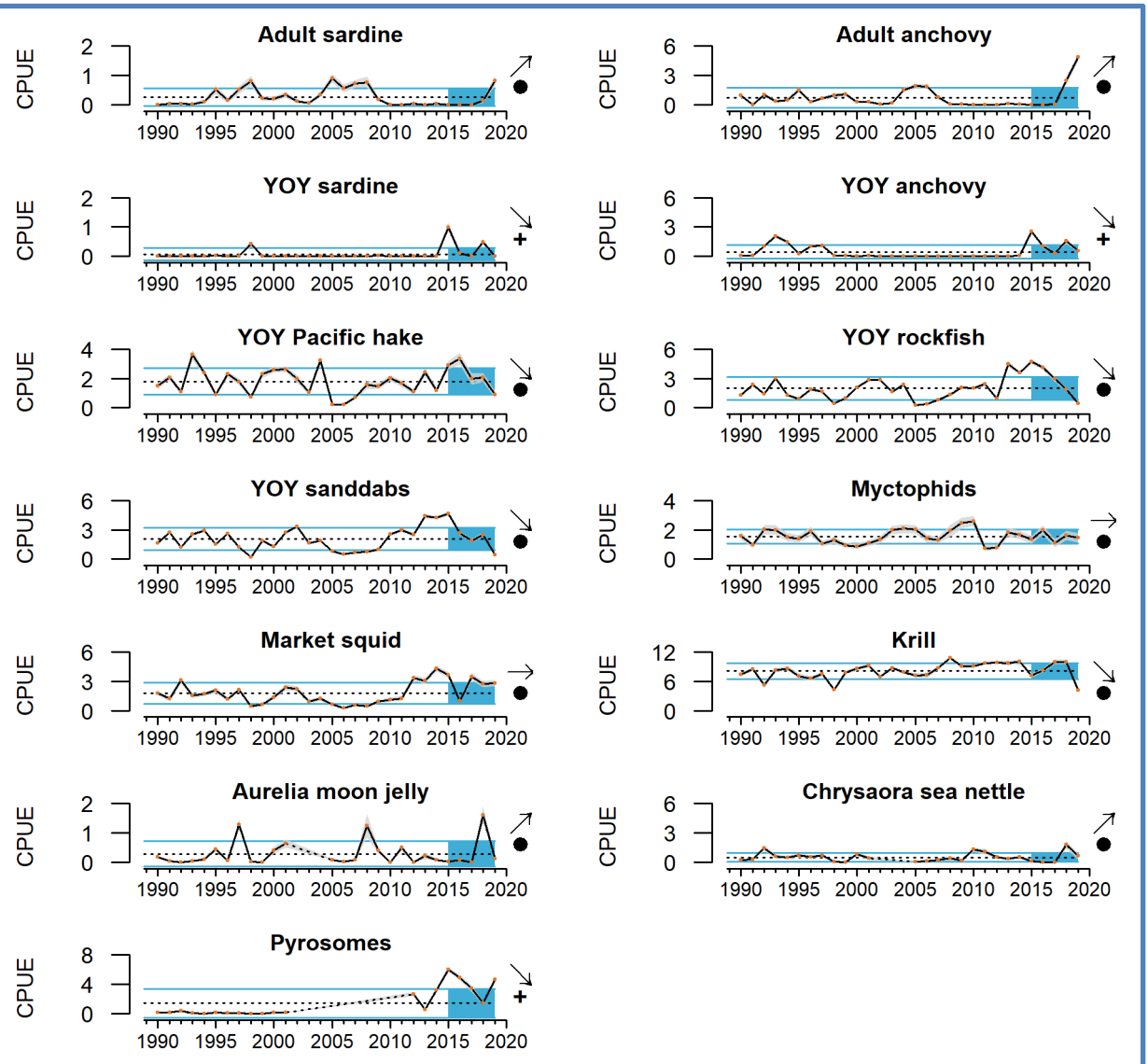

Figure G.2.1 Geometric mean CPUEs (mean (ln catch+1)) of key forage groups in the Central CCE, from the SWFSC Rockfish Recruitment and Ecosystem Assessment during 1990-2019. Lines, colors, and symbols are as in Fig. 1. Shaded errors in these figures represent standard deviations of log transformed catches.

G.3 SOUTHERN CALIFORNIA CURRENT FORAGE

The abundance indicators for forage in the Southern CCE come from fish and squid larvae collected in the spring across all core stations of the CalCOFI survey using oblique vertical tows of fine mesh Bongo nets to 212 m depth. The survey collects a variety of fish and invertebrate larvae (<5 d old) from several taxonomic and functional groups. Larval data are indicators of the relative regional abundances of adult forage fish, such as sardines and anchovy, and other species, including certain groundfish, market squid, and mesopelagic fishes. Noteworthy observations from 2019 surveys include the ongoing increase in relative abundance of anchovy—among the highest catches of the time series—and ongoing high catches of market squid and southern mesopelagic fish larvae (Figure G.3.1). In contrast, several groups experienced low or declining catches, including jack mackerel, sanddab, and sardine. Rockfish catches were average in 2019, but they have declined over the past 5 years.

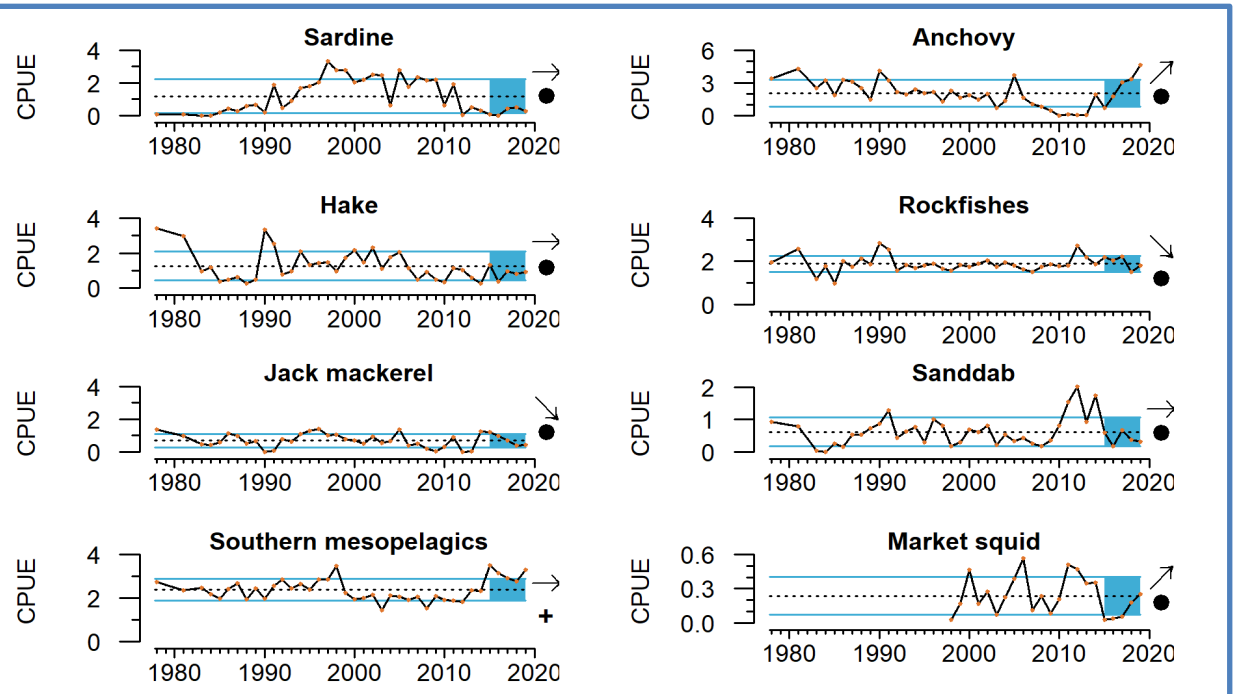

Figure G.3.1 Mean abundance (ln(abundance+1)) of the larvae of key forage species in the southern CCE, from spring CalCOFI surveys during 1978-2019. Lines, colors, and symbols are as in Fig. 1.

G.4 PYROSOME BIOMASS

Pyrosomes (*Pyrosoma atlanticum)* are pelagic tunicates known to have a subtropical distribution, and historically have been occasionally observed in southern and central California waters of the CCE; over the past several years they have become far more abundant, and the increases have been attributed to the marine heatwave that affected the CCE from 2014-2016, when anomalously warm ocean conditions may have favored pyrosome feeding and reproduction. Pyrosomes are aggregate filter feeders that consume pico- and microplankton, and in some areas have been shown to cause the depletion of chlorophyll-*a* standing stocks. Mass occurrences of pelagic tunicates have impacts on human activities, such as damaged fishing nets and clogging cooling water intakes of coastal hydropower facilities.

Recent work by Miller et al. (2019) examined the spatial distribution, abundance, and size variability of pyrosomes in the CCE. Pyrosome abundance was significantly greater in 2012–2019 compared to 1983–2001, and recent persistent abundance peaks were unprecedented. Relative biomass trends showed abundance in the CCE shifting from south to north from 2013 to 2018, while in 2019 abundance was vastly reduced in northern regions and predominately located in the central region (Figure G.4.1). In 2014-2015, pyrosome biomass was mostly off California, but spread north in 2016. In 2017 and 2018, pyrosome biomass was greater in the Oregon and Blanco regions, reaching peak relative abundance levels in the waters off of Washington, Oregon, and Northern California. By 2019, a single pyrosome was caught in surveys in the Oregon region, while pyrosome biomass was greatest in the central California region.

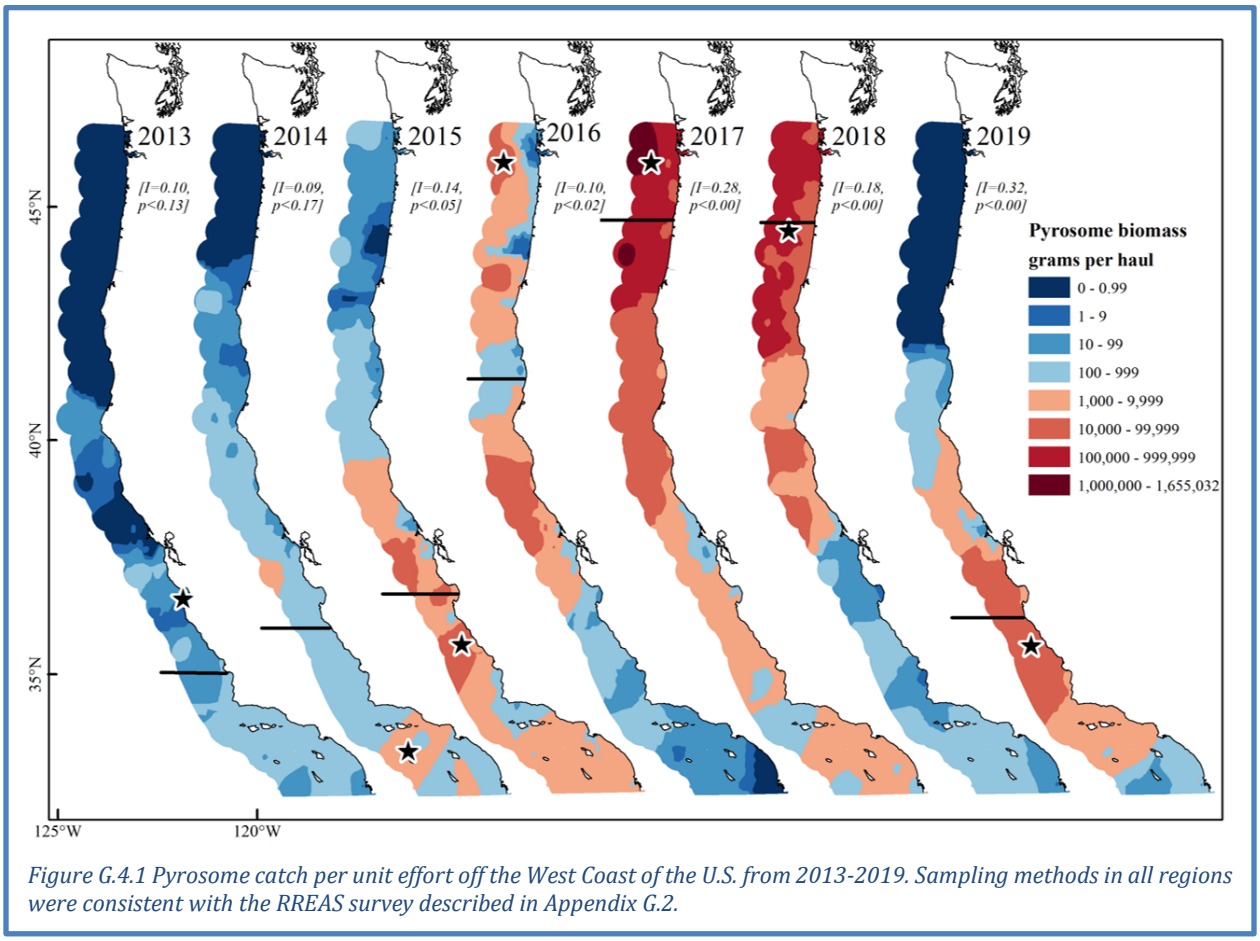

Figure G.4.1 Pyrosome catch per unit effort off the West Coast of the U.S. from 2013-2019. Sampling methods in all regions were consistent with the RREAS survey described in Appendix G.2.

Appendix H CHINOOK SALMON ESCAPEMENT INDICATORS

Salmon escapement data provide indicators of abundance and reproductive potential of naturally spawning salmon stocks. Population-specific status and trends in Chinook salmon escapement are provided in Section 4.3 of the Main Report. Figure 4.3.1 uses a quad plot to summarize recent escapement status and trends relative to full time series. These plots are useful for summarizing large amounts of data, but they may hide informative short-term variability in these dynamic species. The full time series for all populations are therefore presented here. We note again that these are escapement numbers, not run-size estimates, which take many years to develop. Status and trends are estimated for the most recent 10 years of data (unlike 5 years for all other time series in this Report) in order to account for the spatial segregation of successive year classes of salmon.

H.1 CALIFORNIA CHINOOK SALMON ESCAPEMENTS

The Chinook salmon escapement time series from California include data from as recent as 2018 extending back over 20 years, with records for some populations stretching back to the 1970s. No population showed short-term trends over the past 10 years of available data (Figure H.1.1), but escapement estimates in 2018 for two populations (Central Valley Spring, Central Valley Late) were 1 s.d. below the long-term mean for their respective time series, and several others were close to 1 s.d. below the mean. On the other hand, Klamath Fall Chinook were close to the time series average escapement in 2018. Many populations have experienced decreasing escapements from 2013-2018 after some increases in the preceding years.

The California Coast ESU data have not been updated since 2015, so the plot below is likely not representative of recent California Coast ESU escapement levels.

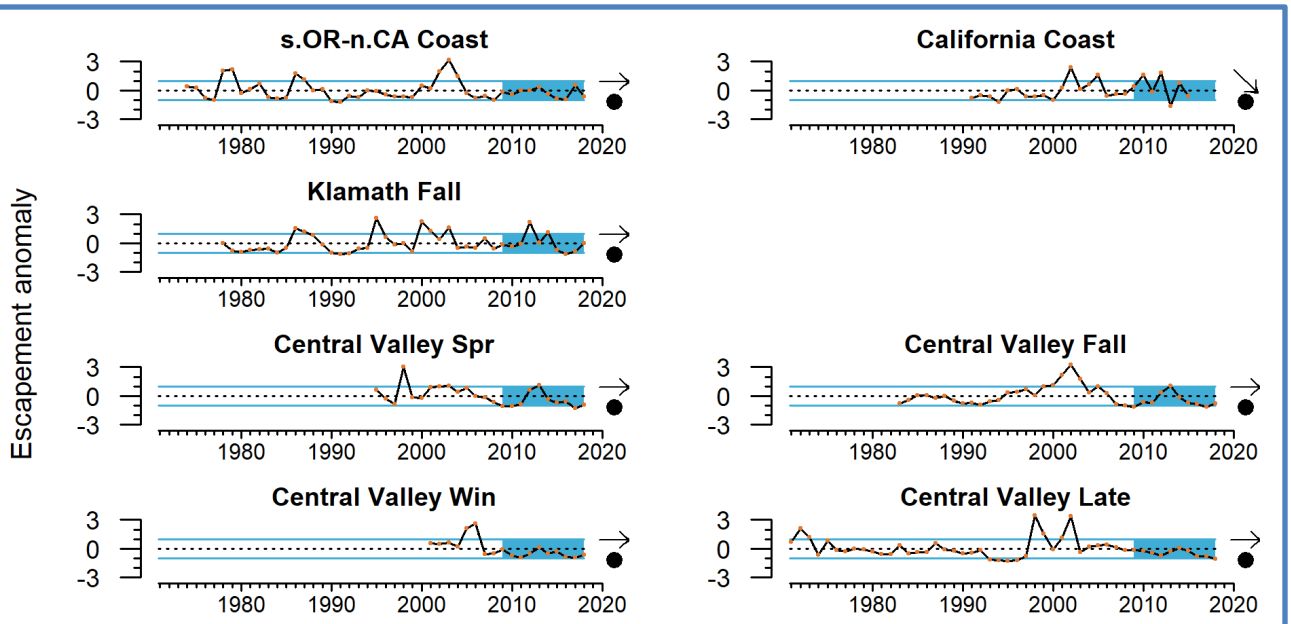

Figure H.1.1 Anomalies of escapement of wild Chinook salmon in California watersheds through 2018. Lines, colors, and symbols are as in Fig.1.

H.2 WASHINGTON/OREGON/IDAHO CHINOOK SALMON ESCAPEMENTS

The escapement time series used for Chinook salmon populations from Washington, Idaho, and Oregon extend back for up to 40+ years, and the most recent data currently available are through 2018 (Figure H.2.1). Stocks are often co-managed and surveyed by a variety of state and tribal agencies. Patterns over the past 10 years were mixed: Snake River Spring-Summer Chinook escapement had a negative trend after declining from peaks earlier in the decade, while Willamette River Spring Chinook had an increasing trend. Snake River Fall Chinook escapement in 2018 was near the long-term mean and have declined over the past few years, but several years of relatively high escapements in the middle of the decade resulted in a 10-year average that is >1 s.d. greater than the long-term mean. Upper Columbia Spring Chinook escapement has been below average for most of the last decade, while Lower Columbia Chinook escapement has been average to below average; both populations' recent averages are within 1 s.d. of the long-term mean, and have neutral escapement trends in the last ten years.

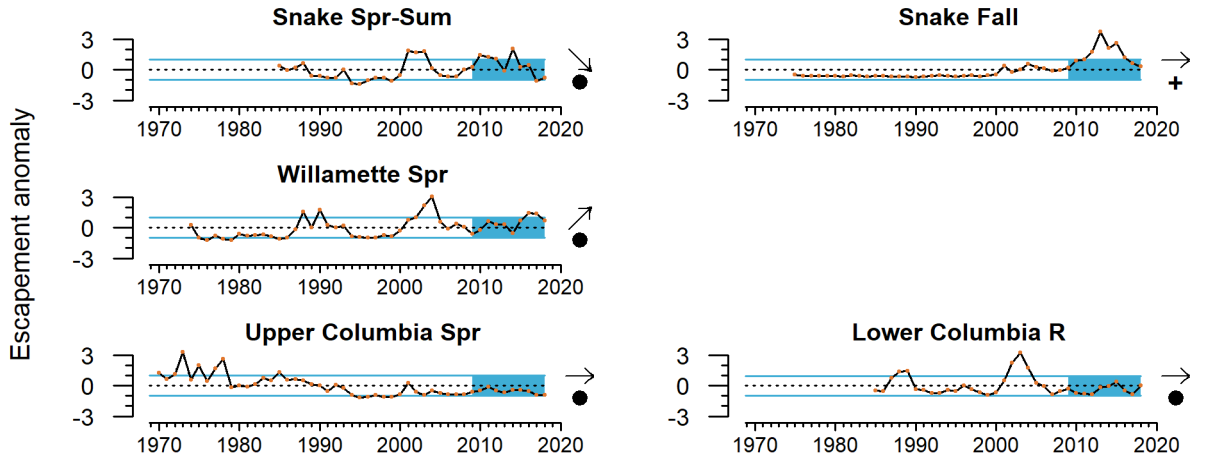

Figure H.2.1 Anomalies of escapement of wild Chinook salmon in Washington, Oregon, and Idaho watersheds through 2018. Lines, colors, and symbols are as in Fig. 1.

H.3 OUTLOOKS FOR 2020 SALMON RETURNS TO THE COLUMBIA RIVER AND OREGON PRODUCTION INDEX AREA

The main body of the report features the "stoplight" table (Table 4.3.1) that shows a ranking of indicators of conditions affecting marine growth and survival of Chinook salmon returning to the Columbia Basin, and coho salmon returning to streams in the Oregon Production Index (OPI) area. The stoplight table provides a qualitative perspective on the likely relative run sizes of salmon in the current year, based on indicator measures in the years since returning salmon originally went to sea as smolts. A somewhat more quantitative analysis based on the stoplight table is depicted at the right. Here, annual Chinook salmon counts at Bonneville Dam (Figure H.3.1, top and middle) and OPI coho smolt-to-adult survival (Figure H.3.1, bottom) over the last two decades are plotted against the aggregate mean ranking of indicators in the stoplight table, with 1-year lag for coho and 2-year lag for Chinook. The highest ranking years at the left tend to produce the highest returns and survival. The 2018 stoplight indicators had a relatively low mean rank of 11.8, for which the model equation projects returns of 131,000 Spring and 379,000 Fall Chinook salmon at Bonneville Dam in 2020 (Figure H.3.1, top and middle panels, solid arrows). The 2019 stoplight indicators had a higher mean rank of 15.1, for which the model projects smolt-to-adult survival of 1.9% for OPI coho in 2019 (Figure H.3.1, bottom, solid arrow). The stoplight indicator ranking of 15.1 in 2019 also corresponds to 2021 Bonneville counts of 104,000 Spring Chinook and 294,000 Fall Chinook (Figure H.3.1, top and middle, dashed arrows). The relationships of past salmon returns to stoplight means explain between 25% (coho) and 58% (Fall Chinook) of variance. This is a fairly simple analysis, however, given that each indicator in the stoplight table is given equal weight.

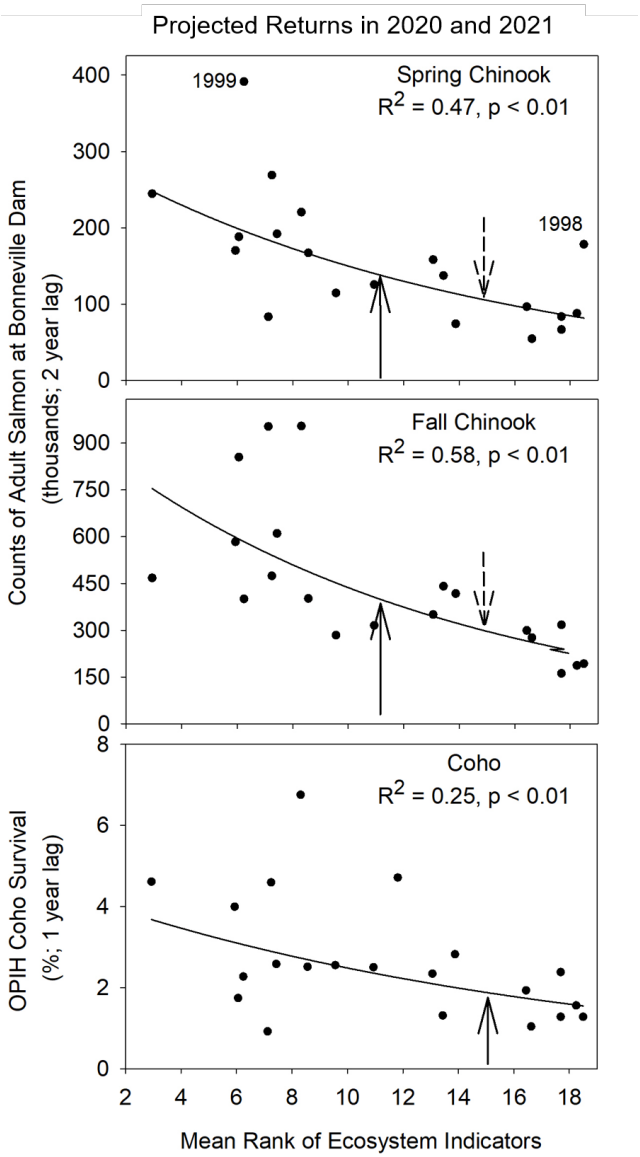

Figure H.3.1. Salmon returns versus the mean rank of ecosystem "stoplight" indicators from Table 4.3.1. Arrows show the projected returns of Chinook salmon to Bonneville Dam in 2020 (solid) and 2021 (dashed), and of coho salmon to Oregon coast streams in 2020 (solid). Data courtesy of Dr. Brian Burke (NOAA NWFSC).

A more robust quantitative analysis uses an expanded set of ocean indicators plus principal components analysis and dynamic linear modeling to estimate outlooks for salmon returns for the same region. The principal

components analysis essentially is used for weighted averaging of the ocean indicators, reducing the total number of indicators while retaining the bulk of the information from them. The dynamic linear modeling technique relates salmon returns to the principal components of the indicator data, and the approach used here also incorporates dynamic information from sibling regression modeling. The model fits very well to data for Spring Chinook and Fall Chinook at the broad scale of the Columbia River (Figure H.3.2). Model outputs with 95% confidence intervals estimate 2020 Bonneville counts of Spring Chinook salmon that are similar to returns from 2017-2019 (Figure H.3.2, top), and potential increases of Fall Chinook at Bonneville in 2020 relative to 2019, but still well below the returns of 2013-2015 (Figure H.3.2, bottom).

(In past years, a similar model was run for coho salmon returns to the Oregon Production Index region, but that model was not available this year.)

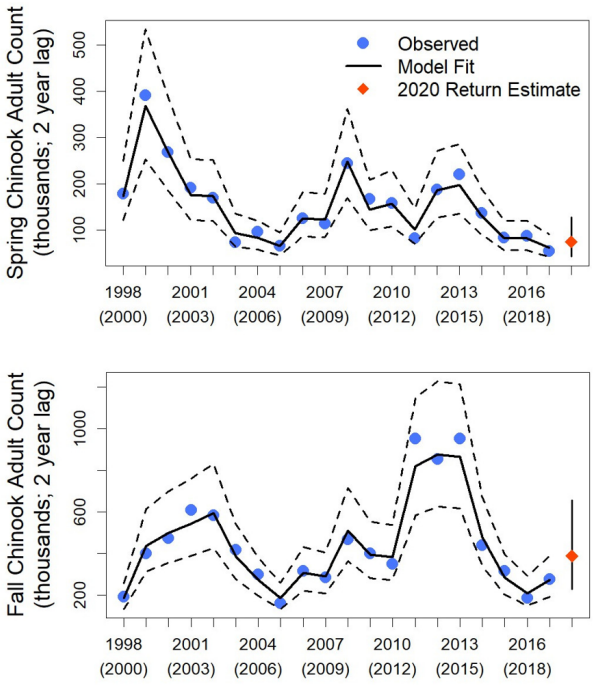

Figure H.3.2. Time series of observed and projected spring Chinook salmon adult counts (top), and fall Chinook salmon adult counts (bottom) by out-migration year. In each plot, the dark line represents the model fit and lighter lines represent 95% confidence intervals. Projections (for return year 2020) were created from a DLM (Dynamic Linear Models) with log of sibling counts and first principal component of ocean indicators as predictor variables. Courtesy of Dr. Brian Burke (NOAA, NWFSC).

Although these analyses represent a general description of ocean conditions, we must acknowledge that the importance of any particular indicator will vary among salmon species/runs. NOAA scientists and partners are working towards stock-specific salmon projections by using methods that can optimally weight the indicators for each response variable in which we are interested (Burke et al. 2013). We will continue to work with the Council and advisory bodies to identify data sets for Council-relevant stocks for which analyses like these could be possible.

Appendix I HIGHLY MIGRATORY SPECIES

Highly migratory species are discussed Section 4 of the main document (Section 4.5). The time series for abundance (Figure I.1) and recruitment (Figure I.2) are plotted here, although these time series have not been updated since our 2019 report and are thus included primarily for reference. We will update these plots in future reports as new information becomes available.

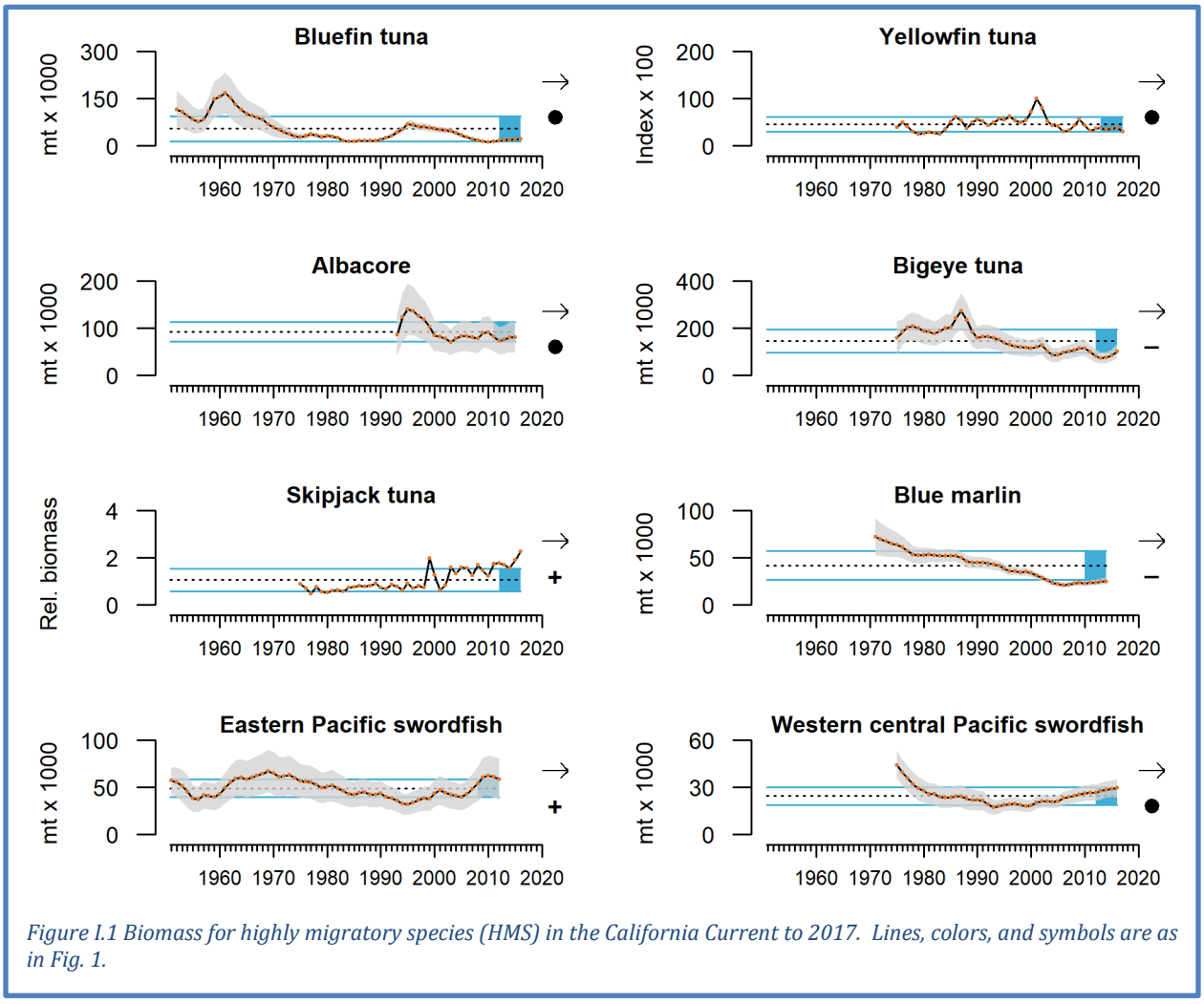

Figure I.1 Biomass for highly migratory species (HMS) in the California Current to 2017. Lines, colors, and symbols are as in Fig. 1.

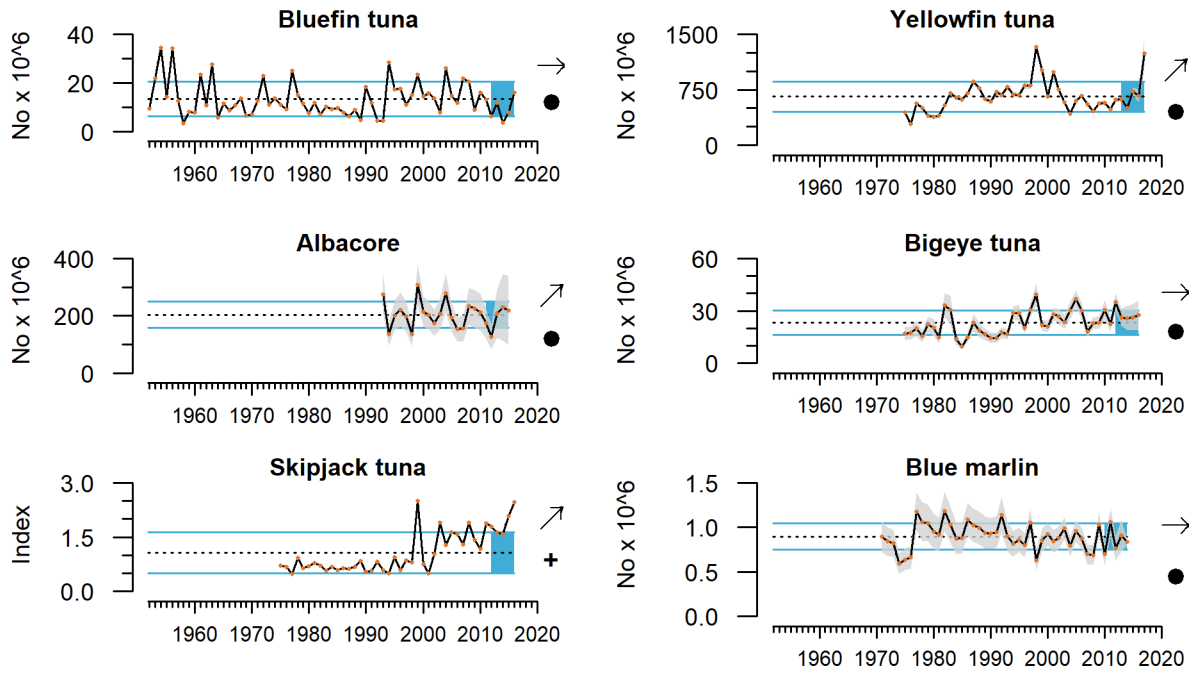

Figure I.1 Recruitment for highly migratory species (HMS) in the California Current through 2017. Lines, colors, and symbols are as in Fig. 1.

Appendix J SEABIRD DENSITY AND MORTALITY

Indicators and other information suggest that seabirds experienced mixed success throughout the California Current in 2019. Seabird indicators (at-sea densities, productivity, diet, and mortality) constitute a portfolio of metrics that reflect population health and condition of seabirds as well as links to lower trophic levels and other conditions in the California Current Ecosystem. To highlight the status of different seabird guilds and relationships to their marine environment, multiple focal species are monitored throughout the CCE. The species we report on in the sections below represent a breadth of foraging strategies, life histories, and spatial ranges.

J.1 SEABIRD AT-SEA DENSITIES

Seabird densities on the water during the breeding season can track marine environmental conditions and may reflect regional production and availability of forage. Data from this indicator type can establish habitat use and may be used to detect and track seabird population movements or increases/declines as they relate to ecosystem change. We monitor and report on at-sea densities of three focal species in the northern, central, and southern regions of the CCE. Sooty shearwaters migrate to the CCE from the southern hemisphere in spring and summer to forage near the shelf break on a variety of small fish, squid and zooplankton. Common murres and Cassin's auklets are resident species that feed primarily over the shelf; Cassin's auklets prey mainly on zooplankton and small fish, while common murres target a variety of pelagic fish (see Appendix J.4).

At-sea density patterns varied within and across seabird species among the three regions of the CCE. Sooty shearwater at-sea density anomalies underwent significant short-term declines in both the northern (NCC) and southern (SCC) regions from 2015–2019 and a significant short-term increase in the central (CCC) region (Figure J.1.1). The negative trends in the northern and southern regions

were driven by steep declines after a peak in 2015, while the 2019 positive anomaly for sooty shearwaters in the central region was the highest in the time series. Cassin's auklet at-sea density anomalies were high in the northern region 2019 but showed no recent trends in any of the regions, and recent average densities have been within ±1 s.d. of the long-term regional means. Common murre at-sea density anomaly trends were neutral over the last five years in the northern region, but showed a significant short-term increase in the central region and short-term decrease in the southern region; despite an average anomaly in 2019, recent common murre density anomalies in the south continued to be high relative to the long-term mean. In the northern region, sooty shearwaters and common murres were again aggregated near the Columbia River plume, likely attracted to concentrations of forage fishes, squid, or krill. In the southern region, it appears that recent sooty shearwater and common murre upticks relative to the 1990s and much of the 2000s have subsided.

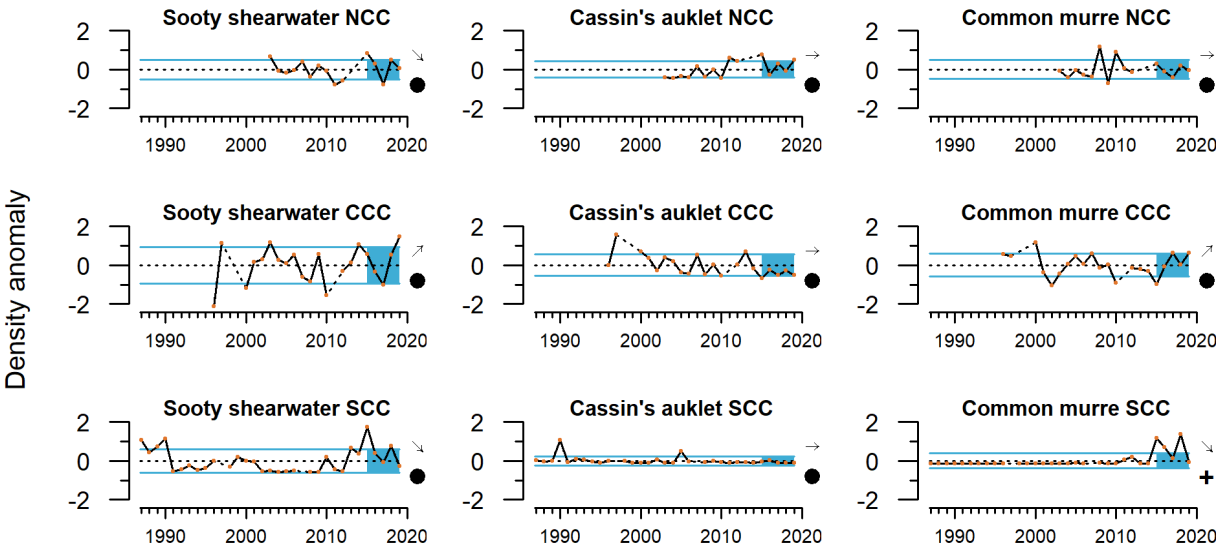

Figure J.1.1 Recent (5-year) trend and average of seabird at-sea densities during the spring in the California Current in three regions through 2019. NCC = northern California Current; CCC = central California Current; SCC = southern California Current. Lines, colors, and symbols are as in Fig. 1.

J.2 SEABIRD PRODUCTIVITY

Seabird population productivity, as measured through variables related to reproductive success, tracks marine environmental conditions and often reflects forage production near breeding colonies. We monitor and report on standardized anomalies of fledgling production per pair of breeding adults for five focal species on Southeast Farallon Island in the central region of the CCE. Data and interpretation are in the main body of the report in Section 4.7.

J.3 SEABIRD MORTALITY

Seabird mortality can track seabird populations as well as environmental conditions at regional and larger spatial scales. Monitoring beached birds (often by citizen scientists) provides information on the health of seabird populations, ecosystem health, and unusual mortality events. CCIEA reports from the anomalously warm and unproductive years of 2014–2016 noted major seabird mortality events in each year. These "wrecks"—exceptional numbers of dead birds washing up on widespread beaches—impacted Cassin's auklets in 2014, common murres in 2015, and rhinoceros auklets in

2016. (Note: The most recent wreck data for most species generally lag by one year because data collection is primarily in winter, and thus data for the 2019-2020 winter are still being collected at the briefing book deadline for the March PFMC meeting.)

In the northern CCE (Washington to northern California), the University of Washington-led Coastal Observation And Seabird Survey Team (COASST) documented beached birds at average to below-average levels for four focal species in the winter of 2018-2019 (Figure J.3.1). The Cassin's auklet encounter rate was at baseline levels in 2018 (the latest year of data), as it has been since its unusual mortality event in 2014. The common murre encounter rate was average in 2019 and showed a significant negative short-term trend since its unusual mortality event in 2015. The northern fulmar encounter rate was just below average in 2018 (the latest year of data) and showed a significant negative short-term trend. The sooty shearwater encounter rate in 2019 was below average, as it has been since a peak from 2011-2013. As mentioned in the main body of the report, preliminary information suggests that an unusual post-breeding mortality event involving rhinoceros auklets was also documented in Washington and Oregon in the fall of 2019, possibly indicating declining foraging conditions for these primarily piscivorous birds in the latter half of 2019 in the northern CCE.

Although encounter rates of indicator species in the COASST survey were near their long-term means in 2019, there was a significant mortality event in COASST's southern-most regions that is not evident in the spatially aggregated data shown in Figure J.3.1. Elevated numbers of dead adult common murres on beaches were documented during the breeding season in Humboldt and Mendocino counties in northern California. In Mendocino County, spring encounter rates were roughly an order of magnitude above normal (data not shown), and birds appeared emaciated.

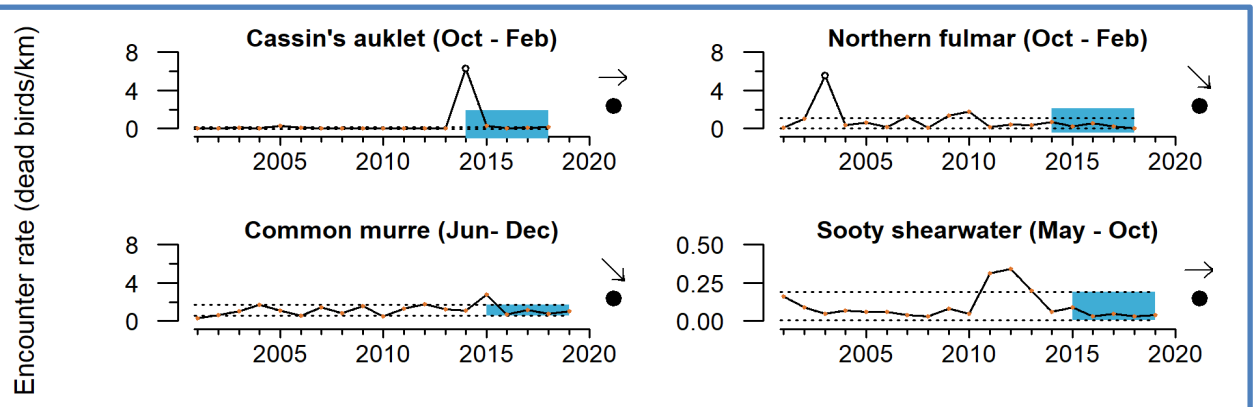

Figure J.3.1 Encounter rate of dead birds on beaches of Washington, Oregon and northern California through 2019. The mean and trend of the last five years is evaluated versus the mean and s.d. of the full time series but with the outliers removed. Open circles indicate outliers. The dashed lines indicate upper and lower s.d. of the full time series with outliers removed. Blue shaded box indicates the evaluation period and the upper and lower s.d. of the full time series with the outliers included. Data provided by the Coastal Observation and Seabird Survey Team (https://depts.washington.edu/coasst/).

In the central region of the CCE (Bodega Bay, CA to Point Año Nuevo, CA), the BeachWatch program documented beached birds at average to below average levels for five focal species in 2018 (Figure J.3.2). The Brandt's cormorant encounter rate was just below average in spring-fall 2019 and showed a significant negative short-term trend following the peak in 2015. The Cassin's auklet encounter rate continued at low baseline levels in 2017-2018 (the most recent year of data), as it has since a peak in 2013-2014. The common murre encounter rate was above average in 2019; common murre encounter rates have been increasing in recent years but remain well below the peak from the wreck in 2014-2015. The sooty shearwater encounter rate was close to average in spring-fall 2019; the peak it also experienced in 2015 was not sharp enough to result in a short-term negative trend. The northern fulmar encounter rate was just below average in 2017-2018, as it has been since a peak in 2009-2010.

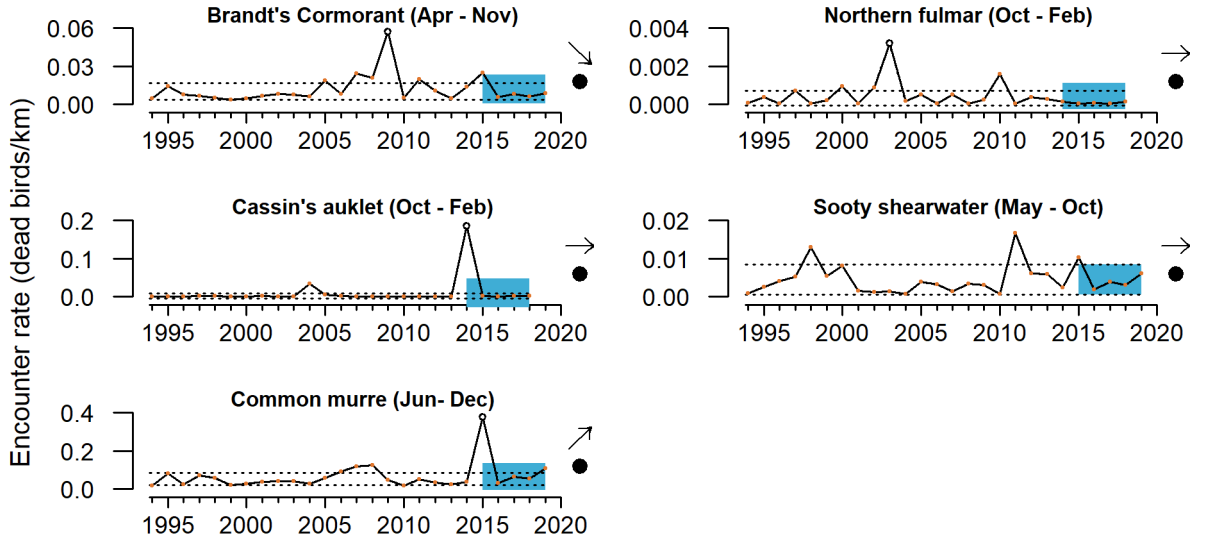

Figure J.3.2. Encounter rate of bird carcasses on beaches in north-central California through 2019. The mean and trend of the last five years is evaluated versus the mean and s.d. of the full time series but with the outliers removed. Open circles indicate outliers. Dotted lines indicate the upper and lower s.d. of the full time series with outliers removed. The blue box indicates the evaluation period and the upper and lower s.d. of the full time series with the outliers included. Annual data for Cassin's auklet and northern fulmar are calculated through February of the following year. Data provided by BeachWatch (https://farallones.noaa.gov/science/beachwatch.html).

Another survey of beached seabirds on California beaches occurs from Point Año Nuevo to Malibu, conducted by the BeachCOMBERS program. In the past, we have reported on two survey regions: north (Point Año Nuevo to Lopez Point, CA) and central (Lopez Point to Rocky Point, CA). These data have not been updated since last year's report, which was current through 2018 and generally found encounter rates at average to below-average levels (Figure J.3.3).

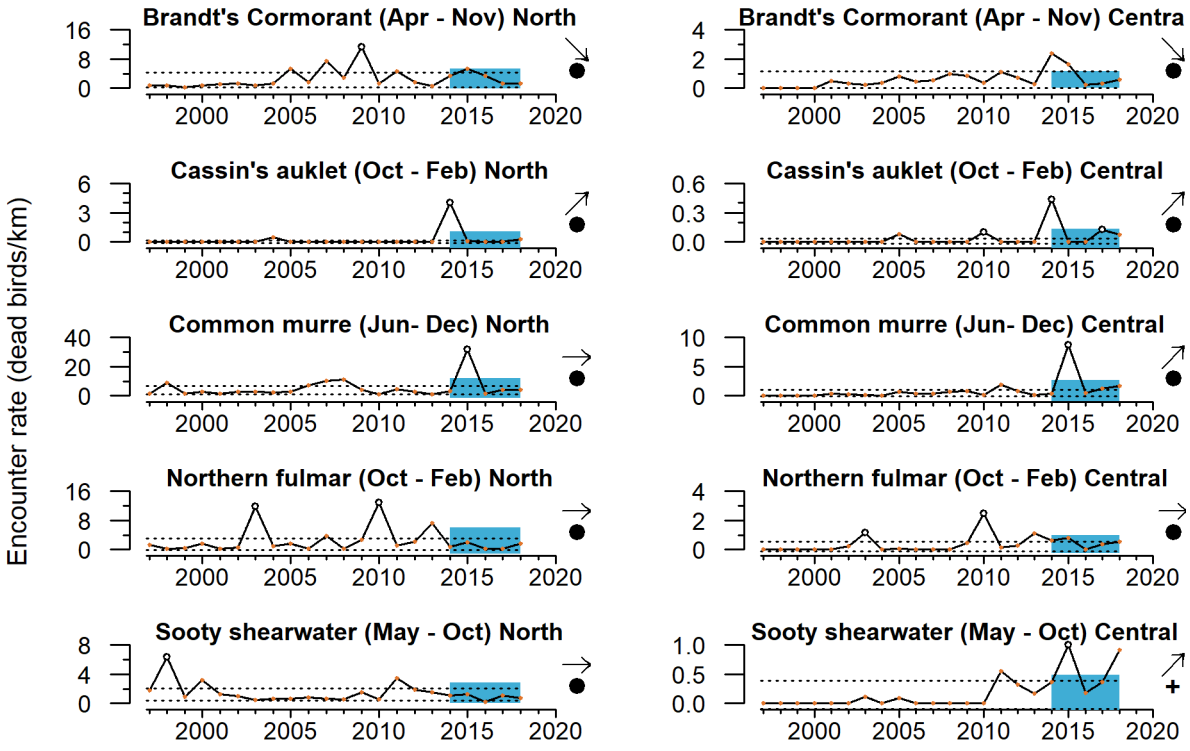

Figure J.3.1. Encounter rate of dead birds on west coast beaches through 2018. The mean and trend of the last five years is evaluated versus the mean and s.d. of the full time series but with the outliers removed. Open circles indicate outliers. Dotted lines indicate the upper and lower s.d. of the full time series with outliers removed. The blue shaded box indicates the evaluation period and the upper and lower s.d. of the full time series with the outliers included. Data from BeachCombers.org

J.4 SEABIRD DIETS

Seabird diet composition during the breeding season tracks marine environmental conditions and often reflects production and availability of forage within regions. Here, we present some seabird diet data that may shed light on foraging conditions along the west coast in 2019. We are working with partner research organizations to better integrate this information into our reporting.

West coast researchers have long-term diet data for five key species in the northern and central CCE. Rhinoceros auklets forage primarily on pelagic fishes in shallow waters over the continental shelf, generally within 50 km of colonies, and they return to the colony after dusk to deliver multiple whole fish to their chicks. Common murres forage primarily on pelagic fishes in deeper waters over the shelf and near the shelf break, generally within 80 km of colonies, and they return to the colony during daylight hours to deliver single whole fish to their chicks. Cassin's auklets forage primarily on zooplankton in shallow water over the shelf break, generally within 30 km of colonies; they forage at day and night and return to the colony at night to feed chicks. Brandt's cormorants forage primarily on pelagic and benthic fishes in waters over the shelf, generally within 20 km of breeding colonies, and they return to the colony during the day to deliver regurgitated fish to their chicks. Pigeon guillemots forage primarily on small benthic and pelagic fish over the shelf, generally within 10 km of colonies, and they return to the colony during the day to deliver a single fish to their chicks.

The first key finding from seabird diet studies pertains to the relatively good production of fledglings at seabird colonies in the northern CCE, such as at Destruction Island, Washington and Yaquina Head, Oregon. Birds at these colonies tend to feed in relatively nearshore waters, where forage species such

as smelts are abundant and may supplement forage from open waters; smelts are not sampled effectively by the forage surveys described elsewhere (Section 4.2, Appendix G), but seabird diets from these colonies suggest that smelt were abundant in 2019 (Figure J.4.1 and Figure J.4.2). At Destruction Island, the proportion of smelts in the diets of rhinoceros auklets provisioning chicks was the highest that has been recorded and showed a significant positive short-term trend (Figure J.4.1). The proportions of anchovies and herring in rhinoceros auklet diets were below average in 2019, and the proportion of juvenile rockfish continued to be low since it peaked in 2016.

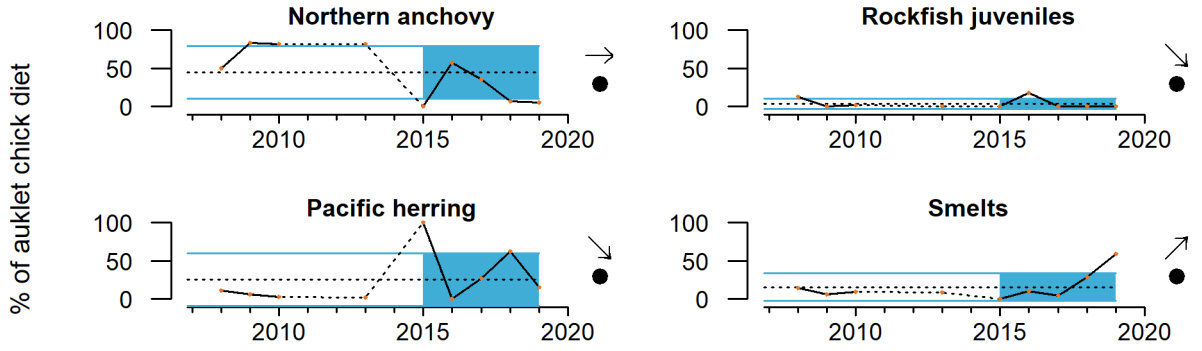

Figure J.4.2. Rhinoceros auklet chick diets at Destruction Island through 2019. Rhinoceros auklet chick diets at Destruction Island through 2019. Lines and symbols as in Fig. 1. Data courtesy of the Washington Rhinoceros Auklet Ecology Project (scott.pearson@dfw.wa.gov). Lines, colors, and symbols are as in Fig. 1.

Similarly, at Yaquina Head, the proportion of smelts in the diet of common murres provisioning chicks was above average in 2019, after a below-average value in 2018 (Figure J.4.2). The proportions of herring and sardine in the murre diet were below average in 2019 and showed a significant short-term decline. The proportion of Pacific sandlance in the murre diet was below average in 2019. The proportion of flatfishes in the murre diet was above average for the second straight year and showed a significant positive short-term trend. The proportion of rockfish in the murre diet in was well below average for the fourth straight year, considerably lower than peaks in 2008 and 2010.

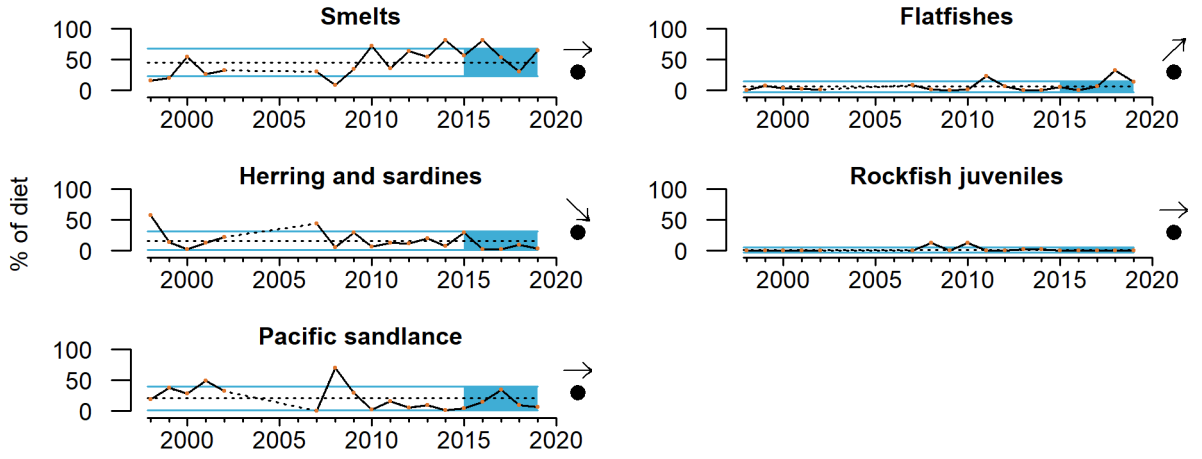

Figure J.4.3.Common murre chick diets at Yaquina Head through 2019. Data provided by the Yaquina Head Seabird Colony Monitoring Project (rob.suryan@noaa.gov). Lines, colors, and symbols are as in Fig. 1.

At colonies off central California, there are diet trends available for seabirds from Southeast Farallon Island (SEFI). Among piscivores, there has been increasing reliance on anchovy and decreasing

reliance on juvenile rockfish over the past five years. The proportions of anchovy in the diets of Brandt's cormorants, rhinoceros auklets and common murres provisioning chicks on SEFI were well above average in 2019 and showed significant positive short-term trends, while the proportions of rockfish in these species' diets were well below average in 2019 and showed significant negative short-term trends (Figure J.4.3). Pigeon guillemots showed a similar decline in juvenile rockfish. In addition, the proportion of salmonids in common murre diets at SEFI was well below average in 2019. Finally, Cassin's auklets, which feed heavily on krill, are only current through 2018, prior to the 2019 decline in krill seen off central California (Figure G.2.2). The proportion of *Euphausia pacifica* in the diet of SEFI Cassin's auklets was above average and showed a significant positive short-term trend, while the proportion of *Thysanoessa spinifera* in the auklet was near average but the recent mean is significantly greater than the long-term mean.

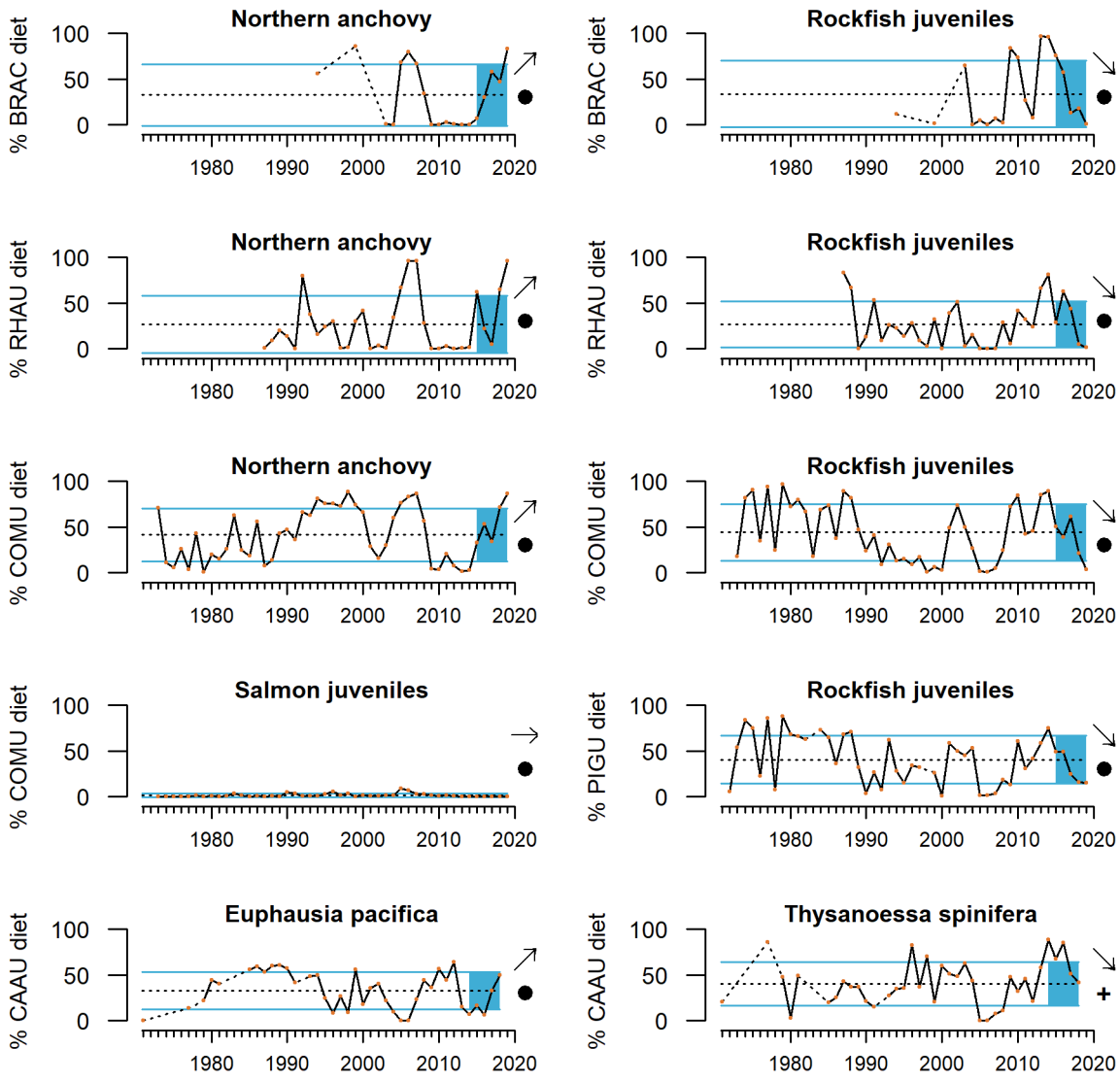

Figure J.4.4. Southeast Farallon Island seabird diets 2019. BRAC = Brandt' cormorant; CAAU = Cassin's auklet; COMU = common murre; PIGU = pigeon guillemot; RHAU = rhinoceros auklet. Lines, colors, and symbols are as in Fig. 1.

At another central California site, Año Nuevo Island, researchers noted that anchovy accounted for nearly 100% of the diets of rhinoceros auklets provisioning chicks in both 2018 and 2019; other prey resources like rockfish juveniles, market squid and Pacific saury, were very rarely delivered to chicks (data not shown). The size of anchovies returned to chicks on Año Nuevo Island in 2019 was above average and has increased since 2014-2016 (Figure J.4.4). Researchers expressed concern that these anchovy were too large to be ingested by rhinoceros auklet chicks, which may have contributed to the poor fledgling production in central California (e.g., Figure 4.7.1) despite the apparent abundance of anchovy.

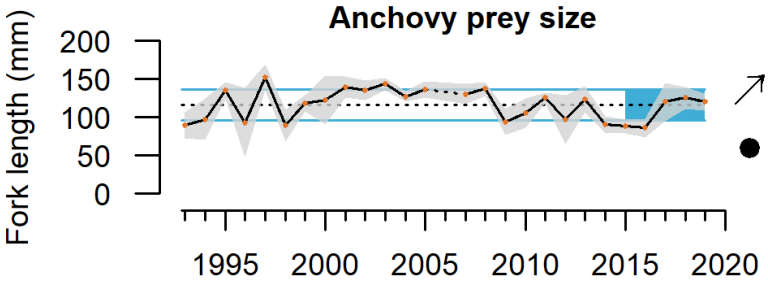

Figure J.4.4 Fork length of anchovy brought to rhinoceros auklet chicks at Año Nuevo from 1993-2019. Error envelope shows +/- 1.0 s.d. Data provided by Oikonos/Point Blue (ryan@oikonos.org). Lines, colors, and symbols are as in Fig. 1.

Appendix K STATE-BY-STATE FISHERY LANDINGS AND REVENUES

The Council and the EWG have requested information on state-by-state landings and revenues from fisheries; these values are presented here. Data for landings and revenue were available for all states through 2018 at the March 2020 Briefing Book deadline. Fishery landings and revenue data are best summarized by the Pacific Fisheries Information Network (PacFIN, http://pacfin.psmfc.org) for commercial landings and by the Recreational Fisheries Information Network (RecFIN, http://www.recfin.org) for recreational landings. Landings provide the best long-term indicator of fisheries removals. Revenue was calculated based on consumer price indices for 2018.

K.1 STATE-BY-STATE LANDINGS

Total fisheries landings in California have decreased to the lowest levels of the time series in recent years, primarily due to steep decreases in landings of market squid in 2015, 2016 and 2018 (Figure K.1.1). Commercial landings of CPS finfish were >1 s.d. below long-term averages, while salmon, groundfish (excluding hake) and other species were near the lowest levels observed over the last 5 years. Crab landings have varied within ±1 s.d. of time series averages over the last 5 years, but were above average in 2017 and 2018. Methods for sampling and calculating total mortality in recreational fisheries changed recently, leading to shorter comparable time series than shown in previous reports. Recreational landings in California (excluding salmon and Pacific halibut) had increased from 2008 to 2015 due to large increases in catches of yellowfin tuna, yellowtail and lingcod, but subsequent decreased landings in these three species are now responsible for the current decreasing trend

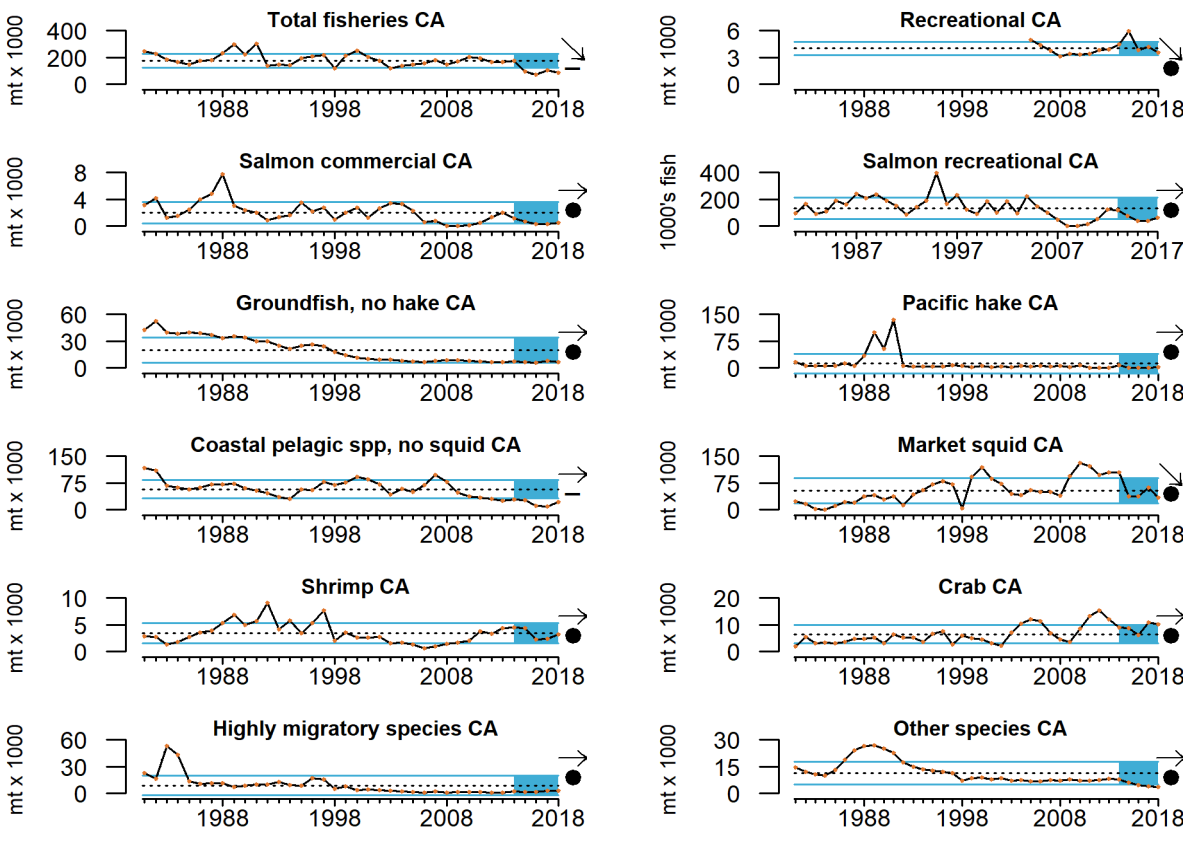

Figure K.1.1 Annual landings of West Coast commercial (data from PacFIN) and recreational (data from RecFIN) fisheries, including total landings across all fisheries from 1981-2018 in California (CA). Lines, colors, and symbols as in Fig. 1.

observed from 2014-2018 (Figure K.1.1). Recreational salmon landings (Chinook and coho) were relatively unchanged and at the lower boundary of the time series from 2014–2018.

Total fisheries landings in Oregon have varied but were above the time series average from 2014–2018 (Figure K.1.2). These patterns were primarily driven by recent landings of hake that were the highest of the time series. Commercial landings of salmon, shrimp and HMS species decreased from 2014–2018. Groundfish (excluding hake) and crab landings increased by >1 s.d. from long-term averages over the last five years. CPS finfish and other species landings were consistently within ±1 s.d. of time series averages. Landings of market squid in Oregon have been at or near 0 across the time series, but landings over 1200 tons in 2016 and 3200 tons in 2018 suggests the potential for new fishing opportunity.

Methods for sampling and calculating total mortality in recreational fisheries changed recently, leading to shorter comparable time series than shown in previous reports. Recreational fisheries landings (excluding salmon and Pacific halibut) in Oregon showed a decreasing trend from 2014–2018 (Figure K.1.2). This decrease is primarily due to decreases in albacore and black rockfish landings. Chinook and coho salmon recreational landings showed no recent trends but were near the lower limits of the time series observations over the last five years.

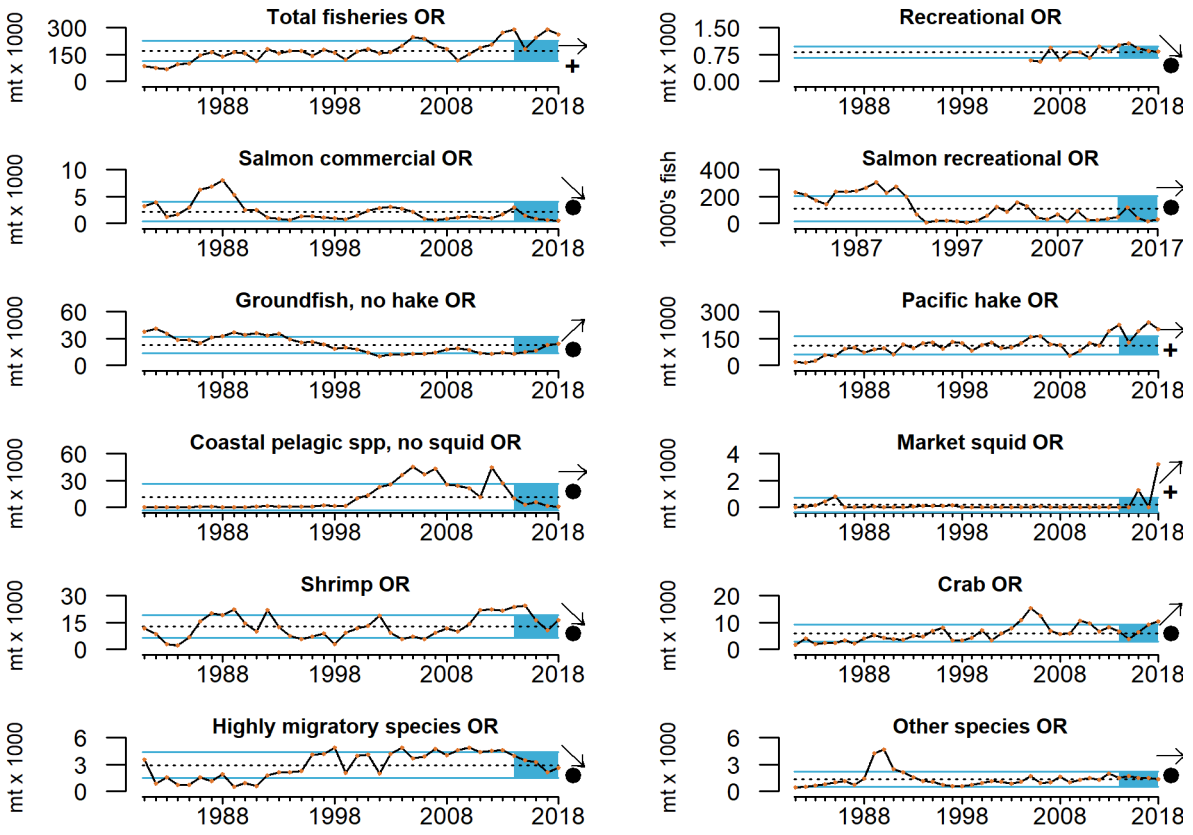

Figure K.1.2 Annual landings of West Coast commercial (data from PacFIN) and recreational (data from RecFIN) fisheries, including total landings across all fisheries from 1981-2018 in Oregon (OR). Lines, colors, and symbols as in Fig. 1.

Total fisheries landings in Washington increased sharply from 2014–2018, with particularly low landings in 2015 and a large increase in 2017 (Figure K.1.3). These patterns were driven by large increases in hake landings from 2015–2017. Shrimp and HMS landings decreased over the last five years. Landings of groundfish (excluding hake) were consistently below time series averages from 2014–2018, while landings of salmon, CPS finfish, crab and other species showed no current trends and were within ±1 s.d. of time series averages over the last five years.

Methods for sampling and calculating total mortality in recreational fisheries changed recently, leading to shorter comparable time series than shown in previous reports. Total landings of recreational catch (excluding salmon and halibut) in Washington state decreased from 2014–2018, but remained within ±1 s.d. of the full time series average (Figure K.1.3). The decrease is primarily due to decreases in albacore and black rockfish landings since 2016. Recreational landings of Chinook and coho salmon were highly variable, but within ±1 s.d. of time series averages over the last five years.

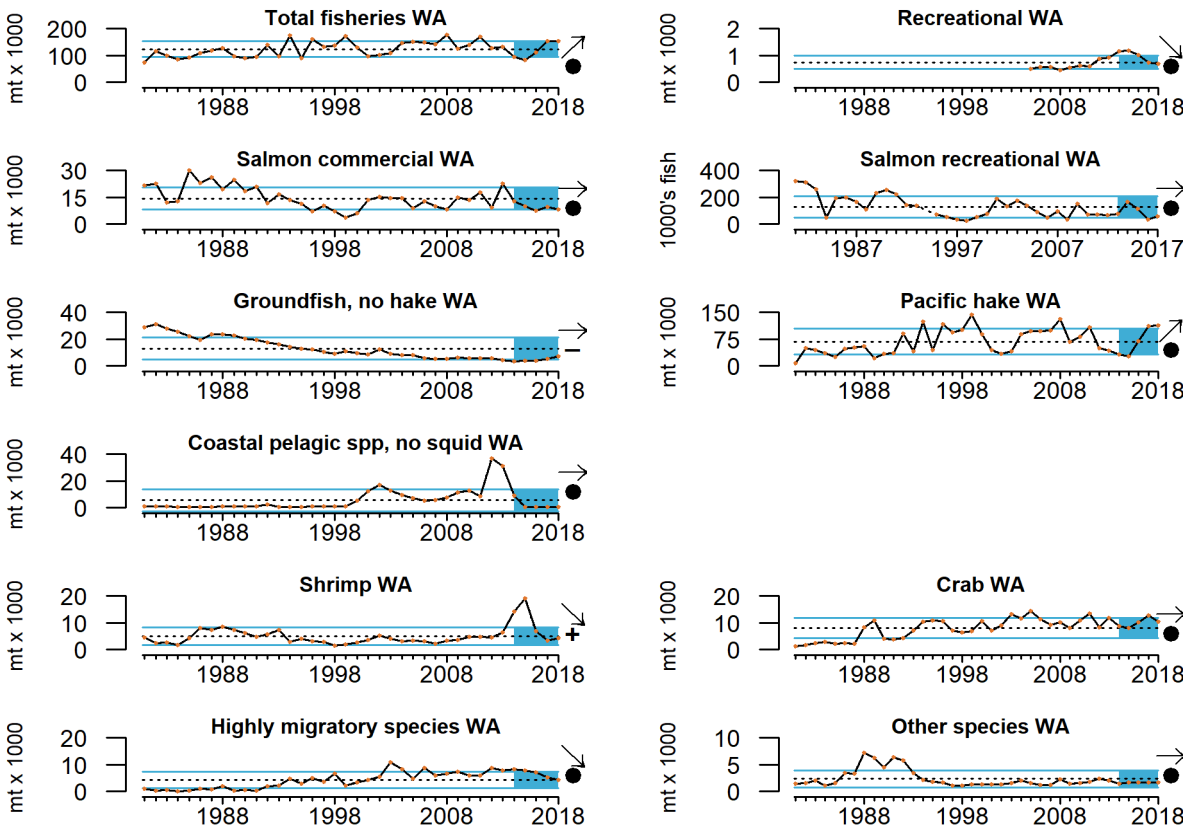

Figure K.1.3 Annual landings of West Coast commercial (data from PacFIN) and recreational (data from RecFIN) fisheries, including total landings across all fisheries from 1981-2018 in Washington (WA). Lines, colors, and symbols as in Fig. 1.

K.2 COMMERCIAL FISHERY REVENUES

Total revenue across West Coast commercial fisheries from 2014–2018 has been near the upper range of the observed time series (Figure K.2.1). Recent patterns were driven primarily by interactions between high revenue from Pacific hake, market squid and crab fisheries, and decreasing revenue in the shrimp fishery over the last 5 years. Revenue from CPS finfish was >1 s.d. below long-term averages from 2014–2018. Revenue from HMS species, commercial salmon, Other species and groundfish (excluding hake) were relatively unchanged and within 1 s.d. of long-term averages over the last 5 years.

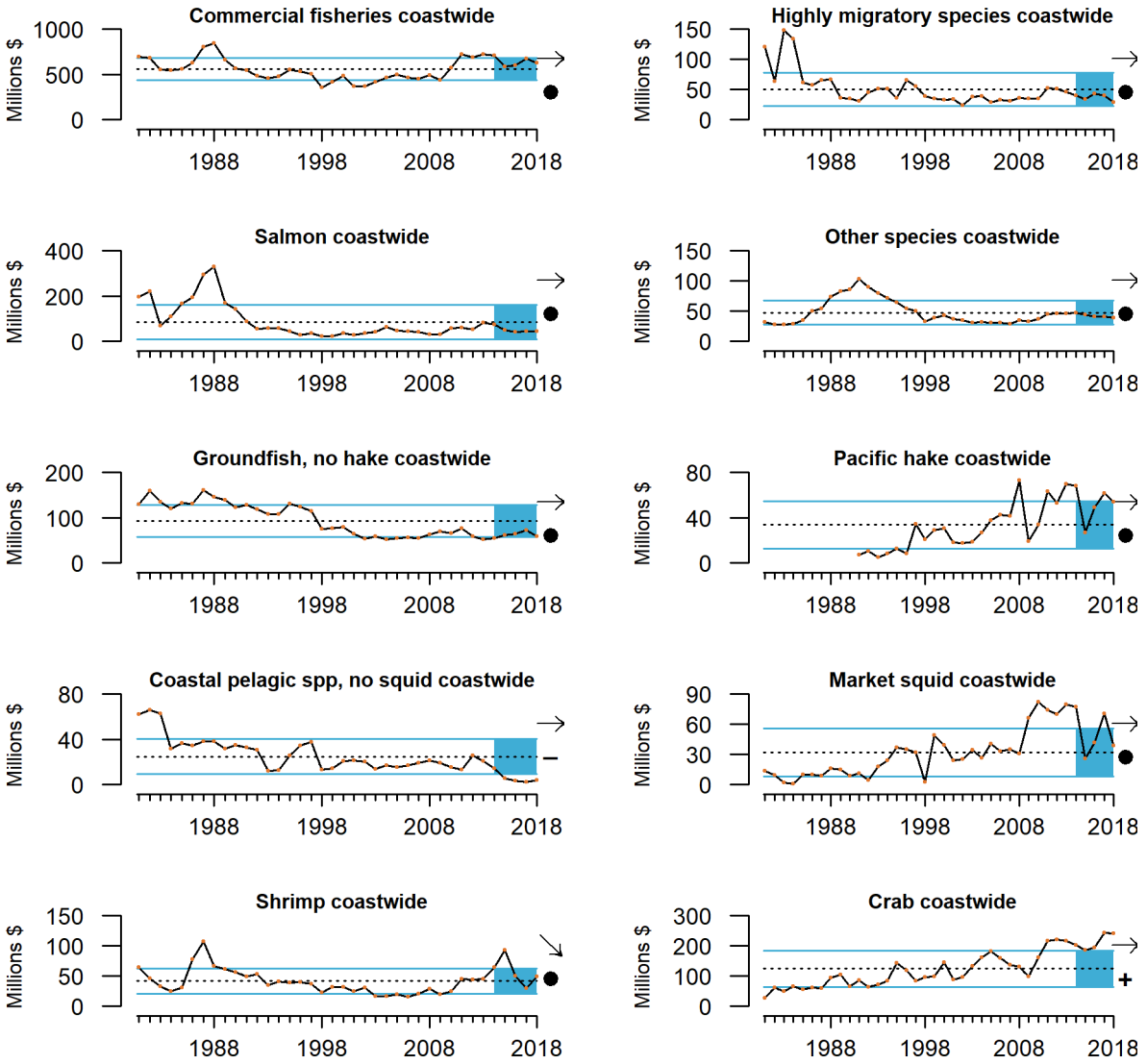

Figure K.2.1 Annual revenue (ex-vessel value in 2015 dollars) of West Coast commercial fisheries (data from PacFIN) from 1981-2018. Pacific hake revenue includes shore-side and at-sea hake revenue values from PacFIN, NORPAC (North Pacific Groundfish Observer Program) and NMFS Office of Science & Technology. Lines, colors, and symbols are as in Fig. 1.

Total revenue across commercial fisheries in California varied within ±1 s.d. of the time series average from 2014–2018 (Figure K.2.2). Revenue from crab fisheries is the most lucrative and was >1 s.d. above long-term averages, while CPS finfish revenue was >1 s.d. below long-term averages in recent years. Pacific hake revenue decreased, but this fishery accounts for a very small portion of total revenue in California. Revenue from HMS species, commercial salmon, Other species, groundfish (excluding hake), market squid and shrimp showed no recent trends and varied within historical averages over the last five years.

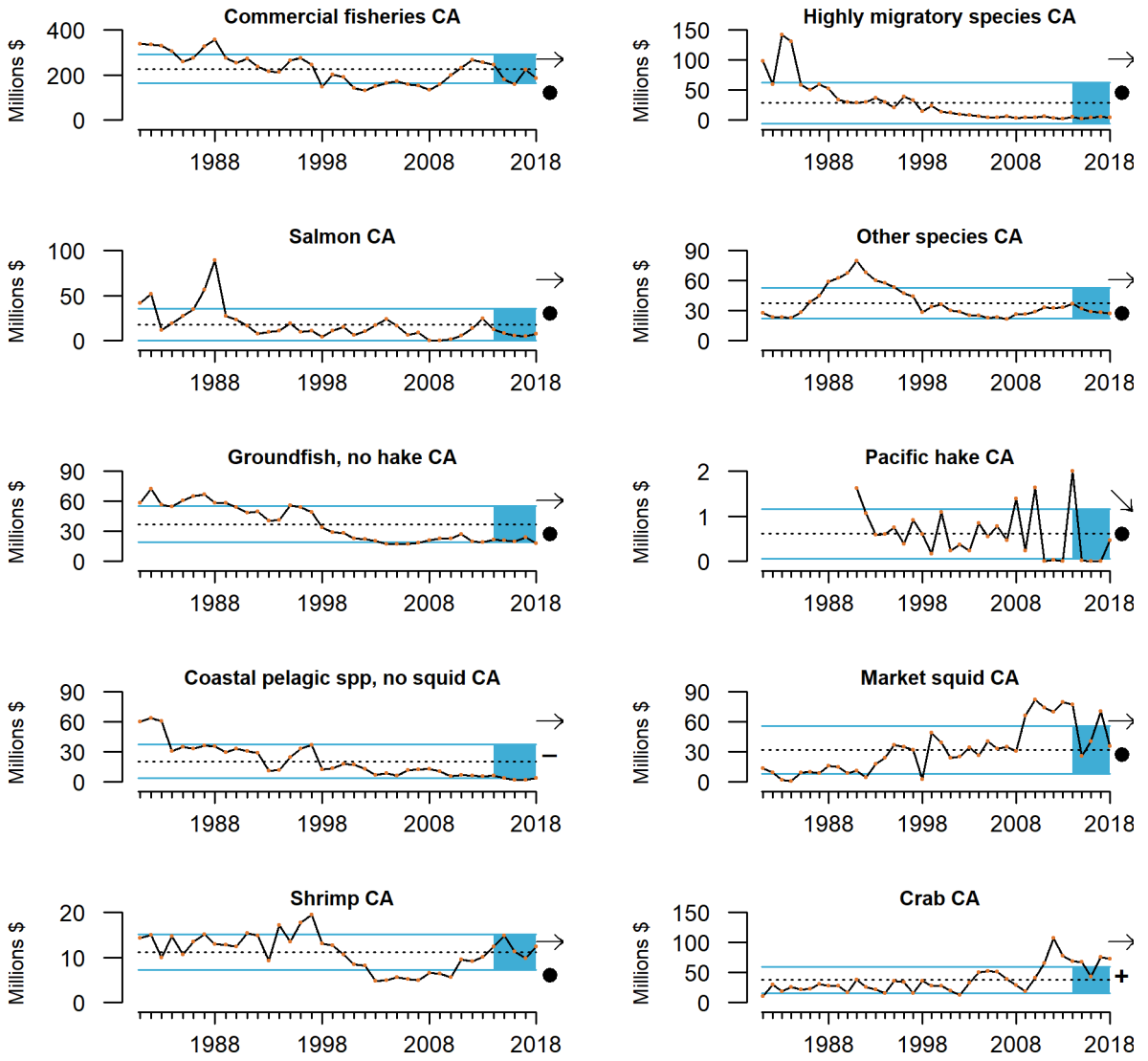

Figure K.2.2 Annual revenue (ex-vessel value in 2015 dollars) of West Coast commercial fisheries in California (CA) (data from PacFIN) from 1981-2018. Pacific hake revenue includes shore-side and at-sea hake revenue values from PacFIN, NORPAC (North Pacific Groundfish Observer Program) and NMFS Office of Science & Technology. Lines, colors, and symbols are as in Fig. 1.

Total revenue across commercial fisheries in Oregon was near the upper range of the time series in 2014–2018 (Figure K.2.3). This was driven by higher than average revenues for Pacific hake and crab, along with increases in revenue from groundfish fisheries. CPS finfish and shrimp revenue declined over the last 5 years. Market squid showed a large increase in revenue in 2016 and another in 2018 that may be related to unusual oceanographic conditions that have pushed market squid north in the system. All other fisheries revenues in Oregon showed no trends and were within ±1 s.d. of long-term averages over the last 5 years.

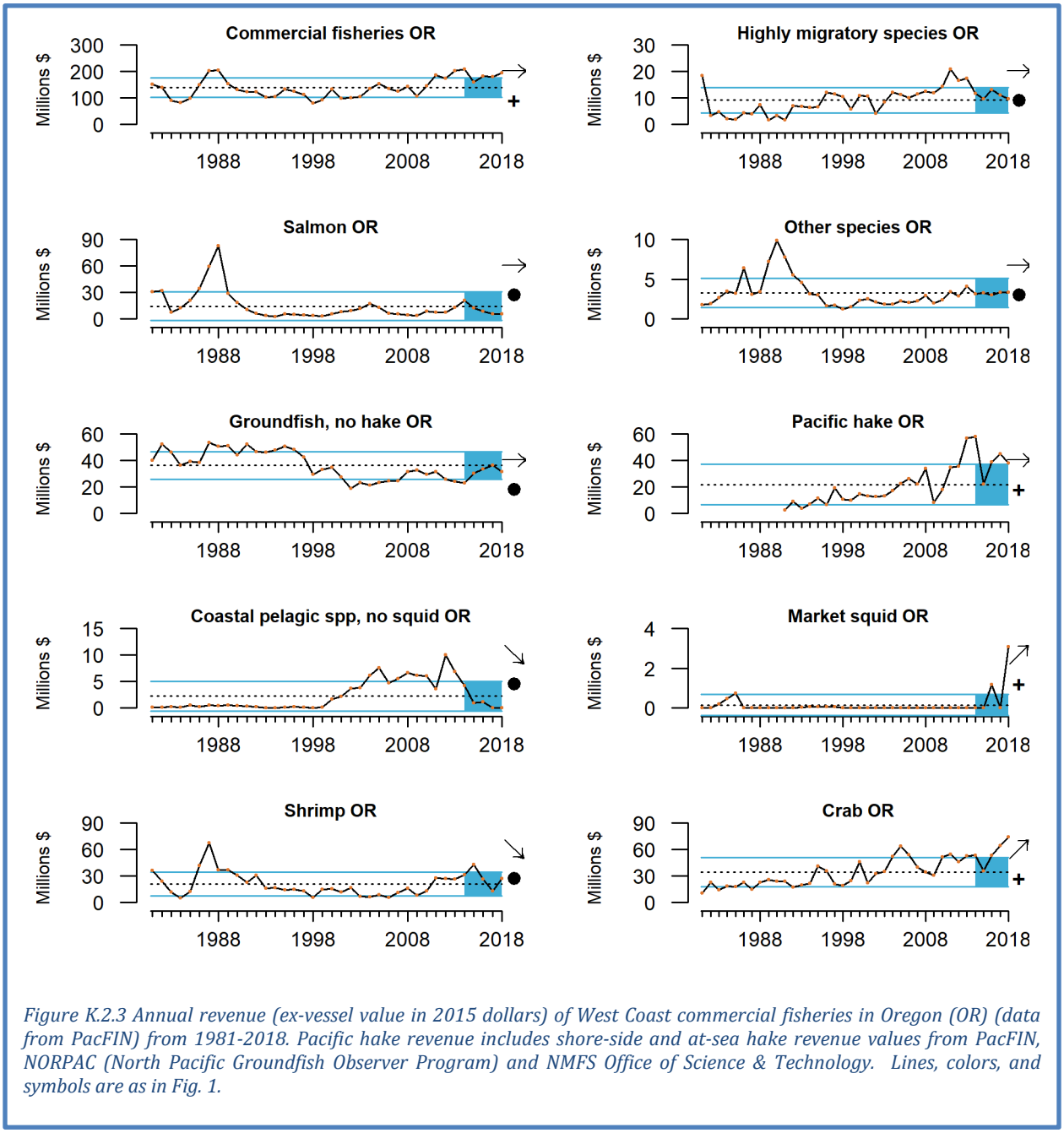

Figure K.2.3 Annual revenue (ex-vessel value in 2015 dollars) of West Coast commercial fisheries in Oregon (OR) (data from PacFIN) from 1981-2018. Pacific hake revenue includes shore-side and at-sea hake revenue values from PacFIN, NORPAC (North Pacific Groundfish Observer Program) and NMFS Office of Science & Technology. Lines, colors, and symbols are as in Fig. 1.

Total revenue across commercial fisheries in Washington remained relatively unchanged and above the long-term average from 2014–2018 (Figure K.2.4). This was a similar pattern to that observed in Oregon over the same time period (Figure K.2.3). The pattern in Washington is primarily driven by the relatively consistent and above-average levels of revenue for crab and HMS, the increasing trend in hake, and the peak in revenue in the shrimp fisheries observed in 2015. Revenue for CPS finfish decreased from 2014-2018 and is near zero. Revenue of non-hake groundfish remained near the lower range of the time series from 2014-2018, while revenue from salmon and Other species showed no significant trends and were within 1 s.d. of long-term averages over the last 5 years.

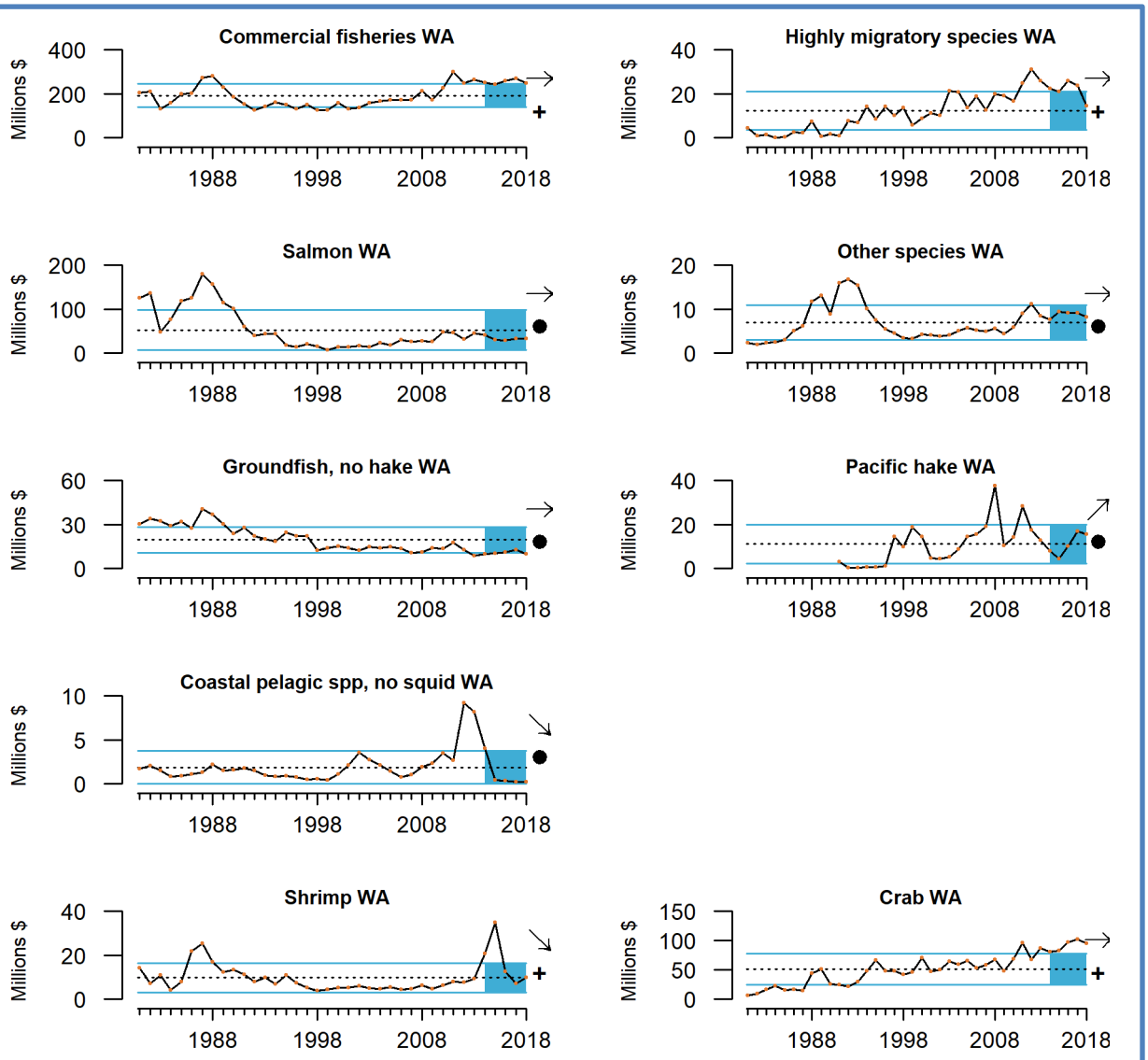

Figure K.2.4 Annual revenue (ex-vessel value in 2015 dollars) of West Coast commercial fisheries in Washington (WA) (data from PacFIN) from 1981-2018. Pacific hake revenue includes shore-side and at-sea hake revenue values from PacFIN, NORPAC (North Pacific Groundfish Observer Program) and NMFS Office of Science & Technology. Lines, colors, and symbols are as in Fig. 1.

Appendix L FISHING GEAR CONTACT WITH SEAFLOOR HABITAT

In Section 5.2 of the report, we presented a spatial representation of the status and trends of gear contact with the seafloor as a function of distances trawled. We used estimates of coastwide distances exposed to bottom trawl fishing gear along the ocean bottom from 1999–2018. We calculated trawling distances based on set and haul-back locations. Data come from logbooks analyzed by the Northwest Fisheries Science Center's West Coast Groundfish Observer Program. Here, we present time series of the data at a coastwide scale and broken out by ecoregion (Northern, north of Cape Mendocino; Central, Cape Mendocino to Point Conception; and Southern, south of Point Conception), substrate type (hard, mixed, soft) and depth zone (shelf, upper slope, lower slope).

At the scale of the entire coast, bottom trawl gear contact with seafloor habitat remained consistently at historically low levels from 2014–2018 (Figure L.1, top). During this period, the vast majority of bottom trawl gear contact occurred in soft, upper slope and soft, shelf habitats (Figure L.1, bottom). The Northern ecoregion has seen the most bottom trawl fishing gear contact with seafloor habitat with nearly five times the magnitude as observed in the central ecoregion in soft, upper slope habitat. Very little to no bottom trawling has occurred in the Southern ecoregion within the time series. A shift in trawling effort from shelf to upper slope habitats was observed during the mid-2000's, which in part corresponded to depth-related spatial closures implemented by the Council. With new spatial closures and openings beginning in 2020, this indicator will be of interest to monitor over the next few years for changes in bottom trawl fishing effort. Reduced bottom trawl gear contact may not coincide with recovery times of habitat depending on how fast recovery happens, which is likely to differ among habitat types (e.g., hard and mixed habitats will take longer to recover than soft habitat).

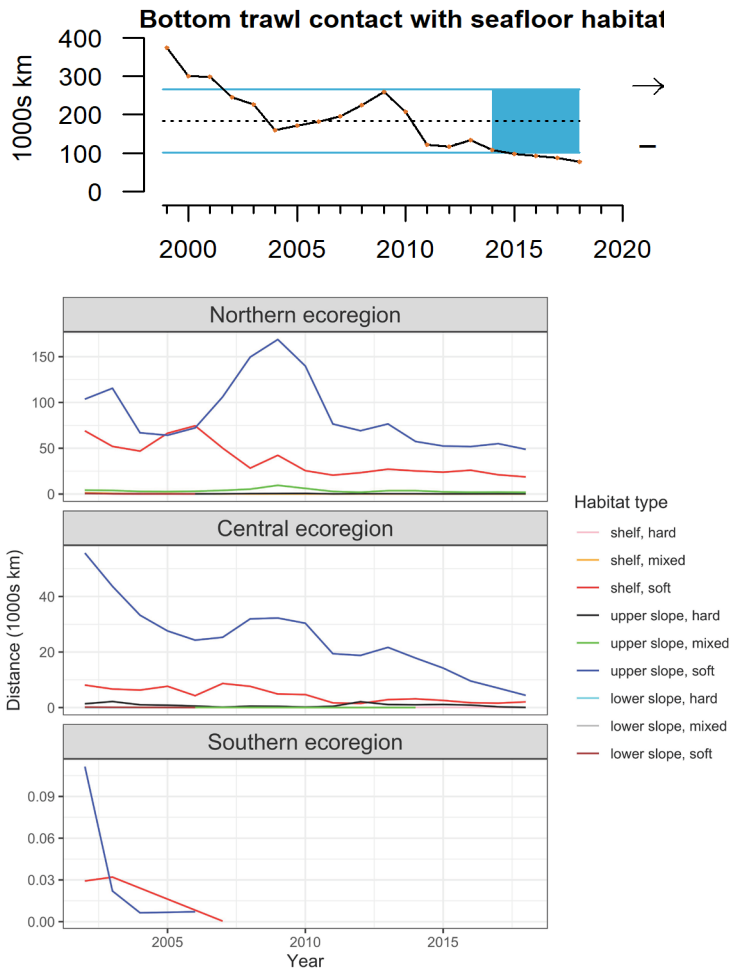

Figure L.1 Weighted distance (1000s km) of fishing gear contact with seafloor habitat across the entire CCE (top; 1999-2018) and within each ecoregion (bottom three panels; 2002-2018). Lines, colors and symbols in top panel are as in Fig. 1.

Appendix M SOCIAL VULNERABILITY OF FISHING-DEPENDENT COMMUNITIES

In Section 6.1 of the main report, we present information on the Community Social Vulnerability Index (CSVI) as an indicator of social vulnerability in coastal communities that are dependent upon commercial fishing. Fishery *dependence* can be expressed by two terms, or by a composite of both. Those terms are engagement and reliance. *Engagement* refers to the total extent of fishing activity in a community; engagement can be expressed in terms of commercial activity (e.g., landings, revenues, permits, processing, etc.) or recreational activity (e.g., number of boat launches, number of charter boat and fishing guide license holders, number of charter boat trips, number of bait and tackle shops, etc.). *Reliance* is the per capita engagement of a community; thus, in two communities with equal engagement, the community with the smaller population would have a higher reliance on its fisheries activities.

In the main body of the report, Figure 6.1.1 plots CSVI in 2017 against commercial reliance for the five most dependent communities in each sector from each of five regions of the CCE. Here, we present a similar plot of CSVI relative to commercial fishing engagement scores from 2017. Figure M.1 shows commercial fishing-engaged communities and their corresponding social vulnerability results. Communities above and to the right of the dashed lines are at least 1 s.d. above the coastwide averages of both indices. Of note are fishing-oriented communities like Westport, Crescent City, Coos Bay, Newport, Fort Bragg, Eureka, and Winchester Bay, which have relatively high commercial fishing engagement results and also a high CSVI composite result.

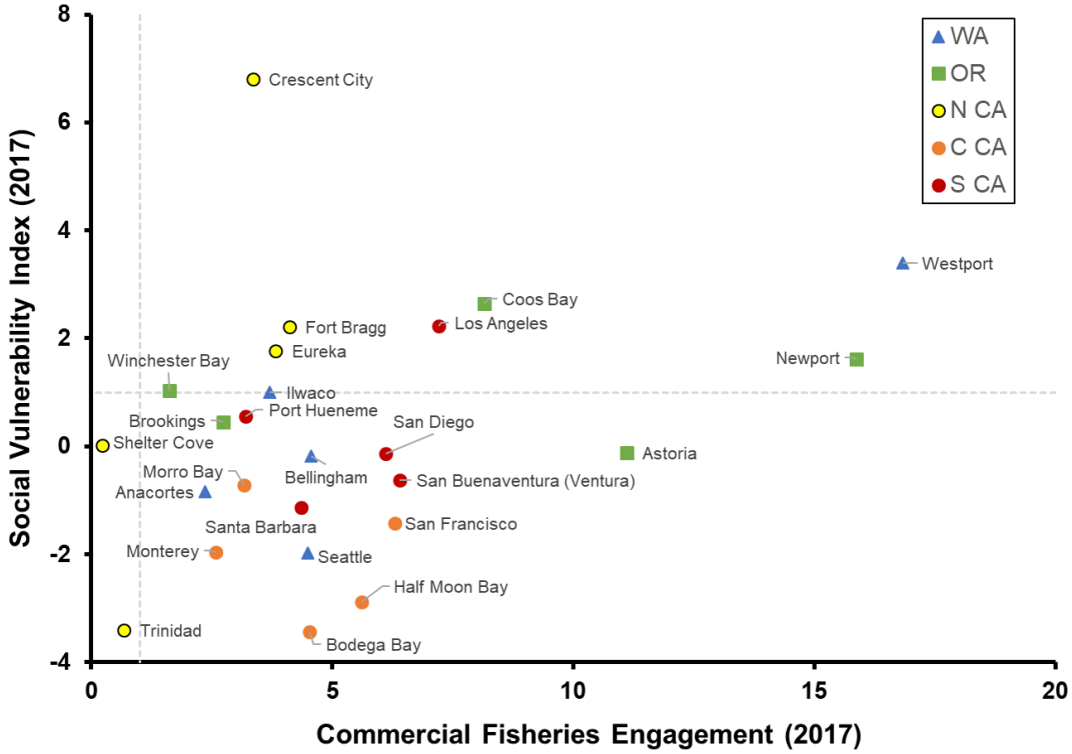

Figure M.1 Commercial fishing engagement (2017) and social vulnerability (2017) scores, plotted for twenty-five communities from each of the 5 regions of the California Current: WA, OR, Northern, Central, and Southern California. The top five highest scoring communities for fishing reliance were selected from each region.

Appendix N FLEET DIVERSIFICATION INDICATORS FOR MAJOR WEST COAST PORTS

Catches and prices from many fisheries exhibit high interannual variability, leading to high variability in fishermen's revenue, but variability can be reduced by diversifying activities across multiple fisheries or regions (Kasperski and Holland 2013). It should be noted that there may be good reasons for individuals to specialize, including reduced costs or greater efficiency; thus while diversification may reduce income variation, it does not necessarily promote higher average profitability. Kasperski (AFSC) and Holland (NWFSC) examined diversification of fishing revenue for more than 28,000 vessels fishing off the West Coast and Alaska over the last 38 years. As a measure of diversification, we use the effective Shannon index (ESI). ESI increases as revenues are spread across *more* fisheries, and as revenues are spread more *evenly* across fisheries; ESI = 1 when a vessel's revenues are from a single species group and region; ESI = 2 if revenues are spread evenly across 2 fisheries; ESI = 3 if revenues are spread evenly across 3 fisheries; and so on. If revenue is not evenly distributed across fisheries, then the ESI value is lower than the number of fisheries a vessel enters.

As is true with individual vessels, the variability of landed value at the port level is reduced with greater diversification of landings. Diversification of fishing revenue has declined over the last several decades for some ports (Figure N.1). Examples include Seattle and most but not all ports in Southern Oregon and California. However, a few ports have become more diversified including Bellingham Bay and Westport in Washington. Diversification of Astoria, in Oregon, had been increasing but has decreased in recent years while Brookings has had an erratic increasing trend. Diversification scores are highly variable year-to-year for some ports, particularly those in Southern Oregon and Northern California that depend heavily on the Dungeness crab fishery, which has highly variable landings. Some ports saw a decrease in diversification between 2017 and 2018, but others saw an increase.

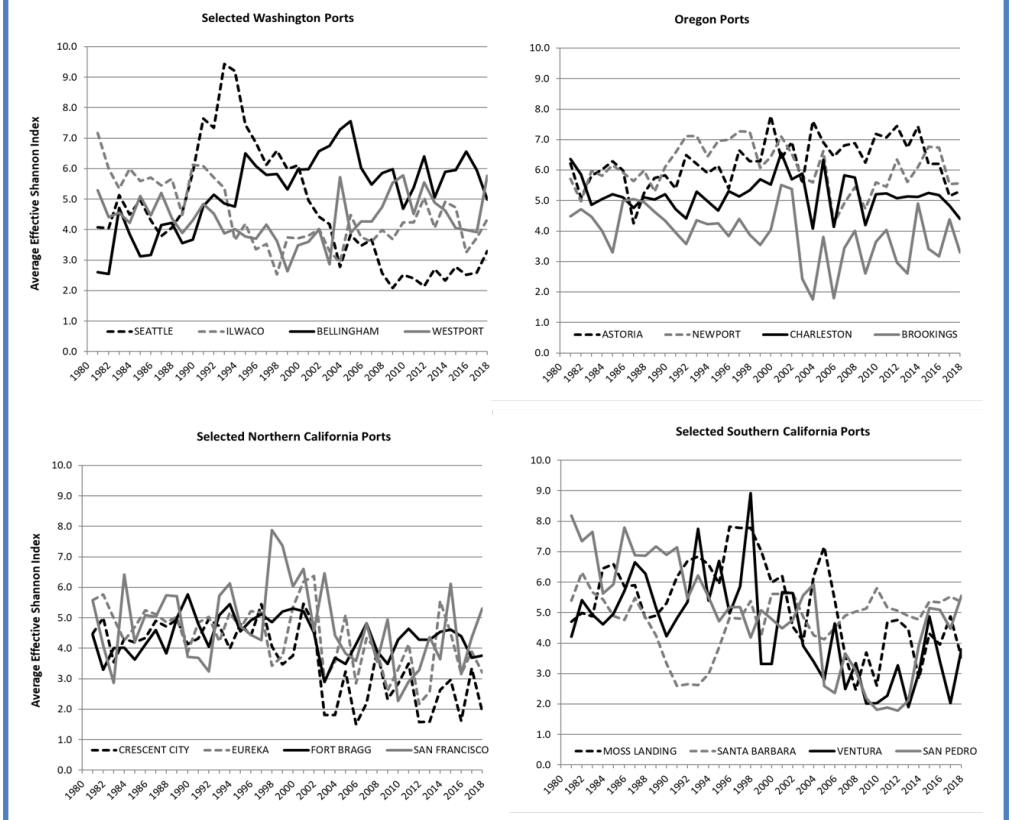

Figure N.1 Trends in fishery revenue diversification in major west coast ports by state. Data from D. Holland (NMFS/NWFSC) and S. Kasperski (NMFS/AFSC).

Appendix O REVENUE CONSOLIDATION BY FISHERY MANAGEMENT PLAN

At the request of the Ecosystem Advisory Subpanel, we are working to develop indicators relevant to National Standard 8 (NS-8) of the Magnuson-Stevens Act. NS-8 states that: "Conservation and management measures shall, consistent with the conservation requirements of this Act (including the prevention of overfishing and rebuilding of overfished stocks), take into account the importance of fishery resources to fishing communities by utilizing economic and social data that meet the requirement of paragraph (2) [i.e., National Standard 2], in order to (a) provide for the sustained participation of such communities, and (b) to the extent practicable, minimize adverse economic impacts on such communities." (NS-2 states that "Conservation and management measures shall be based upon the best scientific information available.")

Following initial discussions with economists in the NOAA IEA network, we chose to examine ex-vessel revenue as a potential indicator of progress toward NS-8. In particular, we are looking at how the proportion of revenues taken in by commercial fishing operations by different ports has changed over time. Consolidation of revenue into a smaller number of ports may indicate that fishery access opportunities are changing and potentially constraining some communities (Kuriyama et al. 2019).

Methods: Total revenue per year was calculated annually for ports in Washington, Oregon and California from 1982 to 2018, and compared to the cumulative revenue for all ports by year generating percent revenue share by port. Revenue was calculated in cpi-adjusted dollars reported by port. FMP-specific fishery revenues were calculated by aggregating revenues based on management species groups and comparing them to the coast-wide cumulative annual revenues. Salmon, HMS, CPS, and groundfish fisheries were all considered; we evaluated groundfish both with and without Pacific hake. For space considerations, we present only the 16 ports with the highest revenue proportions over the full time series (except for CPS, for which only 12 ports were frequent participants). The proportional revenue represented the revenue share for a single port's landings compared to cumulative revenue by all ports with landings that matched the given fishery type. A LOESS model was applied to estimate a smoothing curve with a 95% confidence interval.

Results: For all groundfish, revenue has become more concentrated in a few ports since 1982, most notably Astoria and Newport (Figure O.1). Several other ports have had small increases on average over the full time period (Neah Bay, Port Orford, Brookings, Eureka) while others have had increases since ~2000 (Westport, Ilwaco/Chinook, Morro Bay). Other ports in this top-16 list saw declines

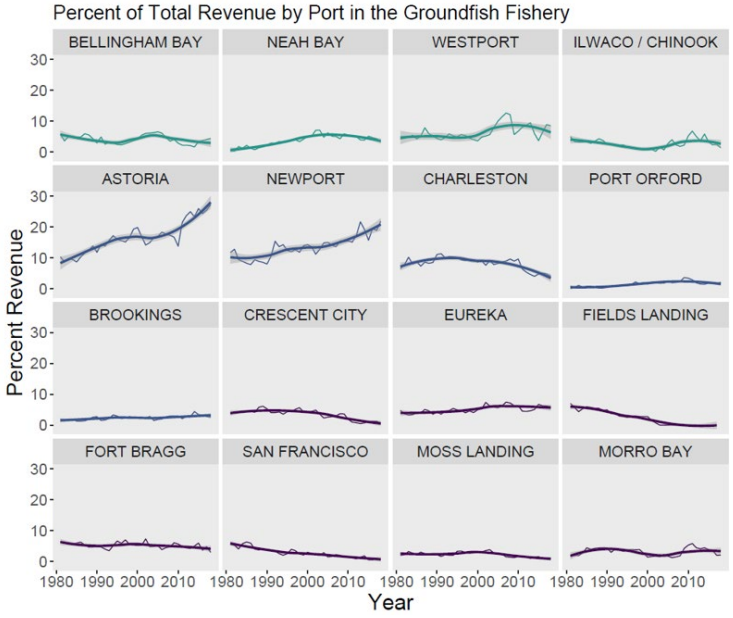

Figure O.1 Port-specific percentages of total commercial groundfish fishing revenue, 1982-2018, for the top 16 ports by groundfish revenue during this period. Data are based on port specific groundfish revenue share relative to coastwide groundfish revenue in a given year. Heavy line is LOESS model fit with 95% CI. Revenue data are from PacFIN.

in percent of total groundfish revenue, some gradually over the full time series (e.g., Fields Landing, Fort Bragg, San Francisco) and others more recently (Charleston, Crescent City, Moss Landing).

When we excluded hake revenue from this analysis, the list of top-16 ports did not change, but patterns changed for some ports (Figure O.2). Westport saw a downturn in non-hake groundfish revenue, dating to the 1990s, in contrast to the relative increase that Westport experienced in the 2000s when hake are included (Figure O.1). Also, the increasing trend for Astoria was more gradual in non-hake groundfish. Otherwise, changes were minor, likely reflecting that many of these communities do not have hake landings.

For CPS, only 12 ports were regular-enough recipients of CPS landings to be included in the analysis. Patterns of CPS revenue percentage were highly dynamic for most ports, both from year to year and over the long term (Figure O.3). Ventura experienced a long-term increase, as did Moss Landing and Half Moon Bay, although not to the extent of Ventura. Sausalito, San Francisco and Terminal Island all declined. Monterey had been declining until an increase that began prior to 2010, while Port Hueneme increased for the first half of

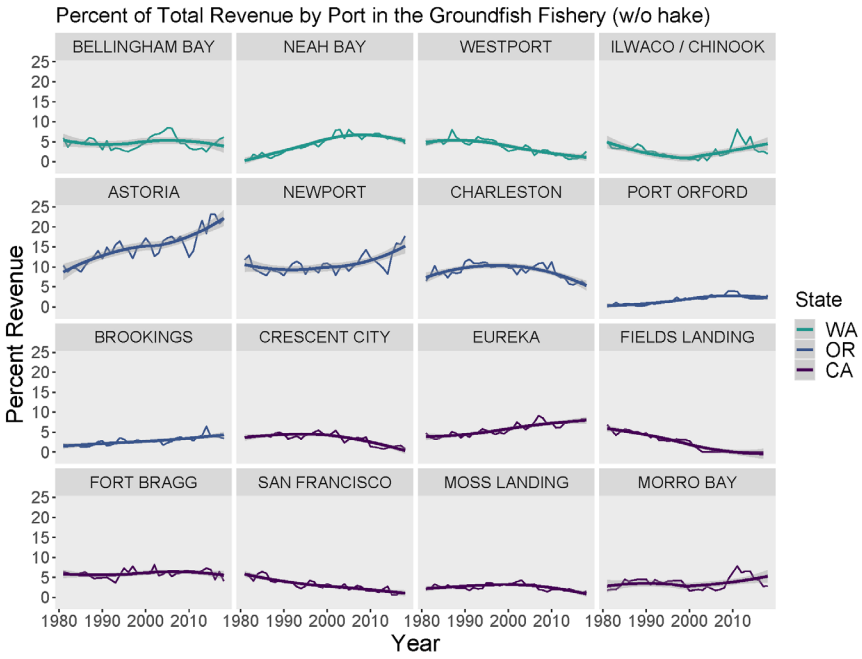

Figure O.2 Port-specific percentages of total commercial groundfish fishing revenue (excluding hake), 1982-2018, for the top 16 ports by groundfish revenue during this period. Data are based on port specific groundfish revenue share relative to coastwide groundfish revenue in a given year. Heavy line is LOESS model fit with 95% CI. Revenue data are from PacFIN.

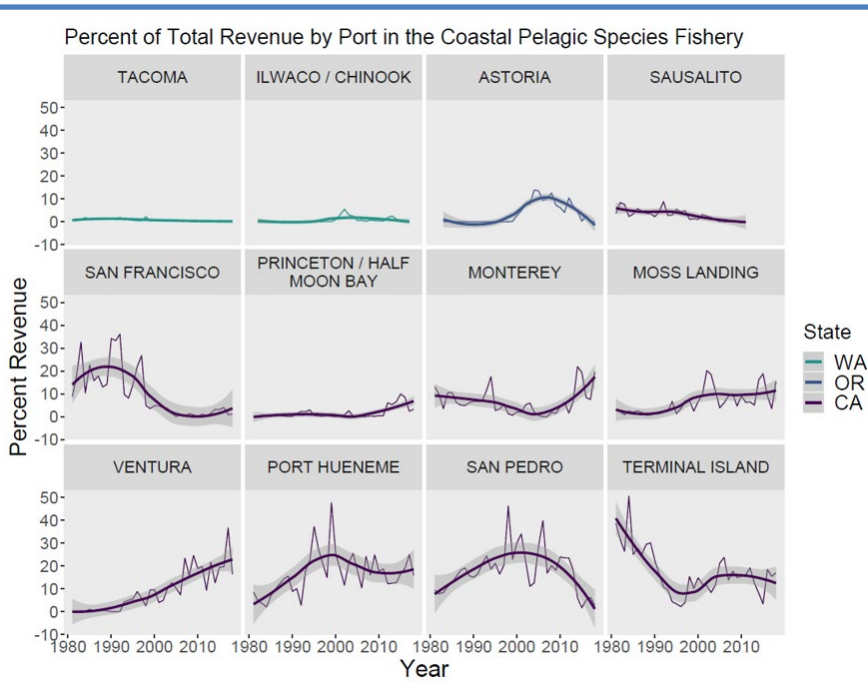

Figure O.3 Port-specific percentages of total commercial CPS fishing revenue, 1982-2018, for the top 12 ports by CPS revenue during this period. Data are based on port specific CPS revenue share relative to coastwide CPS revenue in a given year. Heavy line is LOESS model fit with 95% CI. Revenue data are from PacFIN.

the time series then leveled off. Astoria and San Pedro had dome-shaped patterns. Very little CPS revenue came from Washington.

The list of top-16 commercial salmon ports was very different, and half were located in the Salish Sea (Puget Sound and the Strait of Juan de Fuca). Most patterns showed high interannual variability and several long-term trends (Figure O.4). Several ports in the Salish Sea experienced long-term declines in revenue percentage (Blaine, Bellingham, La Conner, Port Angeles) while others generally had long-term increases (Neah Bay, Shelton). Aggregated ports along the Washington outer coast and in the Columbia River also saw increases. Top commercial salmon ports in coastal Oregon and California typically experienced long-term oscillating patterns, and it is difficult to discern any clear long-term trends over the full course of the time series.

The list of top-16 commercial HMS ports is again different from the other FMPs, and the trends from these ports show dramatic changes (Figure O.5), primarily an increase in commercial HMS revenue percentage for several northern ports where albacore are landed (Westport, Ilwaco /Chinook, Newport, Charleston) and declines in southern ports (San

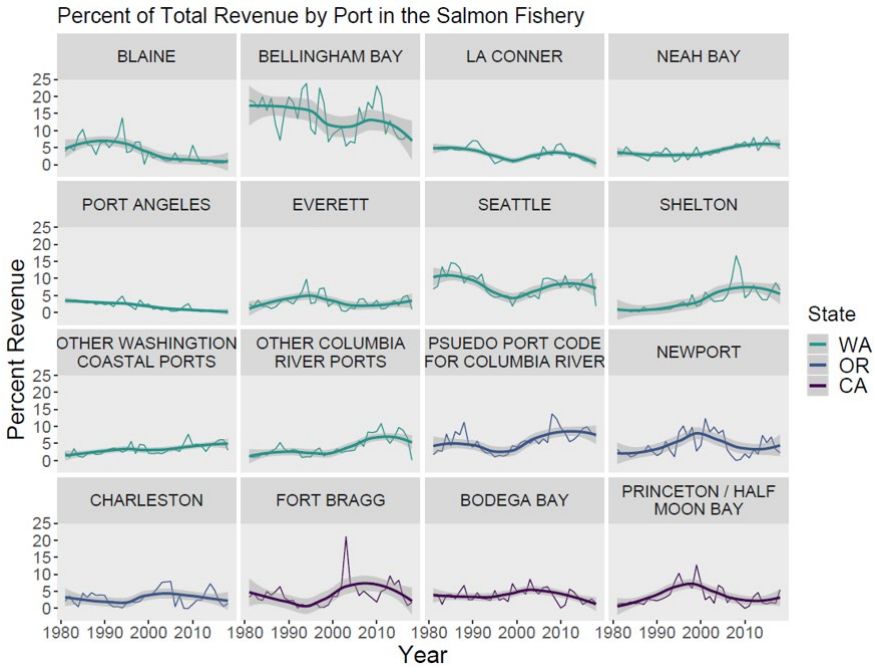

Figure O.5 Port-specific percentages of total commercial salmon fishing revenue, 1982-2018, for the top 16 ports by salmon revenue during this period. Data are based on port specific salmon revenue share relative to coastwide salmon revenue in a given year. Heavy line is LOESS model fit with 95% CI. Revenue data are from PacFIN.

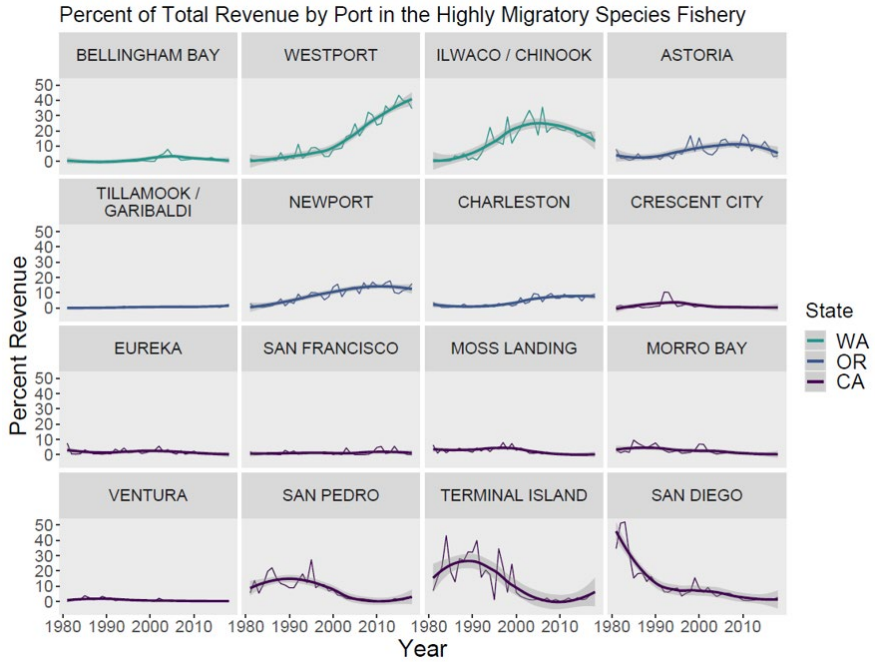

Figure O.4 Port-specific percentages of total commercial HMS fishing revenue, 1982-2018, for the top 16 ports by HMS revenue during this period. Data are based on port specific HMS revenue share relative to coastwide HMS revenue in a given year. Heavy line is LOESS model fit with 95% CI. Revenue data are from PacFIN.

Pedro, Terminal Island, and San Diego). For most of the other ports, the percentage of commercial HMS revenue was quite low.

We must stress several key points regarding these analyses:

- The analyses are preliminary, and we will be doing subsequent work internally and ideally with the PFMC SSC to ensure the analyses are appropriate. For example, as of the briefing book deadline, we have not determined if communities that are experiencing negative trends in percent revenue are also experiencing net decreases in revenue, an important consideration for making judgments about impacts.
- We also have made no effort yet to attribute changes in revenue percentage with management actions, environmental changes, food web changes, or changes within coastal communities. It is therefore premature to link any of these changes explicitly to revenue consolidation as a measure of community-level economies or opportunities in the context of NS-8. We will work with the Council and advisory bodies on how to best approach such interpretation so that this indicator is evaluated for its usefulness.
- The analyses only consider a subset of communities with relatively high revenues for each FMP, and NS-8 is not meant to be selective in that manner. We will thus work to identify ways to classify changes in revenue across a wider range of communities, if this indicator proves to be useful. Because port communities have different levels of coastal community vulnerability (see Section 6.1), they likely experience changes in revenue in different contexts.

Appendix P REFERENCES

Abell, R., *et al.* 2008. Freshwater ecoregions of the world: A new map of biogeographic units for freshwater biodiversity conservation. *BioScience* 58:403-414.

Bednaršek, N., *et al.* 2020. Exoskeleton dissolution with mechanoreceptor damage in larval Dungeness crab related to severity of present-day ocean acidification vertical gradients. *Science of the Total Environment*, article no. 136610.

Burke, B.J., *et al.* 2013. Multivariate models of adult Pacific salmon returns. *PLoS One* 8:e54134.

Chan, F., *et al.* 2008. Emergence of anoxia in the California current large marine ecosystem. *Science* 319:920-920.

Dyson, K., Huppert, D.D. 2010. Regional economic impacts of razor clam beach closures due to harmful algal blooms (HABs) on the Pacific coast of Washington. *Harmful Algae* 9: 264-271.

Feely, R.A., *et al.* 2008. Evidence for upwelling of corrosive "acidified" water onto the continental shelf. *Science* 320:1490-1492.

Fisher, J.L., *et al.* 2015. The impact of El Niño events on the pelagic food chain in the northern California Current. *Global Change Biology* 21:4401-4414.

Friedman, W.R., *et al.* 2019. Modeling composite effects of marine and freshwater processes on migratory species. *Ecosphere* 10:e02743.

Hobday, A.J., *et al.* 2016. A hierarchical approach to defining marine heatwaves. *Progress in Oceanography* 141:227-238.

Jacox, M.G., *et al.* 2016. Impacts of the 2015–16 El Niño on the California Current System: Early assessments and comparison to past events. *Geophysical Research Letters* 43:7072–7080.

Jacox, M.G., et al. 2018. Coastal upwelling revisited: Ekman, Bakun, and improved upwelling indices for the U.S. west coast. *Journal of Geophysical Research: Oceans* 123:7332-7350.

Jepson, M. and L.L. Colburn. 2013. Development of social indicators of fishing community vulnerability and resilience in the U.S. Southeast and Northeast Regions. NOAA Tech. Memo. NMFS-F/SPO-129.

Kasperski, S., and D.S. Holland. 2013. Income diversification and risk for fishermen. *Proceedings of the National Academy of Sciences of the United States of America* 110:2076-2081.
Keister, J.E., *et al.* 2011. Zooplankton species composition is linked to ocean transport in the Northern California Current. *Global Change Biology* 17:2498-2511.
Kuriyama, P.T., et al. 2019. Catch shares drive fleet consolidation and increased targeting but not spatial effort concentration nor changes in location choice in a multispecies trawl fishery. *Canadian Journal of Fisheries and Aquatic Sciences* 76:2377-2389.
Lefebvre, K.A., et al. From sanddabs to blue whales: the pervasiveness of domoic acid. *Toxicon* 40:971-977.
Leising, A.W., in prep. Marine heatwaves of the North East Pacific from 1982-2019: a Blobtrospective. For submission to *Journal of Geophysical Research: Oceans*.
Lindgren, F., and H. Rue. 2015. Bayesian spatial modelling with R-INLA. *Journal of Statistical Software* 63(19):1-25.
McCabe, R.M., *et al.* 2016. An unprecedented coastwide toxic algal bloom linked to anomalous ocean conditions. *Geophysical Research Letters* 43:10366-10376.
McKibben, M., *et al.* 2017. Climatic regulation of the neurotoxin domoic acid. *Proceedings of the National Academy of Sciences* 114:239-244.
Melin, S.R., *et al.* 2012. California sea lions: an indicator for integrated ecosystem assessment of the California Current system. *CalCOFI Reports* 53:140-152.
Miller, R.R., et al. 2019. Distribution of pelagic thaliaceans, *Thetys vagina* and *Pyrosoma atlanticum*, during a period of mass occurrence within the California Current. *CalCOFI Reports* 60:xx-xx.
Peterson, W.T., *et al.* 2014. Applied fisheries oceanography ecosystem indicators of ocean condition inform fisheries management in the California Current. *Oceanography* 27:80-89.
Reynolds, R.W., *et al.* 2007. Daily high-resolution-blended analyses for sea surface temperature. *Journal of Climate* 20:5473–5496.
Ritzman, J., *et al.* 2018. Economic and sociocultural impacts of fisheries closures in two fishing-dependent communities following the massive 2015 US West Coast harmful algal bloom. *Harmful Algae* 80:35-45.
Santora, J.A., *et al.* 2020. Habitat compression and ecosystem shifts as potential links between marine heatwave and record whale entanglements. *Nature Communications* 11:536.
Thompson, A.R., *et al.* 2019a. Indicators of pelagic forage community shifts in the California Current Large Marine Ecosystem, 1998–2016. *Ecological Indicators* 105:215-228.
Thompson, A.R., *et al.* 2019b. State of the California Current 2018-19: a novel anchovy regime and a new marine heatwave? *CalCOFI Reports* 60:xx-xx.
Waples, R.S. 1995. Evolutionarily significant units and the conservation of biological diversity under the Endangered Species Act. *American Fisheries Science Symposium* 17:8-27.